PROPAGATION OF CU/ZN SUPEROXIDE DISMUTASE MISFOLDING VIA TISSUE-DERIVED EXTRACELLULAR VESICLES IN AMYOTROPHIC LATERAL SCLEROSIS

by

Sarah Fernando

BSc., Aston University, 2010

A THESIS SUBMITTED IN PARTIAL FULFILLMENT OF

THE REQUIREMENTS FOR THE DEGREE OF

DOCTOR OF PHILOSOPHY

in

THE FACULTY OF GRADUATE AND POSTDOCTORAL STUDIES

(Pathology and Laboratory Medicine)

THE UNIVERSITY OF BRITISH COLUMBIA

(Vancouver)

August 2017

ABSTRACT

Amyotrophic Lateral Sclerosis (ALS) is a fatal neurodegenerative disease wherein motor neurons progressively degenerate over time, and pathology spreads spatiotemporally throughout the neuroaxis. Mutations in the Cu/Zn superoxide dismutase (SOD1) gene are linked to inherited cases of ALS, and misfolded SOD1 protein has been reported in neural tissues from all ALS subtypes. We have previously shown that human wild-type SOD1 (HuWTSOD1) in cultured HEK cells can be induced to misfold by transgenically-expressed mutant SOD1, and that cell-to-cell transmission of HuWtSOD1 misfolding can occur *in vitro*. However, the mechanism(s) by which misfolded SOD1 could be propagated *in vivo* remain unknown. In this study, we investigated the capability of central nervous system (CNS) tissue-derived exosomes and microvesicles to propagate SOD1 misfolding. The overarching hypothesis of the work is that **CNS tissue-derived EVs from ALS mouse models bear misfolded SOD1 cargo, and can induce SOD1 misfolding in recipient cultured cells.** The hypothesis was investigated using the following specific aims: **1)** Isolate and characterize CNS tissue-derived EVs from ALS mouse models **2)** Investigate the presence and localization of misfolded SOD1 in isolated EVs **3)** Examine capability of ALS mouse model tissue-derived EVs to propagate SOD1 misfolding to cell culture systems, and **4)** Explore physiological relevance of findings using EVs isolated from human ALS patients.

Using primary spinal motor neuron and glial cultures from HuWTSOD1 transgenic mice, and a misfolded SOD1 conformation-specific antibody, we show for the first time that both CNS-derived EV subtypes are capable of transmitting SOD1 misfolding to recipient cells. Our study provides novel evidence consistent with a potential role of CNS-derived extracellular vesicles in human ALS, and highlights the ability to use the more abundant microvesicle population to investigate the functional effects of EVs in protein misfolding diseases.

LAY SUMMARY

Amyotrophic Lateral Sclerosis (ALS) is a fatal disease that causes death of motor neurons in the brain and spinal cord of affected patients. Over time, disease spreads through the central nervous system, causing worsening paralysis in ALS patients. Inherited ALS cases have been linked to gene mutations in superoxide dismutase (SOD1), a protein that acts as an antioxidant enzyme in the body. Abnormally folded forms of SOD1 protein which potentially cause motor neuron death are reported in neural tissues of ALS patients. Using a cell culture system that models aspects of ALS biology, our group showed that normal SOD1 protein folds abnormally when mutated SOD1 is introduced to cells. We also showed that this misfolded protein can spread from cell-to-cell, mimicking the systematic progression of symptoms through the spinal cord in ALS patients. However, the biological mechanisms by which misfolded SOD1 can be propagated in this manner are unknown. Using mouse models of ALS, the work in this thesis shows new evidence that small vesicles secreted from cells termed extracellular vesicles are involved in the transmission of SOD1 protein misfolding in ALS. In addition to informing our understanding of disease biology, the findings here provide insight into the potential use of extracellular vesicles as much-needed biomarkers and therapeutic targets in ALS.

PREFACE

Chapter 1 of this thesis is a review of the current state of ALS research, SOD1, the prion-like propagation of protein misfolding as a mechanism for disease transmission in ALS, and what is currently known about extracellular vesicles as they pertain to the above. Figure 1.1 was generated with assistance by Luke McAlary. Some portions of Chapter 1, as well the conclusion of this thesis, have been previously published in the following invited review articles:

- J.M. Silverman, **S.M. Fernando**, L.I. Grad, A.F. Hill, B.J. Turner, J.J. Yerbury, N.R. Cashman, Disease Mechanisms in ALS: Misfolded SOD1 Transferred Through Exosome-Dependent and Exosome-Independent Pathways, *Cellular and molecular neurobiology* 36(3) (2016) 377-81.
- L.I. Grad, **S.M. Fernando**, N.R. Cashman, From molecule to molecule and cell to cell: prion-like mechanisms in amyotrophic lateral sclerosis, *Neurobiology of disease* 77 (2015) 257-65.

In Chapter 2 The experimental setup for side-by-side comparison of isolation protocols was designed by Dr. Judith Silverman and myself, and the work performed by myself. The protein yield experiment was designed by myself and carried out by Chieh-Chieh Shyu. TEM images were obtained with the help of Brad Ross from the UBC Bioimaging facility, and Nanoparticle tracking analysis experiments were performed with the assistance of Dr. Elham Behesti. I designed and carried out the remainder of experiments in this Chapter with technical assistance by Chieh-Chieh Shyu and scientific input by Dr. Judith Silverman.

Chapter 3: The experiments investigating surface misfolded SOD1 on EVs via immunoprecipitation were designed by Drs. Judith Silverman and Leslie Grad, and performed by Dr. Leslie Grad. TEM experiments probing individual EVs for misfolded SOD1 were designed by myself and performed by Dr. Catherine Cowan.

Cytotoxicty experiments were designed by myself and performed by Chieh-Chieh Shyu. Darren Christy performed the misfolded SOD1 ELISA on spinal cord tissue-derived EVs. All other experiments were designed and performed by myself with scientific input from Drs. Judith Silverman and Neil Cashman.

Chapter 4: Primary spinal cord mixed neuronal and glial cells were cultured and maintained by Dr. Jing Wang. Immunoprecipitation experiments were performed by myself with technical input from Dr. Leslie Grad. The propagation experiment was designed with input from Dr. Neil Cashman. All other experiments were designed and carried out by myself with scientific input from Drs. Neil Cashman and Judith Silverman.

Chapter 5: The human tissue material we used was kindly provided by Drs. Lyle Ostrow and John Ravits from Target ALS, and Dr. Ian Mackenzie from UBC. Experimental setup in this chapter is complementary to the work in animal models conducted in previous chapters, and designed in the same manner. 3H1 and 10C12 immunoprecipitations of spinal cord exosomes were designed by Drs. Judith Silverman and Leslie Grad, and carried out by Dr. Leslie Grad and myself. The remainder of experiments were designed and performed by myself with scientific input from Dr. Neil Cashman.

All experiments involving animals were conducted according to the Canadian Council on Animal Care guidelines, approved by the Animal Care Committee of the University of British Columbia, and were sacrificed according to the guidelines of the Institutional Animal Care and Use Committee (IACUC) under protocol A15-0203.

Portions of this thesis are written up in a manuscript currently under review.

TABLE OF CONTENTS

LIST OF FIGURES

LIST OF ABBREVIATIONS

AD	Alzheimer's disease
ALS	Amyotrophic lateral sclerosis
AMPA	Amino-3-hydroxy-5-methyl-4-isoxazoleproprionic acid
ANG	Angiotensin
ANOVA	Analysis of variance
ATF6	Activating transcription factor 6
BCA	Bicinchoninic acid
C9ORF72	Chromosome 9 open reading frame 72
CHMPB2	Charged multivesicular body protein 2B
DSE	Disease-specific epitope
ELISA	Enzyme-linked immunosorbent assay
EM	Electron microscopy
ER	Endoplasmic reticulum
ESCRT	Endosome sorting complex required for transport
EV	Extracellular vesicles
FALS	Familial ALS
FBS	Fetal bovine serum
FTD	Frontotemporal dementia
FTLD	Frontotemporal lobar dementia
FUS	Fused in sarcoma
HD	Huntington's disease
HEK	Human embryonic kidney cells (HEK293FT)
HSP	Heat shock protein
HuWTSOD1	Human wild-type SOD1
IB	Immunoblot (western blot)
ICC	Immunocytochemistry
IF	Immunofluorescence
ILV	Intraluminal vesicles
IP	Immunoprecipitation
IRE1	Inositol-requiring enzyme 1
LMN	Lower motor neuron
MHC	Major histocompatibility complex
MV	Microvesicle
MVE/MVB	Multivesicular endosome/Multivesicular body
NMDA	N-methyl-D-aspartate

NonTg	Non-transgenic
NSC-34	mouse motor neuron-like
NTA	Nanoparticle tracking analysis
OPTN	Optineurin
PBS	Phosphate buffer solution
PBST	0.3% Triton X-100 in phosphate buffer solution
PD	Parkinson’s disease
PERK	Protein-kinase RNA like ER kinase
PFA	Paraformaldehyde
PK	Proteinase K
PVDF	Polyvinylidene difluoride
ROS	Reactive oxygen species
SALS	Sporadic ALS
SDS	Sodium dodecylsulphate
SDS-PAGE	SDS-polyacrylamide gel electrophoresis
SEM	Standard error of mean
SETX	Senataxin
siRNA	Small interfering RNA
SOD	Superoxide dismutase
SOD1	Cu/Zn Superoxide dismutase 1
SQSTM1	Sequestosome 1
TDP-43	Tar DNA-binding protein 43
TEM	Transmission electron microscopy
TSE	Transmissible spongiform encephalopathy
UBQLN2	Ubiquilin 2
UMN	Upper motor neuron
UPR	Unfolded protein response
VAPB	Vesicle associated membrane protein associated protein B
WtSOD1	Wild-type SOD1

ACKNOWLEDGEMENTS

I am grateful to have received salary support from the UBC Four Year Doctoral Fellowship, and to Dr. Haydn Pritchard and the Department of Pathology and Laboratory Medicine for the nomination. This work was performed with the peace of mind that comes with the lack of “money worries”.

I am immensely thankful for the mentorship of my supervisor, Dr. Neil Cashman, who has encouraged me to not only to do good science and think broadly, but also to look to the future. I am grateful for your guidance, financial support, and for the opportunities you provided me throughout the years to travel, attend conferences, and grow as a scientific speaker and presenter. A big thank you goes to my committee members: Drs. Yu Tian Wang, Emma Guns, Cheryl Wellington and Ed Pryzdial. Your mentorship, support, and advice have meant so much to me, and this journey would not have been possible without your contributions. A heart-felt thank you goes to Emma Guns who encouraged and motivated me to keep pursuing my PhD.

I am fortunate to have shared my highs and lows with the members of the Cashman lab who have enriched my experience at UBC: Dwayne Ashman, Edward Pokrishevsky, Sarah Louadi, Jing Wang, Dean Airey, Beibei Zhao, Catherine Cowan, Jeremy Nan, Masoud Yousefi, Luke McAlary, Else Van Gerresheim, Juliane Coutts, and all the co-op students past and present. Thank you to Maja Filipovic for all the tissue harvests you performed and your good cheer, and Lisa Bertram for all your help in animal land. Chieh-chieh Shyu provided outstanding and tireless help with this work; the countless EV isolations you performed and cell cultures you maintained were very much appreciated. I am also very grateful for the mentorship of Drs. Judith Silverman, Ebrima Gibbs, and Leslie Grad at various points in this journey. As senior scientists, your guidance has been formative, and I will carry with me the lessons you have taught me. A very special thank you goes to Dr. Leslie

Grad for carefully reviewing large portions of this thesis and providing detailed feedback.

To my friends Namita Mistry, Katharine Shelton, Stephanie, Sam, and Seraphina Bakker, Colleen Soo, Chantelle, Mark and Brooks Agbayani, Mary Pham, Lilliana Wong, Natasha Ibrahim, the Italian cohort, and all others who were part of my life for the past five years. The comradery we shared and the fun times we had together kept my spirits lifted, and gave me energy to continue this journey.

To my closest allies and supporters: Domenico Cutrupi and Priya Aucharagram. You have provided me with every kind of support and inspiration imaginable, and I hope my heart-felt gratitude to you goes at least as far as the depth of your love for me. You are bright shining stars in my universe.

Finally, I am profoundly grateful for the unconditional love and support of my parents, Terrence and Pearley Fernando, my brothers Suneth Fernando, Dillan Fernando, and Benedict Fernando, my sister-in-law Jennifer Fernando, and my darling nephews and niece, Ryan, Shannon, Shania, Levi, Luke, Jacob and Joshua. I would not be here without you.

To Margaret Elsie DeSilva, my grandmother, for your courage and strength amidst adversity, and for the life you did not get to live.

CHAPTER 1. INTRODUCTION

1.1 AMYOTROPHIC LATERAL SCLEROSIS (ALS)

ALS is a rapidly progressive, fatal neurodegenerative disease which affects upper and lower motor neurons in the brain, brain stem, and spinal cord, causing muscle weakness and paralysis in patients [1]. Most patients with ALS die within 2-5 years from when symptoms first begin; disease duration can be highly variable however, with some patients surviving for more than 2 decades while others reach terminal stage within months [1]. Apart from disease duration, ALS is characterized by hetereogeneity at almost every level: age of onset, phenotype, genetic background, etiology, and biological mechanisms implicated [2]. These differences point to the highly complex and multisystemic nature of this disease, and will be explored in greater depth in the following paragraphs. In terms of classification, ALS is traditionally divided into two major subtypes. Approximately 90% of ALS is sporadic with no clear genetic linkage, while ~10% of ALS is familial, and is associated with inheritable gene mutations. Clinical onset of symptoms in ALS patients usually occurs in their fifties or sixties, but can occur at all ages. Apart from a higher average age of onset in sporadic ALS cases, the clinical presentation of the two subtypes of ALS is indistinguishable from each other, suggesting that a common pathobiology may underlie both forms.

1.1.1 HISTORY

The earliest reports of ALS date to 1824 when Charles Bell described several patients with a form of motor weakness [3]. However, the first detailed clinicopathological descriptions of ALS are credited to the French neurologist Jean-Martin Charcot. In 1869 he reported the loss of anterior horn motor neurons in patients and hypothesized that this was due to sclerosis in the lateral columns of the spinal cord [4]. These autopsy findings in patients led him to name the disease amyotrophic lateral sclerosis [3]. The level of clinicopathologic description he

achieved was a remarkable feat for the time since the organization of the motor system and its linkage to different anatomical regions had not yet been elucidated.

In 1930, ALS as a disease became widely known in popular culture when Lou Gehrig, an exceptionally talented and renowned major league baseball player, was abruptly struck with a rapidly worsening muscular weakness, eventually leading to the diagnosis of ALS. Gehrig, a beloved sports figure, brought the awareness of many to the devastating aspects of the disease itself, but also to the courage displayed by many in the face of ALS when he gave his retirement speech in 1939 titled “The luckiest man on the face of the earth” [5]. ALS is now colloquially referred to as Lou Gehrig’s disease in North America.

1.1.2 Epidemiology

The worldwide incidence of ALS is approximately 1-2 cases per 100,000 individuals, and the prevalence around 4-6 per 100,000 individuals [6]. There is a slightly higher incidence of ALS among males with sporadic ALS (SALS), but not familial (FALS) [7]. However, this phenomenon could potentially be accounted for by the increased incidence of ALS among smokers and war veterans, and is currently trending towards equality of incidence between genders [7]. There is evidence from population-based studies of variation in ALS incidence according to ethnic background; ALS is less common in mixed race persons in Europe, and in Asian, Hispanic and African American individuals compared to Caucasians in North America [8, 9].

There are also certain geographical hot-spots with high levels of reported ALS cases. For example, the island of Guam, at one time, had almost a hundred fold higher incidence rate of ALS than in the mainland United States, although disease rates have declined steadily since the 1940s [10]. This epidemic was associated with the accidental ingestion of β-methyl-amino-L-alanine by the local Chamorro

population who consumed flying foxes which feed on cycad seeds, a plant containing high concentrations of the neurotoxin [9, 11].

Cigarette smoking, exposure to environmental toxins, high lifetime physical exertion, and active military service have all been linked to higher risk of developing ALS [9]. A retrospective study performed on soccer players from Italian professional leagues identified a higher incidence of ALS among players, particularly in those who have played over 5 years in an active midfield position[9]. The same higher incidence was observed in a group of amateur English soccer players, suggesting that intensive physical exertion poses a risk for developing ALS [9]. However, the etiology and definitive risk factors for most cases of ALS are currently unknown.

1.1.3 Clinical symptoms

Most ALS patients present clinically with spinal onset where symptoms first appear in limbs. Approximately 25% of patients have bulbar (lower brainstem) onset, with accompanying symptoms in jaw/mouth, tongue and facial muscles [7]. A small cohort–5% of all cases–present with trunk or respiratory symptoms [9]. ALS patients typically present with a mixture of upper and lower motor neuron (UMN & LMN) symptoms. UMN symptoms include dysarthria, emotionality, spasticity, and hyperactive reflexes, while LMN symptoms are commonly cramps, decreased reflexes, muscle wasting, and twitching [7]. Muscle weakness is common to both UMN and LMN involvement. In all instances, symptoms spread from the region of onset to other regions in a progressive manner. There is a wide heterogeneity in clinical symptoms even among patients from the same family, presumably carrying the same mutation. This phenomenon is posited to be due to variability in 3 primary factors: rate of progression, body region of onset, and the relative mix of UMN and LMN involvement [4].

1.1.4 Overlap with FTD

Although ALS is mainly a disease of motor neurons, there can be prefrontal and temporal cortex involvement to varying degrees, resulting in cognitive dysfunction and/or frontotemporal lobar dementia (FTLD) [1]. The presence of FTLD with symptoms of ALS is characterized as ALS-FTD, with approximately 15% of patients falling under this category [1]. Indeed, there is significant overlap in clinical, pathological and genetic characteristics between ALS and FTD, leading many to recognize that the two diseases lie on opposite ends of a spectrum encompassing a single disease [1, 12]. The current consensus in the field is that these two neurodegenerative diseases are linked, and that findings in one research area should also be tested and potentially applied in the other [13].

1.1.5 Diagnosis and therapy

There is currently no diagnostic test available for ALS, and clinical examination remains the main method of disease diagnosis. One significant challenge in diagnosis is that clinical symptoms of ALS overlap considerably with a variety of conditions such as cervical spondylosis, myopathies, neuropathies, inclusion body myositis, myasthenia gravis, and multiple sclerosis, as well as infections such as Lyme's disease and HIV, among many others [7]. Therefore, disease diagnosis involves a process of elimination of other conditions which could mimic ALS. Misdiagnoses are common, with ~10% of false diagnosis of ALS when the condition is in fact a mimic, resulting in delays in obtaining correct treatment and care [7]. Identification of reliable biomarkers for disease diagnosis and monitoring would reduce the time from symptom onset to diagnosis, and is therefore imperative.

There is currently no cure for ALS, and the only FDA-approved intervention is Riluzole, a drug which extends the lifespan of patients by approximately 3 months [6]. ALS therapy is primarily aimed at halting disease progression and the palliative care of patients [7]. Non-invasive ventilation, for example, is used to alleviate worsening respiratory symptoms in patients, and studies have shown a slight

extension of survival with the addition of ventilation to the care program [7]. Other means of caring for patients include provision of a support team, the preparation of food that is easy to swallow, and medications for weakness, muscle spasticity, sleep, and depression, as well as end-of-life or hospice care. Although these interventions can provide temporary relief and comfort for patients, the ultimate goal of ALS treatment remains a means to halt progression of disease.

1.1.6 Prognosis

50% of all ALS patients usually die within 30 months from when symptoms first appear, and only 20% of patients survive over 5 years [9]. As the disease progresses, fatigue, weakness, dysphagia, malnutrition, and weight loss are common, with the latter two being linked to poor prognosis [9]. At end stage, patients usually die from respiratory failure due to progressively weakening respiratory muscles, a condition which can be accelerated by pneumonia [9]. Early respiratory involvement, older age of onset, and bulbar-onset are associated with poorer prognosis, while predominantly LMN subtypes of ALS such as progressive muscular atrophy and flail-limb variant ALS are associated with slower progression and better prognosis [9].

1.1.7 Genetics

Knowledge regarding the underlying genetic cause of ALS has rapidly advanced in recent decades. As mentioned previously, 10% of all ALS cases have a known genetic association, with patients having at least one affected family member or relative. The majority of FALS cases are inherited autosomal dominantly with high penetrance, but there are cases of autosomal recessive and X-linked inherited mutations as well [14]. The distinction between familial and sporadic ALS is not as clear-cut as one would assume. For example, there is accumulating evidence from twin and family studies that apparently sporadic cases of ALS may have a genetic component as well [15]. FALS cases are also often misclassified as SALS because

of reduced penetrance, low numbers of offspring making the genetic linkage unclear, incomplete family information, phenotypic variability, and non-paternity events [2]. Therefore, it may be misleading to assume that all, or even most, cases of SALS have no genetic association.

There are over 50 ALS-associated genes identified in literature to date. However, proving the causality of these variants in disease is difficult, and only a few are unambiguously linked to the pathogenesis of ALS. Of these, the major players are outlined below:

SOD1

Mutations in the gene encoding Cu/Zn superoxide dismutase 1 (SOD1) were the first genetic mutations to be identified in ALS patients, and account for 20% of all FALS cases and ~1-4% of SALS [6]. To date, over 180 different mutations spanning all 5 exons in the SOD1 gene have been identified in ALS patients [16]. Almost all SOD1 mutations are inherited in an autosomal dominant fashion, although the D90A mutation found in Scandinavian populations is recessive for unidentified reasons [1]. The most common SOD1 mutation found in the United States is the Ala4Val (A4V) mutation, which accounts for ~50% of SOD1-positive FALS, and is associated with a very rapidly progressive form of the disease[13]. The majority of SOD1 mutations are missense mutations, suggesting that most of the molecule must be present for its pathogenic effect. However, a small cohort of truncation mutations at the C-terminal of the protein, such as the G127X mutation, have also been identified in patients [17].

TDP-43 & FUS

Tar DNA binding protein (TDP-43) and fused in sarcoma (FUS) were first discovered in mass spectrometry studies attempting to identify the major protein components of the pathological inclusions found in ALS patients. Mutations in these genes each cause 4-5% of FALS [18]. TDP-43 is an RNA-binding protein that shuttles between the nucleus and the cytoplasm in its wild-type state, and is involved in an array of

RNA-related processes including transcription, RNA maturation, and the processing of miRNAs [9].TDP-43 protein is found within inclusions in SOD1-negative ALS, renamed ALS-TDP, as well as most cases of FTD. Over 40 different mutations in the TARDBP gene have been thus far identified in SALS and FALS patients [19]. Like TDP-43, FUS is an RNA-binding protein whose gene is located on chromosome 16, and share similar functions and properties.

C9ORF72

Two landmark studies published in 2011 identified that mutations in a region of chromosome 9 open reading frame 72 (C9ORF72) were linked to both ALS and FTD [20, 21]. Hexanucleotide repeat expansions in the C9ORF72 gene are now known to account for over 30% of FALS and 10% of SALS, making it the largest contributing mutation in ALS discovered to date [22]. Expansions in ALS patients can reach upto hundreds of copies and present clinically with an FTD/ALS phenotype as well as TDP-43-positive inclusion pathology [23]. The exact mechanism by which C9ORF72 mutations lead to disease is thus far unknown, but observations point to a toxic gain-of-function possibly in a pathway affecting RNA processing [23].

Others

The remainder of FALS are due to mutations in ubiquilin 2 (UBQLN2), optineurin (OPTN), angiogensin (ANG), senataxin (SETX), alsin, Sequestosome 1 (SQSTM1) vesicle associated membrane protein associated protein B (VAPB), charged multivesicular body protein 2B (CHMPB2), and spasticin, among others [6]. For an updated list of gene mutations involved in ALS, please refer to Appendix 1. Interestingly, C9ORF72 and several other ALS-associated mutations such as CHMPB2 and VAPB, encode proteins linked to vesicle trafficking, intimating that this pathway may play an important role in the pathogenesis of ALS [24-26].

1.1.8 NEUROPATHOLOGY

Autopsies of ALS patients reveal degeneration of motor neurons in the motor cortex, brain stem, and anterior horns of the spinal cord [14]. The neuropathology of ALS is characterized by the presence of ubiquitinated inclusions in the cytoplasm of affected motor neurons and surrounding oligodendrocytes [27]. These inclusions consist of one or more aggregated proteins encoded by ALS-associated genes such as TDP-43, FUS, SOD1, SQSTM1, and UBQLN2. The fact that these protein components are also found in the inclusions of SALS patients make a compelling case for both forms of ALS being linked at the pathological level.

Ubiquitinated and hyperphosphorylated TDP-43 protein is found within inclusions in almost all ALS cases investigated, with the notable exception of cases with FUS or SOD1 mutations [14]. TDP-43 aggregates form skein-like inclusions, and are located near stress granules in the cytosol of neural and glial cells of the anterior horn [13]. In its wild-type state, TDP-43 is known to shuttle between the cytoplasm and the nucleus, but in disease it's found primarily localized to the cytosol with corresponding nuclear depletion [28].

FUS, which is structurally and functionally similar to TDP-43, is also found mislocalized to the cytoplasm in disease. Post-mortem analysis of tissue from ALS patients with FUS mutations shows severe loss of motor neurons in the spinal cord and brain stem, and mild to moderate loss of UMNs of the motor cortex [13]. Immunohistochemical studies show that nuclear levels of FUS are normal in most parts of the CNS, but that spinal cord motor neurons and dystrophic neurites contain large globular or elongated inclusions [13]. However, FUS-specific pathology seems to be rarer than TDP-43 in ALS cases overall [13]. Interestingly, the characteristic ubiquitin and p62 positive inclusions, as well as TDP-43 inclusions, are rarely seen in patients with FUS mutations [13].

Certain neuropathological features in ALS are associated with specific gene mutations. For example, ALS cases with TDP-43 mutations display neuropathology

with gliosis, motor neuron degeneration, pallor of corticospinal tracts, and the presence of Bunina bodies in the anterior horns of the spinal cord [13]. In addition to UMN and LMNs, TDP-43 positive inclusions are also found in other regions of the CNS such as the frontal and temporal cortex in affected individuals [13]. In ALS patients with SOD1 mutations, there is a loss of anterior horn motor neurons with accompanying skein-like or rounded inclusions immunopositive for ubiquitin and p62 and negative for TDP-43 [13]. ALS caused by C9ORF72 mutations is accompanied by intranuclear RNA foci and cytoplasmic inclusions of the protein sequestosome-1 (encoded by SQSTM1), and are distinct from TDP-43 inclusions [14]. Misfolded forms of SOD1 protein has been identified in some immunohistochemical analyses of post-mortem tissues from both sporadic and familial ALS patients **(Figure 1.1)** [29]. However, this finding is subject to some controversy as not all research groups have found results consistent with this finding [30].

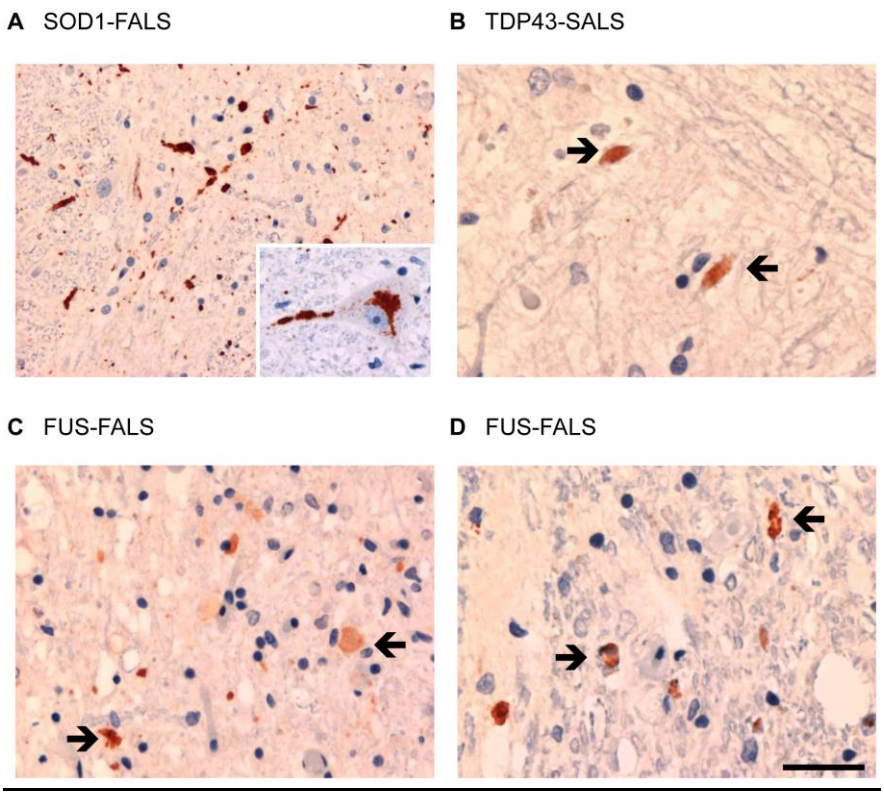

Figure 1.1 Misfolded SOD1 in ventral grey matter and corticospinal tracts of ALS patient cervical spinal cord.

A. Cases of SOD1 gene mutation-positive FALS show accumulation of misfolded SOD1 in axons and in perikarya of some lower motor neurons (inset). **B.** SALS with TDP-43 pathology had accumulation of misfolded SOD1 in a small number of axons with a normal appearance (arrows). **C,D.** Cases of FALS with FUS mutations show aggregates of misfolded SOD1 in swollen axons within the ventral grey matter (**C.** arrows), and within a number of axons with a normal appearance within the corticospinal tract (**D,** arrows). Scale bar, 60 µm (**A,C**); 30 µm (**B,D**)
Figure and caption reproduced from Pokrishevsky E, *et al.* Aberrant Localization of FUS and TDP43 Is Associated with Misfolding of SOD1 in Amyotrophic Lateral Sclerosis. *PLoS One 7.*

1.1.9 Biological mechanisms implicated

Multiple cellular mechanisms have been implicated in ALS disease pathogenesis. One of the major challenges is to elucidate the convergence point of these pathways to cause neurodegeneration. Many now believe that ALS is primarily a disease caused by the loss of protein homeostasis, or proteostasis, leading to cell stress and ultimately death. The other major biological mechanisms implicated in ALS include glutamate excitoxicity, endoplasmic reticulum (ER) stress, dysfunctional autophagy, and mitochondrial stress, some of which are explored in greater depth below.

Glutamate Excitotoxicity

Several lines of evidence, garnered from animal models and patients, indicate that glutamate-induced excitotoxicity may be an initiating event in the pathogenesis of ALS. Glutamate is the main excitatory neurotransmitter in the central nervous system (CNS), and binds to N-methyl-D-aspartate (NMDA) and (-amino-3-hydroxy-5-methyl-4-isoxazoleproprionic acid (AMPA) receptors at the post-synaptic membrane [31]. Excessive activation or overstimulation of these receptors can cause neuronal death through Ca^{+2}-mediated pathways. Insufficient clearance of glutamate from the synaptic cleft, as well as increased release, can cause excitotoxicity [32]. Re-uptake of glutamate is primarily facilitated by the glutamate transporter EAAT2/GLT-1 which is highly expressed in astrocytes [32].

The only available ALS therapeutic, Riluzole, is thought to act by blocking NMDA receptors and inhibiting the action of glutamate, although the exact mechanism of drug action is not known [32]. Motor neurons have also been shown to be especially

susceptible to excitotoxicity. Injection of AMPA-receptor agonists into the intrathecal or intraspinal areas causes selective motor neuron loss in several different animal models, an effect which is not recapitulated by NMDA agonists [33-36]. The same finding of selective motor neuron loss was observed in cell culture models treated with AMPA agonists, but not NMDA [36]

Autophagy

Autophagy is one of two conserved cellular pathways for degrading unwanted or dysfunctional cell components. Although an important process in all cells, autophagy is especially crucial in post-mitotic cells such as neurons where dilution of abnormally folded proteins or dysfunctional organelles by cell division is not possible [37]. Synaptic plasticity, anti-inflammatory function of glial cells, myelination, and maintenance of neuronal homeostasis all require autophagy [38, 39]. Unsurprisingly, defective autophagy is implicated in the pathogenesis of several neurodegenerative diseases such as Parkinson's, Alzheimer's, and Huntington's disease [40].

There is also accumulating evidence for a role of autophagy in ALS, and among the molecular mechanisms implicated in the pathogenesis of ALS dysregulation of autophagy is emerging as an early and pivotal event [41]. A post-mortem immunohistochemical study on spinal cords from SALS patients showed an increased number of autophagosomes in close association with characteristic protein inclusions in all samples investigated [42]. ALS mouse models transgenic for SOD1 mutations also displayed enhanced autophagosome formation by immunoassay [43, 44]. However, the overall impact of autophagy induction on ALS disease course is subject to some controversy. Studies show conflicting results as some report beneficial clearance of mutant SOD1 and TDP-43 by induction of autophagy [4, 45], while others show a more pathological role with decreased survival of mutant SOD1 mice treated with rapamycin, an inducer of autophagy [46, 47]. Regardless of whether its induction is protective or pathological, all reports agree that autophagy is dysregulated in ALS.

Dysfunctional Proteostasis

Approximately 30% of newly synthesized proteins are misfolded, indicating the need for continuous protein quality control in the cell [48, 49]. In the event of an overload of aberrantly folded proteins within a cell, the unfolded protein response (UPR) acts to restore protein homeostasis by modulating ER function. Three transmembrane ER-resident proteins, protein-kinase RNA like ER kinase (PERK), inositol-requiring enzyme 1 (IRE1), and activating transcription factor 6 (ATF6) work together to orchestrate the UPR. If ER-stress remains unresolved for an extended time period, pro-apoptotic factors are upregulated, leading to initiation of apoptotic cell death.

The UPR is increasingly implicated in the pathogenesis of almost all neurodegenerative diseases. Many disease-associated proteins are inherently prone to misfolding, and often polymerize to form aggregates which can be further compacted into inclusion bodies [50]. Although proteins within an inclusion body are prevented from de-constructing to form oligomers and fibrils, species which are identified to be more toxic to cells, these proteins are also prevented from executing their normal function which can also cause cellular stress and death [50]. There is histological evidence of UPR activation in post-mortem tissues from patients with Alzheimer's disease (AD), Parkinson's disease (PD), tauopathies, frontotemporal dementia, as well as ALS [50].

1.1.10 ALS AS A PROTEIN MISFOLDING DISORDER THAT SPREADS IN A PRION-LIKE MANNER

Correctly functioning proteins are crucial to the health of cells and the organism as whole. The 3-dimensional structure of a protein, governed by its amino acid sequence, determines its function. The folding of proteins into the correct 3-dimensional conformation, assisted by molecular chaperons, and the removal of misfolded proteins from the cell are both strictly regulated processes that ensure

homeostasis within the cell. Accumulating evidence suggests that neurodegenerative diseases such as ALS, AD, PD, Huntington's disease (HD), transmissible spongiform encephalopathies (TSEs) such as prion disease, and spinocerebellar ataxia share in common the underlying molecular signature of being protein misfolding disorders [51]. A hallmark of the mentioned neurodegenerative diseases is the presence of aggregated proteins that accumulate in tissues as inclusion bodies or concentrated deposits of protein. Aggregated proteins are often β-sheet rich in structure, and are termed amyloids. However, the proteins within the inclusion bodies show disease-specificity, differing from one disease to the other.

In ALS, there is a consensus among neurologists that the disease has a focal clinical onset [4, 52]. Clinical observations and neuropathological studies together demonstrate a radial gradient of involvement from a focal site, and provide evidence of disease spread via contiguous anatomical regions in a non-random manner, or spread from one side of the body to the contralateral side. **(Figure 1.2)** [4, 52]. These reports suggest that ALS pathology begins focally and spreads sequentially through the neuroaxis, consistent with a prion-like mechanism of systematic disease transmission.

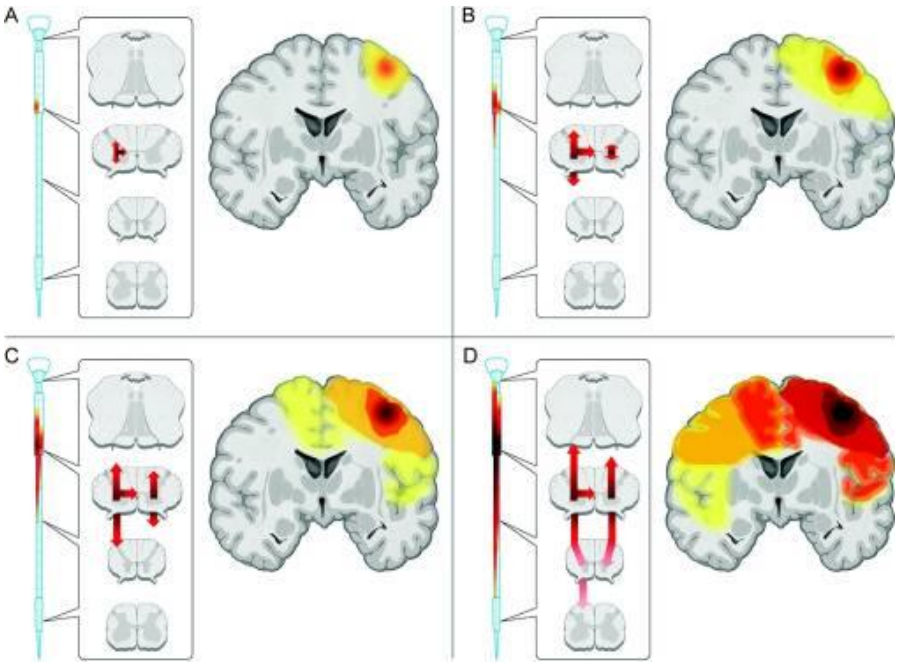

Figure 1.2 A model of the focality and contiguous spread of pathology in ALS

A. At clinical onset, degeneration involves upper motor neurons (UMNs) and lower motor neurons (LMNs) that innervate the same peripheral body region **B.** As the disease process spreads neuroanatomically through UMN and LMN levels, clinical manifestations become complex **C.** For LMN, the ALS disease process continues to spread rostral-caudal. Neurodegeneration may have preferential caudal spread or "directionality". For UMN, however, the ALS disease process continues to spread medial-lateral and more quickly begins to appear as diffuse. **D.** Advanced spread: Ultimately, degeneration appears to be diffuse and symmetric through temporal-spatial summation within and between UMN and LMN levels.

Figure and modified caption reproduced with permission from Ravits JM, La Spada AR. 2009. ALS motor phenotype heterogeneity, focality, and spread: deconstructing motor neuron degeneration. *Neurology* 73: 805-11.

As mentioned previously, the inclusions in ALS patients consist of multiple proteins, the major components being TDP-43, FUS, and/or SOD1 **(Section 1.1.8, page 8)**. Several lines of evidence strongly implicate cell-to-cell transmission of these proteins in the inception and spread of disease pathology, similar to how infectious prions replicate in TSEs. In TSEs, or prion diseases, an abnormal 3-dimensional conformation of the normal prion protein (PrP^{C}) is generated, and is termed Scrapie prions (PrP^{Sc}). PrP^{Sc} can template the conversion of normal PrP^{C} into a misfolded conformation similar to its own, and recruit it into a pathological aggregate. This mechanism is then spread from cell to cell, and/or organism to organism. A prion-like

self-propagation mechanism has been described for several disease-associated proteins such as α-synuclein, amyloid-β, tau, huntingtin with polyQ repeats, TDP-43, and SOD1 [45, 53-55]. This mechanism is termed “prion-like” in all neurodegenerative diseases apart from TSEs because infectivity between organisms has not been demonstrated in these diseases.

In studies investigating the prion-like capacity of TDP-43 and SOD1 proteins, minute amounts of protein aggregates or synthetic fibrils were sufficient to template the conversion of their normally-folded counterparts into an aggregated or misfolded conformation, indicating that it is a robust phenomenon [54, 56-58]. Over two decades of research has been conducted on SOD1 involvement in ALS since the first identification of SOD1 gene mutations in FALS patients in 1993 [59]. A number of biological processes implicated in ALS such as proteostasis impairment, ER and mitochondrial stress, and glutamate excitotoxicity have also been linked to mutant SOD1 [52]. Importantly, mice transgenic for FALS-associated SOD1 mutations faithfully recapitulate several symptoms observed in patients including adult-onset degeneration of motor neurons in the brain and spinal cord [60, 61]. These converging points strongly implicate SOD1 in both the etiology and transmission of ALS, and are explored in greater detail in the proceeding sections.

1.2 SUPEROXIDE DISMUTASE (SOD1)

1.2.1 STRUCTURE AND FUNCTION OF THE SOD1 PROTEIN

SOD1 is a 32 KDa, highly conserved, soluble cytosolic protein which is ubiquitously expressed in the body. SOD1 belongs to the superoxide dismutase (SOD) family of enzymes, and is one of 3 different isoforms that exist in mammalian cells, the other two being SOD2 (a mitochondrial-specific isoenzyme), and SOD3 which mainly exists in the extracellular space [62]. The most commonly described function of SOD1, as well the other superoxide dismutase family members, is to catalyze the

conversion of superoxide anions (O_2^-) to hydrogen peroxide and oxygen via the following reaction:

$$SOD1 - Cu^{2+} + O_2^{\bullet -} \rightarrow SOD1 - Cu^{+} + O_2$$

$$SOD1 - Cu^{+} + O_2^{\bullet -} + 2H^{+} \rightarrow SOD1 - Cu^{2+} + H_2O_2$$

$$O_2^{\bullet -} + O_2^{\bullet -} + 2H^{+} \rightarrow O_2 + H_2O_2$$

Superoxide is formed as a by-product in a number of processes including cellular respiration and oxidative bursts in neutrophils and other immune cells. The SODs are thus the cellular first-defence against damage by reactive oxygen species (ROS) such as superoxide. They, along with other non-enzymatic ROS scavengers such as Vitamins A,C and E work to maintain homeostasis between ROS production and clearance. The loss of redox balance within the cell leads to oxidative stress, a condition characterized by high levels of ROS and low levels of antioxidant defence, and eventually, cellular damage and death. Although it is most well-characterized as an antioxidant enzyme, a study in yeast found that less than 1% of total SOD1 is needed to carry out this function, indicating that SOD1 may have other equally important and yet unknown functions [63, 64]. Other proposed functions of SOD1 include a zinc-sensor causing ER activation under conditions of zinc-depletion, transcription factor, RNA-binding protein, signaling molecule, and a mediator of autophagy since SOD1 was found to co-precipitate with Beclin-1, an important autophagy activator [64].

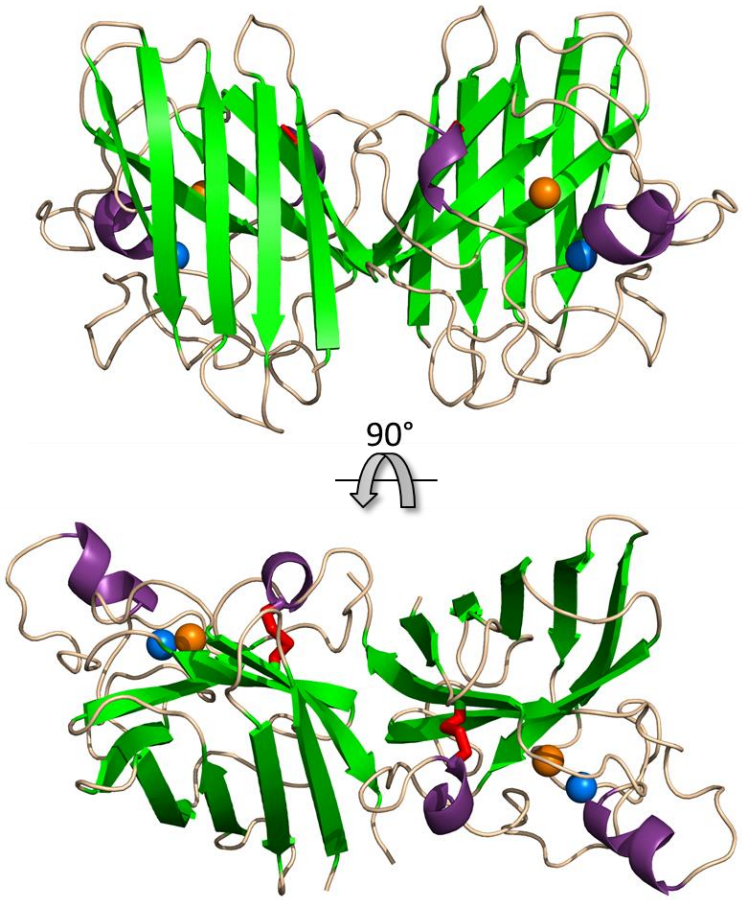

Figure 1.3 3D-ribbon representation of the human SOD1 protein.

SOD1 exists as a homodimer composed of two monomer subunits. 8 β-sheets (green) in each monomer form a barrel conformation when visualized from top-down, α-helices are depicted purple, Cu atom in orange, and Zn in blue. The electrostatic loops can be seen in beige and the disulfide bridge in red. (PDB Code: 1HL5, modelled with The PyMOL Molecular Graphics System, Version 1.8 Schrödinger, LLC.)

The SOD1 gene is located on chromosome 21 and is comprised of 4 introns and 5 exons encoding a 153 amino acid protein. The SOD1 protein normally exists as a homodimer with each subunit containing 8 anti-parallel β-sheets and 4 α-helices connected by 7 loops **(Figure 1.3).** The encoded metalloenzyme binds a copper and zinc atom on each monomer [65]. Fully metallated SOD1 is found to be extremely stable even in highly denaturing conditions, a property that is attributed to an intra-subunit disulfide bond between cysteine residues 57 and 146 on each dimer subunit formed through the coordination of its Cu and Zn ions (**Figure 1.3;red**) [65]. The Zn atom also has a highly stabilizing effect on the molecule, more so than the Cu atom,

since it holds the active site of the enzyme in place [66]. Zn-binding also lowers the free energy of the unfolded SOD1 monomer, driving it towards a folded state [67]. Meanwhile, the Cu atom is mainly required for SOD1 enzymatic activity as redox states of Cu^{+} and Cu^{+2} work to accept and donate electrons from the O-• superoxide anion; indeed, all SOD1 activity is lost when the Cu atom is removed [68].

1.2.2 SOD1 IN ALS

SOD1 is highly abundant in the CNS, comprising 1-2% of the total soluble protein [64]. Over 180 different SOD1 gene mutations have been identified to date in ALS patients [16]. It's been reported that upto 75 of the 153 amino acids in SOD1 are found mutated in ALS; the majority of these are missense point mutations scattered at positions spanning all 5 exons of the gene [64]. Although different SOD1 mutations have varying levels of antioxidant activity there appears to be no correlation between its activity and onset or progression of disease [69]. ALS-like symptoms in SOD1 mutant mouse models is also shown to be driven by an acquired toxicity of the mutant protein since overexpression of the mutant transgene causes motor neuron degeneration and paralysis, but not knockdown [14, 60]. Therefore, rather than a loss of enzymatic activity, mutant SOD1 seems to acquire a gain of toxic function in ALS. However, despite over 23 years of research, the exact causes of SOD1 toxicity in ALS are unknown. Instead, an abundance of potential toxic mechanisms have been proposed.

One such mechanism is the adoption of misfolded 3-dimensional protein conformations. SOD1 protein is shown to be highly sensitive to cellular stress, and undergoes conformational changes leading to aggregation when exposed to stress conditions *in vitro* [44]. Mutations in the SOD1 gene also make the protein more likely to misfold and aggregate within inclusions. Multiple groups have shown that misfolded and aggregated mutant SOD1 is specifically toxic to motor neurons [70-72]. Interestingly, wild-type SOD1 (WtSOD1) with no identified mutation has also been shown to misfold when metal-depleted or oxidized, and is toxic when

exogenously applied to cells [73-77]. Misfolded SOD1 protein has been found within inclusions in FALS patients. Some groups have detected misfolded SOD1 in SALS cases [29, 78], although this finding is not one of consensus [30, 79]. Thus, misfolded SOD1 protein is potentially a common mechanistic link in both SALS and FALS.

1.2.3 SOD1 MOUSE MODELS OF ALS

To date, over 15 different rodent models of ALS transgenic for SOD1 mutants, most of which are murine, have been generated and characterized in the literature [61, 80, 81]. Many of these models faithfully recapitulate aspects of the ALS phenotype such as older age of onset, sequential spread of pathology through the CNS, progressive worsening of motor symptoms, gliosis in CNS tissues, and specific degeneration of motor neurons [81]. Often, these models transgenically express FALS-associated SOD1 mutations rather than a deletion of the SOD1 gene. Indeed, SOD1 knockout mice are reported to develop normally without any symptoms of motor neuron dysfunction, often taken as evidence for a SOD1 toxic gain-of-function being involved in ALS pathobiology [81].

$SOD1^{G93A}$ transgenic mice are one of the most widely used *in vivo* ALS models, and several lines of these mice were initially developed. In this work we will be referring to the high copy number strain B6SJL-TgN(SOD1-G93A)1Gur (Jackson Laboratory, ME), originally characterized by Chiu *et al.*, as $SOD1^{G93A}$ [82]. Clinical disease occurs at around 3 months in these mice, with accompanying tremors in limbs, and paralysis and death ensues by ~136 days of age **(Figure 1.4)** [82]. Pathological changes are reported to begin only by day 37 [82].

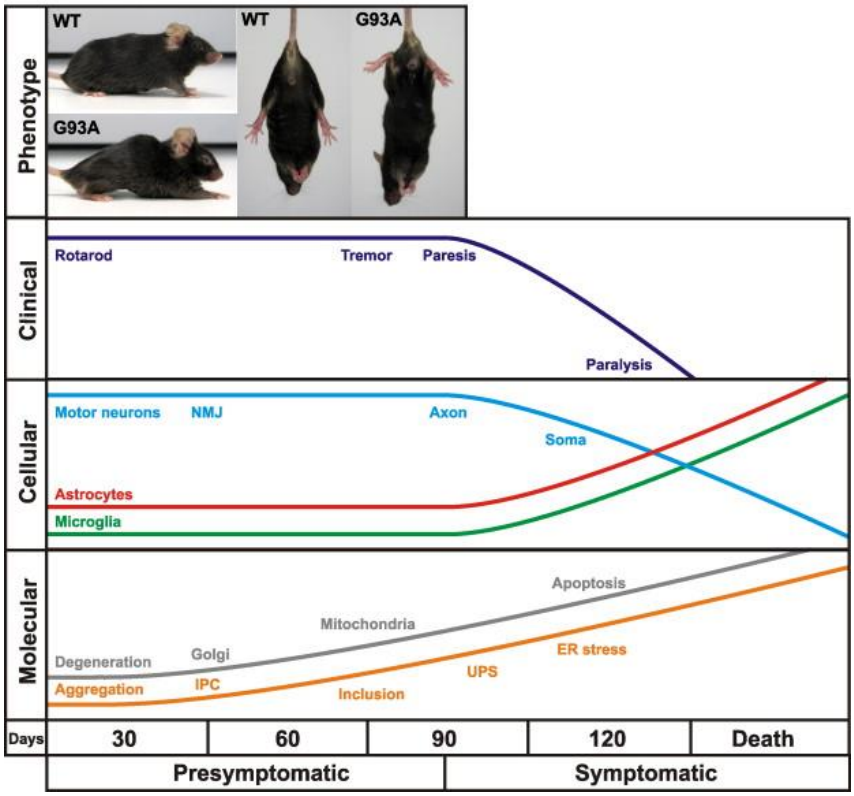

Figure 1.4 Time course of pathobiological events in SOD1^{G93A} transgenic mice

SOD1^{G93A} mice develop motor weakness, hindlimb tremor, and locomotor dysfunction shortly after 3 months of age. Degeneration of axons and distal synapses are observed at the cellular level. At 4 months of age, disease in SOD1^{G93A} mice have progressed to fatal paralysis with accompanying spinal and motor neuron loss and gliosis. Molecular events that potentially underlie pathology are also depicted.
Figure reproduced with permission from Turner BJ, Talbot K. 2008. Transgenics, toxicity and therapeutics in rodent models of mutant SOD1-mediated familial ALS. Prog Neurobiol 85: 94-134 [81].

Other transgenic mutant SOD1 mice express the FALS associated mutations A4V, D90A, G37R, G85R, and G86R, among others [81]. However, these mice do not develop disease at the same speed or to the same extent as do SOD1^{G93A} mice. Transgenic mice expressing C-terminal truncated FALS-associated SOD1 mutants such as SOD1^{G127X} have also been developed [56]. Homozygous SOD1^{G127X} mice of line 716 develop disease at approximately 5 months of age, and paralysis and death at ~8 months [56]. Disease phenotype in SOD1^{G127X} mice appears with foreleg onset, and differs slightly from SOD1^{G93A} mice who develop hind-leg symptoms first [56]. Mice transgenic for truncation mutants such as SOD1^{G127X} also display

disruption of the SOD1 intramolecular disulfide bond at Cys-57 and Cys-146, resulting in less stable forms of the SOD1 protein being expressed [81].

1.2.4 PRION-LIKE PROPERTIES OF SOD1 PROTEIN

Using *in vitro* and cell culture systems, Grad *et al.* have shown that mutant SOD1 has the capability to convert human wild-type SOD1 (HuWTSOD1) into a misfolded conformation, and the subsequent spreading of SOD1 misfolding from cell culture to cell culture successively [83, 84]. Moreover, two studies have shown that HuWTSOD1 induced to misfold by TDP43 also acquires a prion-like property of intercellular transmission [29, 85]. Indeed, the number of *in vitro* studies implicating misfolded SOD1 as the toxic agent which is spread in a prion-like manner in ALS is growing [73, 84, 86-89].

More recently, Ayers *et al.* provided the first *in vivo* demonstration of SOD1 transmissibility by injecting brain homogenates from diseased $SOD1^{G93A}$ transgenic mice into mice transgenic for a GFP-tagged version of G85R ($SOD1^{G85R\text{-}GFP}$) [86]. $SOD1^{G85R}$ mice normally never develop disease phenotype during its lifetime, but injection of $SOD1^{G93A}$ brain homogenates caused ALS-like symptoms and death in the recipient $SOD1^{G85R\text{-}GFP}$ mice within a time-frame of months [86]. Together, these reports demonstrate that there is solid rationale for treating SOD1 as a potential culprit in the spread of neurodegenerative pathology and clinical symptoms in ALS patients. However, the mechanism(s) via which this process occurs are uncertain. We hypothesize that a systemic transfer of mutant misfolded SOD1 occurs from cell to cell in ALS, and that it may be mediated by small cell-secreted vesicles termed extracellular vesicles.

1.3 EXTRACELLULAR VESICLES

Extracellular vesicles (EVs) are increasingly implicated in the disease progression of a variety of conditions including cancer and neurodegenerative diseases. Indeed, many have speculated that the involvement of EVs in disease spread is a mechanism common to both cancer and neurodegenerative disease [90]. Better understanding the role that EVs play in the CNS in both normal physiology and in disease has important implications for understanding the biological underpinning of neurodegenerative diseases, for identifying relevant and specific biomarkers, and for designing effective therapeutic interventions.

1.3.1 DEFINITION

Exosomes

Exosomes are a subtype of EVs, and are small, secreted vesicles ranging from ~50-150 nm which originate in the endosome. Exosomes are formed in the late endosome with the inward budding of the endosomal membrane to form intra-organelle vesicles termed intraluminal vesicles (ILVs) **(Figure 1.5)**. The structure containing ILVs is termed the multivesicular body (MVB), and the fusion of the MVB with the cell plasma membrane results in the exocytosis of the ILVs as exosomes **(Figure 1.5)**. Numerous studies have confirmed that exosomes are secreted from a wide variety of cultured cells including neurons, epithelial cells, immune cell types, and tumour cells, and it is hypothesized that they are secreted from all cells [91] The presence of exosomes in bodily fluids such as urine, blood, plasma, cerebrospinal fluid, and semen, among others, demonstrate that exosomes are also secreted *in-vivo*.

The term “exosome” was first coined in 1987 when Johnstone and colleagues published work on the recycling of transferrin receptor from maturing reticulocytes [92]. Following on the idea that vesicles were merely a mode of clearing unnecessary or toxic components from the cell, work in the field continued without much commotion for the next decade. Interest in these small vesicles was only re-

ignited in the late 1990s when two groups published intriguing work demonstrating a role for exosomes in intercellular communication [93, 94]. In 1996, Raposo *et. al* showed that B cells transformed with Epstein-Barr virus secreted exosomes containing major histocompatibility complex (MHC) class II molecules, and were capable of inducing specific CD4 positive T-cell clones [91, 93]. Their findings suggested that exosomes were acting as vehicles to transfer MHC class-II between cells and induce an immune response.

A second major period of breakthrough in the field came in 2007 when it was discovered that exosomes carry nucleic acids such as miRNA and mRNA, and transfer genetic information between cells [95]. Valadi *et al.* found that exosomes isolated from murine and human mast cells contained functional RNA material which was capable of being translated into proteins, and that human mast cells treated with murine mast cell-derived exosomes caused the production of novel murine proteins not previously present in the human cells [95]. Thus, the data suggested that the transferred nucleic material was capable of being translated within the recipient cells, and could alter gene expression in cells. This finding sparked the imagination of researchers to consider novel functions for exosomes, and heralded the beginning of research into these small vesicles in earnest.

Microvesicles

Extracellular vesicles which directly bud off from the plasma membrane are referred to as microvesicles **(Figure 1.5)**, and are known to be more heterogeneous in size distribution than are exosomes. Microvesicles can be as large as 2 μm in diameter, or as small as exosomes at ~50 nm. Relative to exosomes, microvesicles have not been extensively characterized in literature, and their mechanisms of biogenesis and cargo loading are unclear [96]. Inability to discriminate between exosomes and microvesicles, and inconsistencies in the use of nomenclature that exist within the EV field, have also resulted in difficulties identifying the exact vesicle type authors refer to in their studies [97, 98]. Since many preparations contain mixtures of exosomes and microvesicles, they are often referred to collectively as EVs. The

protein content of microvesicles is also found to overlap with exosomes, making it difficult to distinguish between the two subpopulations [96].

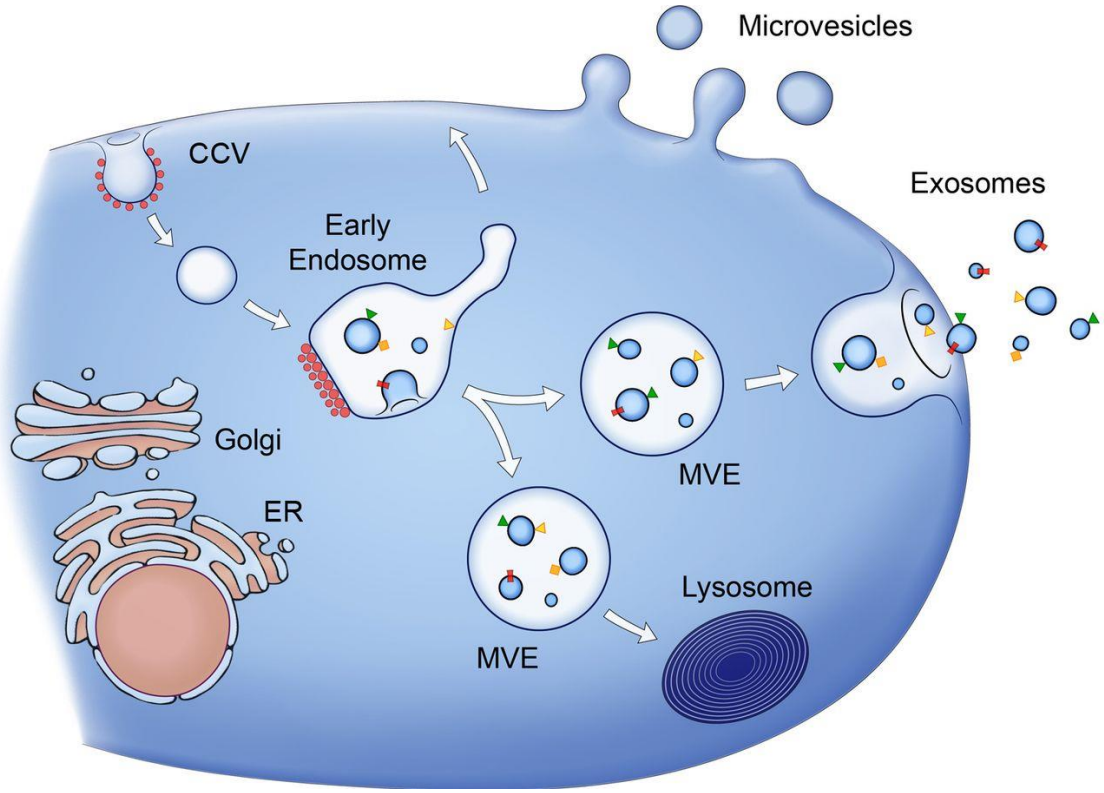

Figure 1.5 Biogenesis and secretion of exosomes and microvesicles.

The exosome biogenesis pathway begins at the early endosome with the formation of invaginations in the endosomal membrane to form intraluminal vesicles (ILVs). Protein and nucleic acid cargo (coloured arrows) are sorted into ILVs, and they mature within the endosome which is now termed the multivesicular endosome (MVE). The MVE can fuse with the lysosome for degradation of constituents, or with the plasma membrane for secretion of ILVs into the extracellular space as exosomes. Conversely, microvesicles bud directly from the plasma membrane.

Figure reproduced with permission from Raposo G, Stoorvogel W. 2013. Extracellular vesicles: exosomes, microvesicles, and friends. *The Journal of cell biology* 200: 373-83

1.3.2 Biochemical & physical features

Morphology

Exosomes and microvesicles can most readily be visualized by transmission electron microscopy (TEM) due to their nanometer size scale, and TEM is the most frequently used technique to observe the size and morphology of extracellular

vesicles. Under TEM, vesicles display a cup-shaped morphology when stained by uranyl acetate and whole-mounted onto grids **(Figure 1.6)**. However, this feature is known to be an artefact of the protocol where fixation causes shrinkage of membrane-enclosed subcellular structures. In fact, extracellular vesicles have a round shape when visualized using cryo electron microscopy (EM) **(Figure 1.6)**, a technique which prevents shrinkage and better preserves physiological shape.

Size

When quantitated, EM studies show that vesicles from biological fluids and supernatants of cell cultures with dying cells are heterogeneous in size distribution, while in comparison, vesicles from homogenous healthy cell cultures show a more uniform size distribution of ~30-150nm [91]. Similarly, microvesicle pellets show a more heterogeneous size distribution than do exosomes in published studies [91]. More recently, a technique called Nanoparticle tracking analysis (NTA) has been used widely in the field to characterize the size distribution of vesicles in a population. NTA tracks the Brownian motion of individual particles in a suspension and uses the Stokes-Einstein equation to convert its motion to size and concentration of particles.

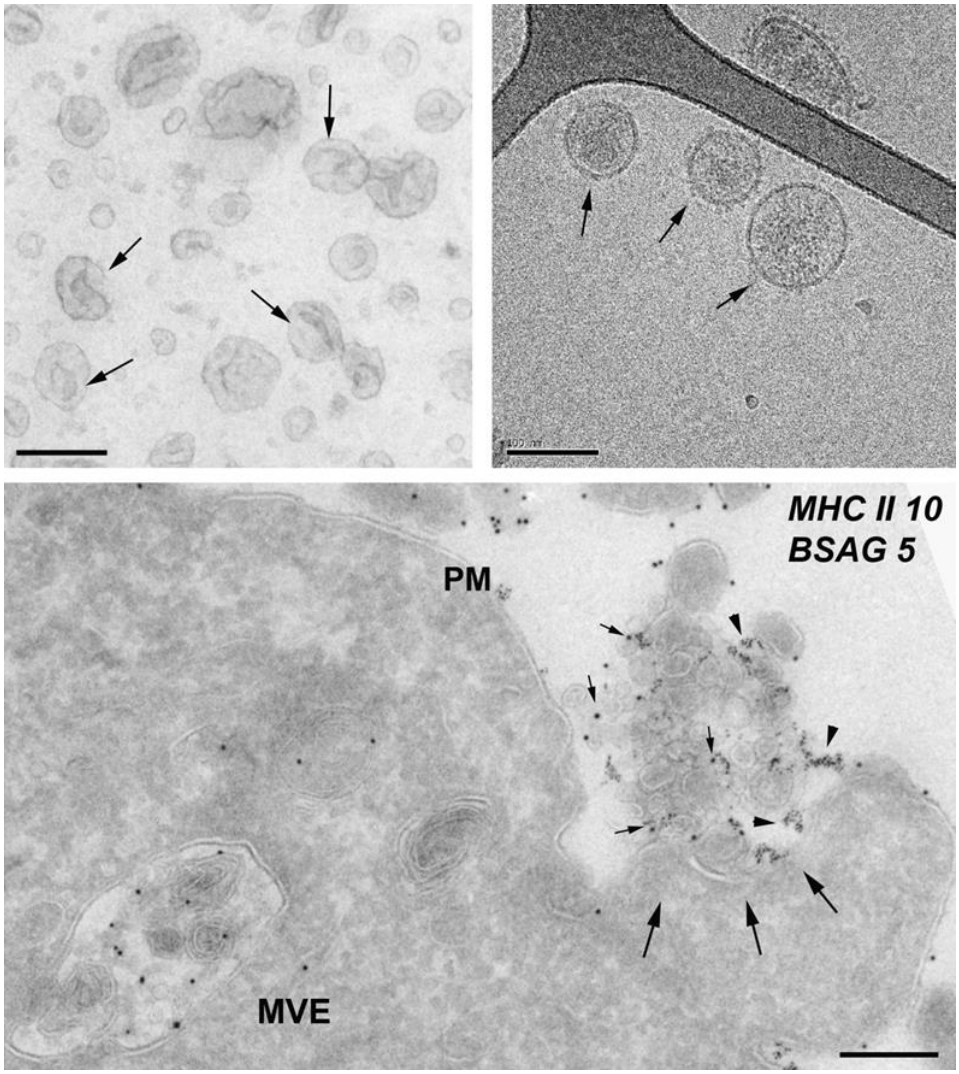

Figure 1.6 Size and ultrastructure of exosomes

Exosomes secreted from melanoma cells were contrasted with uranyl-acetate and embedded as whole mount preparations in methylcellulose. Note their artificial cup shape appearance (examples are indicated with arrows) and heterogeneous size ranging from 30 to 100 nm **(top left panel)**. Exosomes from prostate epithelial cells (prostasomes) were directly frozen and observed by cryo–electron microscopy without chemical fixation or contrasting. Exosomes appear round (arrows) and are visualized with improved resolution **(top right panel)**. EBV-transformed B lymphocytes were allowed to endocytose BSA coupled to 5-nm gold particles (BSAG 5) for 10 min and then chased for 20 min in the absence of BSAG 5. Ultrathin cryosections were immunolabeled for MHC class II with 10-nm protein A gold. The fusion of the multivesicular endosome (MVE) with the plasma membrane is depicted by arrows, and is defined by regurgitated 5-nm BSAG 5 that had previously been endocytosed. In addition to BSAG 5 (arrowheads), the exocytic profile contains exosomes labeled for MHC class II with 10-nm gold (MHC II 10; small arrows). PM, plasma membrane. **(bottom panel)** Scale bars,100 nm.

Figure and modified caption were reproduced with permission from Raposo G, Stoorvogel W. 2013. Extracellular vesicles: exosomes, microvesicles, and friends. *The Journal of cell biology* 200: 373-83

Density

Exosomes are conventionally known to migrate to sucrose densities of 1.13-1.19g/mL within a density gradient when subjected to overnight centrifugation [99]. However, some recent studies have shown that subpopulations of EVs display delayed flotation, and can be identified within distinct sucrose density fractions when bottom-loaded onto a gradient [100-102]. These studies suggest the existence of subpopulations within the classically defined exosome pellet, and call for a deeper and differential analysis of density-gradient fractions.

1.3.3 FUNCTION

Exosomes were initially viewed merely as means for the cell to clear unwanted material. Since then, studies have shown that EVs are vital for a variety of processes including cellular communication, signal transduction, coagulation, antigen-presentation, and others [103]. In 1998, Zitvogel *et al.* published a breakthrough study which showed that exosomes released from human dendritic cells were capable of suppressing the growth of established tumors in mice, demonstrating an important role for EV as mediators of immune responses [104]. Indeed, the most well-characterized functions of EVs are in the immune system, where a great number of *in vitro* and *in vivo* investigations have shown a role for exosomes in disseminating and presenting antigens, promoting proliferation of dendritic cells, and interacting with memory T cells [105]. EVs also play a role in tumour progression and metastases by promoting angiogenesis and tumour cell migration, and many have shown that tumour cells secrete EVs [98]. Although EVs are constitutively released from cells, their levels are increased following stress conditions such as DNA damage, hypoxia, cellular injury, or senescence, suggesting a potential function for EVs in resolving cell stress [90].

EVs have been shown to be secreted from all major cell types in the CNS including neurons, astrocytes, microglia, and oligodendrocytes [106-109]. EVs are also present in cerebrospinal fluid (CSF), highlighting their *in-vivo* relevance to the CNS

[110]. EVs appear to have a number of functions in the CNS including intercellular communication, synaptic plasticity, neuroprotection, antigen presentation, and maintenance of the myelin sheath [96]. However, it is important to note that most studies of EVs in the nervous system have been conducted *in vitro* using cultured cells, and have not been corroborated *in vivo* [111].

1.3.4 Cargo composition

Nucleic Acid

Analysis of genetic material within extracellular vesicles shows small RNA such as mRNA and miRNA of varying sizes, with very little ribosomal RNA. Indeed, it has been suggested that any rRNA present is due to contamination of the vesicle preparation with apoptotic bodies[91]. Low levels of mtDNA have also been detected in EVs[107]. More recently, next-generation sequencing showed the presence of non-coding RNA such as tRNA, vault RNA, and Y-RNA.

Although EV cargo identified in this section are generally applicable to most EVs it is important to note that the protein, nucleic acid, and lipid composition within exosomes and microvesicles can vary depending on the cell type or tissue of origin, as well as environmental factors such as culture conditions, hypoxia & stress, and cellular activation.

Lipid

Extracellular vesicles are enriched in cholesterol, ceramide, sphingomyelin, phosphatidylserine, and phosphatidylinositol in comparison to the parent cell, while phosphatidylcholine is decreased [112, 113], suggesting that lipids are specifically sorted into EVs [114]. The high proportion of cholesterol and sphingomyelin within EV membranes confers structural rigidity to these vesicles, greatly increasing their stability and resistance to physicochemical changes in the surrounding environment. In addition, the importance of lipids to the biogenesis and overall function of EVs is becoming increasingly apparent. Ceramide, for instance, is involved in the formation

of ILVs within MVBs [115], and cholesterol is shown to be important for regulating release of EVs from cells [116]. Lipids also have a demonstrated role in the angiogenic activity of tumour-derived vesicles and the capacitation process of sperm during reproduction, shown to be mediated by the transfer of cholesterol from seminal fluid-derived EVs to sperm cells [114, 117, 118].

Protein

Extracellular vesicle protein content can be examined by antibody-based techniques such as immuno-EM and Western blot. However, proteomic studies allow a more large-scale analysis of the protein content, and the data from many such proteomics experiments have been gathered into online repositories such as Exocarta (www.exocarta.org), Vesiclepedia (www.microvesicles.org), and EVpedia (www.evpedia.info) [119-121].

Proteomic profiling shows that a portion of the protein content in EVs depends on the secreting cell type while others are common to most vesicles regardless of originating cell. In general, the most commonly identified proteins in extracellular vesicles are cytoskeletal, cytosolic, heat shock proteins (HSP), vesicle trafficking, and plasma membrane proteins [114]. Some of the proteins found to be enriched in vesicles, and are thus commonly used as EV-specific markers are as follows: tetraspanins (CD9, CD63, CD81, CD82), MHC molecules, TSG101, HSPs, and the endosome sorting complex required for transport -3 (ESCRT III) binding protein Alix [114]. Nuclear, mitochondrial, endoplasmic reticulum, and golgi proteins are mostly absent from extracellular vesicles [91]. However, proteomic profiles are known to be heavily influenced by vesicle isolation method, making it difficult to perfectly extrapolate findings between different research groups. Extensive studies to differentiate exosomes from microvesicles based on protein content have not yet been conducted, and are warranted to better distinguish between these two subtypes of EVs.

1.3.5 Techniques for isolating extracellular vesicles

Exosomes and microvesicles can be isolated from cell culture supernatants using a variety of techniques such as high-speed ultracentrifugation, size-exclusion chromatography, precipitation using commercially available reagents, and affinity chromatography using antibodies against vesicle surface markers [103]. Most published protocols for isolating EVs use ultracentrifugation at ~10,000 x g to pellet the larger microvesicle population and ~100,000 x g to isolate the smaller exosomes. However, since centrifugation at high speeds also pellets protein aggregates and other vesicles such as synaptic vesicles, ultracentrifugation methods are usually followed by a sucrose purification step where the EVs are allowed to float on a sucrose density gradient or a sucrose cushion [91]. The lipid-containing extracellular vesicles introduced to a sucrose gradient will float at the sucrose fraction corresponding to its own buoyant density, and equilibrate there, while protein aggregates sediment [91].

1.3.6 Transmission of protein misfolding via EVs

Misfolding of PrP^{C} can be induced in prion disease models by the transfer of conditioned media containing PrP^{Sc}, indicating that direct cell to cell contact is not required for this process [122]. Growing evidence suggests that exosomes may be a predominant mechanism for the intercellular transfer of prion protein [122-125]. Indeed, studies have shown that stimulating the release of exosomes increases the infectivity of prion protein [126], adding further evidence to this hypothesis.

In PD, α-synuclein aggregation, seeding, and propagation are notable features of disease pathogenesis, and the transmission of misfolded α-synuclein is a leading hypothesis to explain the systematic progression of pathology [123]. EVs isolated from the CSF of PD patients were shown to carry misfolded α-synuclein, and EVs from *in vitro* systems were shown to both carry α-synuclein and mediate its transfer between neurons [127-129]. α-synuclein within vesicles is also more aggregation-prone than free extracellular α-synuclein [127]. Others have shown an increased

likelihood of cellular uptake of EV-associated α-synuclein in comparison to free protein, suggesting a role for EVs in the transmission of α-synuclein aggregation between cells [123].

EVs appear to play dual roles in neurodegenerative diseases. In AD, for example, a fraction of Aβ peptides were shown to be secreted from cells in association with exosomes, and EV-associated proteins are found in amyloid plaques, suggesting EVs are involved in AD pathobiology [123]. Inhibition of exosome secretion seemed to ameliorate amyloid aggregation and deposition [123]. However, injection of neuroblastoma-derived EVs into a murine model of AD decreases amyloid deposition, suggesting a protective role of EVs in this context [123]. Thus, it is unclear whether secretion of protein via EVs is beneficial or detrimental.

There is also evidence for the involvement of EVs in ALS. TDP-43 is enriched in EV fractions isolated from cell culture media from neuroblastoma cells overexpressing TDP-43, as well as in EVs from the CSF of ALS patients, indicating that TDP-43 can be released from cells via EVs and that it may be disease-relevant [123]. In further support of this, another study demonstrated that exosome-associated TDP-43 is preferentially taken up by cells in comparison to free TDP-43 [123]. Wild-type SOD1 has also been shown to be secreted via exosomes in a cell culture model of ALS [130], and our group has demonstrated a role of EVs in the intercellular propagated misfolding of SOD1 in a cell culture model of ALS [84].

1.4 HYPOTHESIS AND AIMS

The findings thus far described in literature demonstrate *in vitro* evidence for SOD1 secretion via exosomes in normal physiology and in some cell culture models of ALS. However, the physiological relevance of these findings and their applicability to human ALS is not certain. For example, it is not known whether EVs secreted in an *in vivo* environment, either murine or human, contain misfolded SOD1 cargo. Furthermore, though mutant SOD1-bearing exosomes are shown to be taken up by

cells, it is not known whether EVs mediate propagation of SOD1 misfolding. With these points in mind, the overarching hypothesis of this work is that **CNS tissue-derived EVs from ALS mouse models bear misfolded SOD1 cargo and propagate SOD1 misfolding to recipient cell cultures in a prion-like manner.** The hypothesis was investigated using the following specific aims:

Aim 1: Isolate and characterize CNS tissue-derived EVs from ALS mouse models

Aim 2: Investigate the presence and localization of misfolded SOD1 in isolated EVs

Aim 3: Examine capability of ALS mouse model tissue-derived EVs to propagate SOD1 misfolding to cell culture systems

Aim 4: Explore physiological relevance of findings using EVs isolated from human ALS patients

CHAPTER 2. ISOLATION AND CHARACTERIZATION OF CNS TISSUE-DERIVED EXOSOMES AND MICROVESICLES

2.1 INTRODUCTION

Extracellular vesicles (EVs) encompass three major vesicle classes: exosomes, microvesicles, and apoptotic bodies [99, 114, 131]. Exosomes originate primarily in the late endosome in an ESCRT-dependent process, while microvesicles bud directly from the plasma membrane [98]. To date, the majority of published work in the EV field has been conducted using exosomes isolated from cell culture supernatants and biofluids [114]. Since there is increasing evidence that ALS and neurodegenerative diseases are non-cell autonomous, studying one subpopulation of EVs derived from a single cell type is unlikely to give a comprehensive understanding of the role EVs play in these diseases [72, 132, 133]. Biofluids contain EVs secreted from multiple cell types, but EVs specific to disease are often diluted by the presence of EVs secreted from healthy cells. More recently, a handful of studies have explored EVs isolated from tissues [134-137]. Whole-tissue sourced EVs encompass subpopulations of EVs which originate from multiple cell types in the region affected by disease pathology, and can provide a unique window into the role these small vesicles play in health and disease.

Grad *et al.* have previously demonstrated that exosomes isolated from an *in vitro* model of ALS have surface-localized misfolded SOD1 and are efficiently taken up by primary cultured neurons [84]. However, the physiological accuracy of this system is uncertain. To explore the *in vivo* relevance of these findings, and to establish a protocol for downstream analysis of ALS patient EVs, we studied two EV subpopulations secreted into the extracellular space of the mouse central nervous system (CNS). To this end, we isolated exosomes and microvesicles from whole neural tissues of two different ALS mouse models, $SOD1^{G127X}$ and $SOD1^{G93A}$, and

their non-transgenic (NonTg) counterparts, and characterized them according to criteria established in the field.

EVs are often isolated from complex mixtures that have multiple non-EV constituents. This is especially true for EVs isolated from whole tissues. Therefore, the identity and purity of isolated EVs has to be established with multiple means of characterization. A position paper published in 2014 in the *Journal of Extracellular Vesicles* recommends these minimal experimental requirements for definition of EVs [138]: 1) demonstration of EV-enriched cargo by a semi-quantitative method such as immunoblot 2) demonstration of the lack of proteins not expected to be enriched in exosomes 3) comparison of isolated EVs to starting material 4) comparison of EVs to negative controls such as the EV-depleted supernatant remaining after ultracentrifugation, and 5) characterization of single vesicles within a population by transmission electron microscopy (TEM) to give an indication of the heterogeneity within the sample.

Proteomic studies have identified certain proteins that are enriched in EVs such as cytoskeletal, cytosolic, plasma membrane, and vesicle trafficking proteins, whereas intracellular organelle proteins are less abundant [114]. With respect to other characteristics, EVs are increasingly found to be highly heterogeneous [139, 140]. Exosomes were originally thought to migrate to sucrose densities of ~1.16 g/mL and to be ~50-150 nm in diameter, but more recent studies are discovering that they may encompass a broader size range and density profile [102, 140, 141]. These original definitions were based on work conducted on cell culture supernatant-derived EVs. However, true physiological heterogeneity in size, morphology, and cargo of EV populations may not be fully reflected in EVs sourced *in vitro*. There is also evidence of subpopulations that exist within isolated EV preparations that carry varying cargo and mediate different functions in recipient cell types [131, 139, 140]. Separation and proper characterization of EV subpopulations are therefore important when studying EV biology and function.

Several different methods exist for isolating EVs. Differential centrifugation is a method by which a solution is pre-cleared of debris and apoptotic bodies via low-speed centrifugation while other EVs are isolated at higher speeds. It represents the most established protocol for EV isolation [97, 99]. However, in addition to EVs, ultracentrifugation at high speeds can sediment protein complexes, aggregates, high and low density lipoproteins (HDL, LDL), and other vesicle types, and a means of eliminating these contaminants are routinely required in the process [99, 142]. Filtration through a molecular weight cut-off filter can deplete large proteins and complexes from an EV-containing solution, but may also eliminate larger EVs [99]. More commonly, a sucrose density gradient is used to sediment protein aggregates while allowing lipid-bound vesicles migrate to densities of sucrose which correspond to their own buoyant density [93, 99]. Alternate methods of EV isolation include immunoaffinity-based capture using known EV-associated proteins, and size-exclusion chromatography which isolates vesicles of a specific pre-determined size [99]. However, these methods operate on a narrow definition of EV-associated surface cargo or size-range, and are inherently biased against the discovery of subpopulations of vesicles. In the current work, we have used an ultracentrifugation-based protocol in order to capture a broad range of EV subtypes, and a sucrose density gradient to further purify isolated EVs.

With these points in mind, the aims of this chapter are to demonstrate the optimization of a differential ultracentrifugation-based method for isolating EVs from frozen whole CNS tissues from ALS mouse models. Using this protocol we have isolated two different CNS-derived EV subpopulations (exosomes and microvesicles), and confirmed their identity and purity by a variety of criteria. This work provides useful and foundational information regarding the heterogeneity of EVs derived from whole tissues, and identifies similarities and points of divergence between CNS tissue-derived exosome and microvesicle populations.

2.2 METHODS

2.2.1 ANIMAL CARE

Experiments involving animals were conducted according to the Canadian Council on Animal Care guidelines were approved by the Animal Care Committee of the University of British Columbia. C57 BL/6, $SOD1^{G93A}$, HuWTSOD1 (Strains: B6SJL-Tg(SOD1)2Gur/J, Cg-Tg(Sod1-G93A)1Gur/JB6, Cg-Tg(Sod1*G85R)148Dwc/J, B6SJL-Tg(Sod1-hWT)2Gur/J; Jackson Laboratories, Bar Harbor, ME), or $SOD1^{G127X}$ mice (Tg(SOD1*G127X)716Mrkl; Stefan Marklund) were sacrificed according to the guidelines of the Institutional Animal Care and Use Committee (IACUC) under protocol A15-0203. Brain and spinal cord tissues were harvested from sacrificed animals, and flash-frozen in liquid nitrogen.

2.2.2 EV ISOLATION FROM WHOLE CNS TISSUES

Frozen brain or spinal cord tissues from mice were finely sliced in Hibernate A medium (Brain Bits, Springfield, IL), added to a pre-warmed solution of Hibernate A containing 25 U/mL Papain or 125 U/mL Collagenase III to digest the extracellular matrix, and incubated with shaking at 37°C for 15 minutes. Enzymatic digestion was stopped by adding ice-cold Hibernate A containing Protease Inhibitors (EDTA-free protease inhibitor cocktail; Roche Diagnostics, Switzerland). The mixture was centrifuged at 300 x *g* and subsequently at 2000 x *g* to remove cells and cellular debris. Microvesicles were isolated by centrifuging the supernatant at 10,000 x *g* for 30 min. Exosomes were isolated by centrifuging the resultant supernatant at 100,000 x g for 90 min. All ultracentrifugation steps were performed using the Beckman Coulter Type 70Ti Rotor (Break, CA) at 4°C.

2.2.3 SUCROSE DENSITY PURIFICATION

EVs were top-loaded onto a sucrose step-gradient with concentrations ranging from 0.25 - 2.0 M sucrose (top to bottom) diluted in 20 mM HEPES buffer pH 7.4 (Sigma),

and centrifuged at 200,000 x *g* for 16 h in a SW41 swing bucket rotor (Beckman) at 4°C. Following centrifugation, 1 mL fractions were collected from top to bottom, and analyzed to identify the sucrose fraction containing EVs. In subsequent experiments, a sucrose cushion was used in which the pre-determined concentration of sucrose (0.95M for exosomes, 1.3M for MVs) was layered on top of 2M sucrose in a 1.5mL ultracentrifuge tube (Beckman). The EV pellet from the ultracentrifugation step was diluted in PBS, top-loaded onto the cushion, and centrifuged for 2 h at 20,000 x *g* for the MV pellet, or 150,000 x g for the exosome pellet. The 700uL fraction at the interphase between the 2 sucrose densities was collected into a fresh tube, and spun down for 1 h at 10,000 x *g* for MVs and 100,000 x *g* for exosomes to isolate the purified vesicle pellet.

2.2.4 Transmission electron microscopy

A 3 µL sample of exosomes or microvesicles was applied to glow discharged 200 mesh formvar/carbon coated TEM grids (Ted Pella Inc., Redding, CA), and negatively stained with 2% aqueous uranyl acetate. A Hitachi H7600 TEM (Hitachi High-Technologies Corp., Tokyo, Japan) instrument operated at 80kV with a side mounted 1K AMT Advantage digital camera (Advanced Microscopy Techniques, Corp. Woburn, MA) were used to observe samples and capture images.

2.2.5 Immunoblotting

Total protein concentrations were determined by a commercially available BCA assay kit (ThermoFIsher Scientific, Waltham, MA), and 15-30 µg of samples were prepared in phosphate-buffered saline (PBS) for immunoblot analysis. Samples were boiled in sample buffer containing 1% β-mercaptoethanol, and run on 4% Bis-Tris gels (LifeTechnologies, Carlsbad, CA). Proteins were transferred to a PVDF membrane, incubated for 1 h at room temperature in blocking buffer (TBS, 0.1% Tween-20 (TBST), 5% skimmed milk), and incubated with 1 µg/ml SOD100 antibody (Assay Designs, Ann Arbor, MI), 1 µg/ml Flotillin-1, GM130, BiP antibodies (BD

Tranduction Laboratories, USA), 1 µg/ml HSP-70, CD9 (Abcam, USA), 1 µg/ml PrP antibody (Covance, Dedham, MA), or 1 µg/ml β-actin antibody (ABM, Vancouver, BC, Canada) overnight at 4 °C. Membranes were then washed twice in TBST and incubated with anti-mouse or anti-rabbit IgG horseradish peroxidase-linked whole antibody (GE Healthcare, Buckinghamshire, UK) diluted 1:10,000 in blocking buffer for 1 h at room temperature. Membranes were developed using SuperSignal West Femto chemiluminescence substrate (Thermo Fisher Scientific, Waltham, MA), and visualized using a VersaDoc Imager (Bio-Rad Laboratories, Hercules, CA).

2.2.6 Nanoparticle tracking analysis

The NanoSight LM10-HS instrument (Malvern Instruments Ltd., Malvern, UK) equipped with the NTA 2.0 analytical software was used to characterize the diameter of particles in EV samples. Samples were diluted 1:3000 in distilled water, and injected with constant output via syringe-pump into a 405 nm laser chamber. Three recordings were performed for each sample, followed by use of the batch process function in the NTA software to integrate readings to obtain a mode and mean size for each sample.

2.2.7 Confocal microscopy

Confocal images were captured with a Leica TCS SP8 scanning confocal microscope (Leica Microsystems) using LAS-X software. Images were focused using the DAPI signal, and by making minor focal modification to capture signal emitted at 488 nm (PKH67 signal) [143].

2.2.8 Statistical analysis

All data were analyzed using GraphPad Prism version 6.00 for Windows (GraphPad Software, La Jolla, California). One-way ANOVA was performed followed by

Kruskal-Wallis or Mann-Whitney-U tests. Two-way ANOVA was performed followed by Tukey's or Sidak's post-tests. Data is presented as mean ± SEM.

2.3 RESULTS

2.3.1 ISOLATING EXTRACELLULAR VESICLES FROM FROZEN WHOLE NEURAL TISSUES

We optimized a unique method first published in 2012 by Perez-Gonzalez et al. to isolate EVs from whole tissues [135]. Briefly, we minced flash-frozen brain or spinal cord tissue from ALS mouse-model or NonTg mice, and added it to a pre-warmed solution of neuronal maintenance medium, Hibernate A, containing 20 U/mL papain, a digestion enzyme, in order to digest the extracellular matrix and liberate extracellular vesicles. The mixture was incubated at 37°C for 15 min. Enzymatic digestion was stopped by adding ice-cold Hibernate A containing protease inhibitors. We centrifuged the mixture at 300 x *g* and at 2000 x *g* to remove whole cells, cellular debris and apoptotic bodies. One vesicle population was isolated by centrifuging the supernatant at 10,000 x *g* for 30 min and collecting the pelleted material. We then further centrifuged the resultant supernatant at 100,000 x *g* for 90 min to obtain a second population of EVs. **(Figure 2.1).**

We characterized our samples to ensure we were isolating *bona fide* EVs rather than artificially-created vesicles, intracellular organelles, or non-EV vesicle types. Of note, it is typically not possible to reliably distinguish between the endocytic or plasma membrane origin of EV populations isolated from cell culture supernatants, biofluids, or extracellular spaces of tissues. Therefore, in this work we use the term exosomes to denote the vesicle population pelleted at 100,000 x *g* and the term microvesicle for EVs pelleted at 10,000 x *g*.

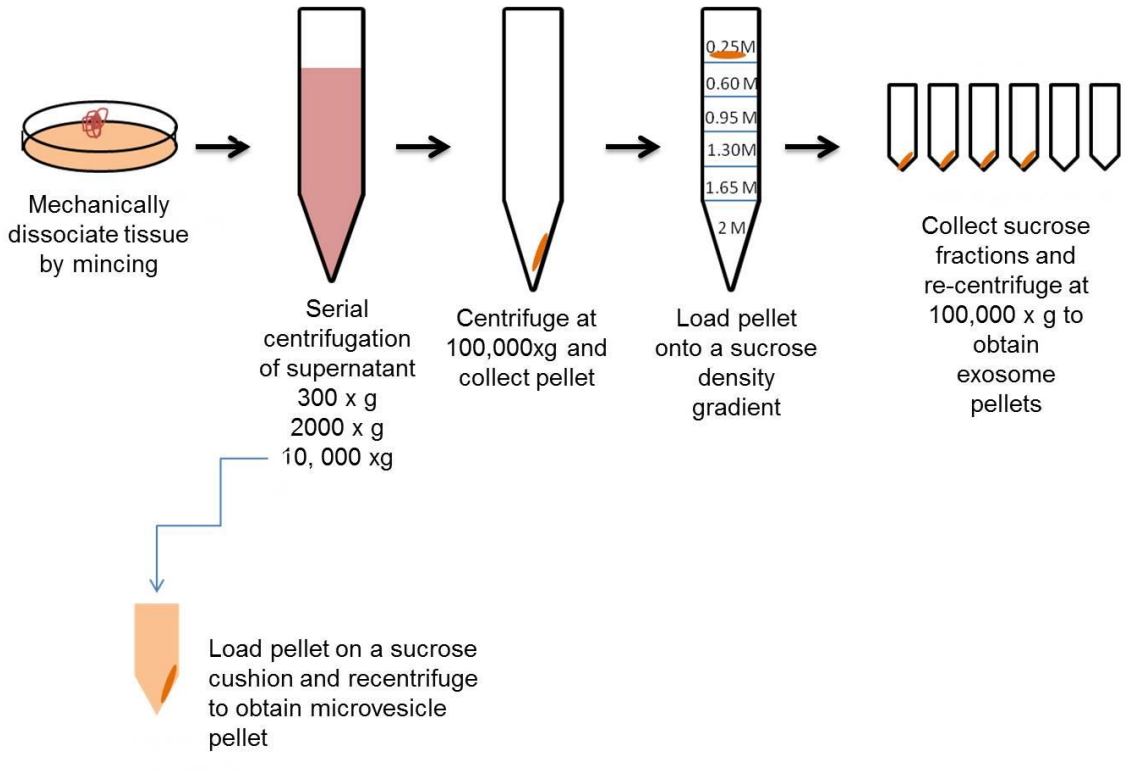

Figure 2.1 Isolation protocol for CNS tissue-derived EVs.

Frozen brain or spinal cord tissue from ALS mouse-model or NonTg mice are minced and added to neuronal maintenance medium, Hibernate A, containing 20 U/mL papain, a digestion enzyme. After 15 min, the enzymatic digestion is stopped by adding ice-cold Hibernate A containing protease inhibitors. The mixture is serially centrifuged at low speeds to remove whole cells, cellular debris and apoptotic bodies. The microvesicle population is isolated by centrifuging the supernatant at 10,000 x g, and exosomes by centrifuging the resultant supernatant at 100,000 x g for 90 min.

2.3.2 Papain causes digestion of EV-associated protein content

We initially obtained low levels of signal across a number of antibody markers when attempting to characterize EV-associated proteins using immunoblot. We suspected that papain may be enzymatically digesting some of the protein material on the vesicle surface, and decided to use a milder digestion process instead. We tested a protocol using 125 U/mL collagenase III as a replacement for papain, and subsequently immunoblotted for two EV-associated markers: the cytoskeletal protein β-actin, and prion protein (PrP) which has previously been demonstrated as a neuronal EV-associated marker [99, 124]. In a side-by-side comparison, EVs

harvested by papain digestion showed little to no β-actin and PrP signal **(Figure 2.2).** When papain was replaced by collagenase III in the isolation protocol, strong β-actin and PrP signals were observed in the isolated EV pellets **(Figure 2.2)**. The above data indicate that papain in the original published protocol should be replaced by a milder digestion process to preserve EV-associated protein content.

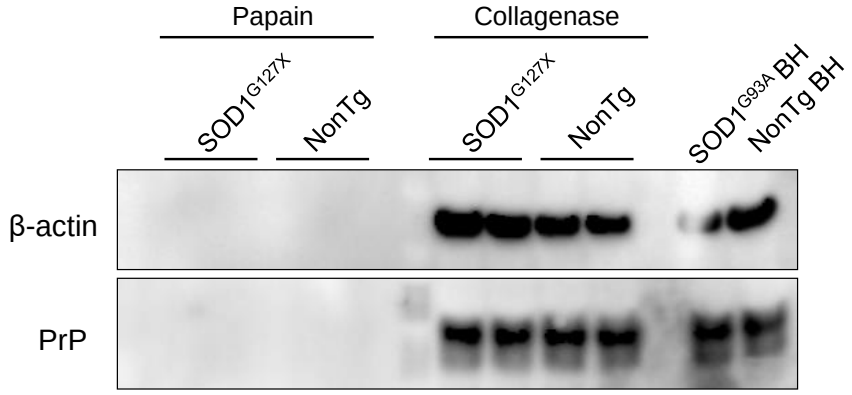

Figure 2.2 Enzymatic digestion by papain causes denaturation of exosome protein content.

Exosomes isolated with papain enzymatic digestion show no β-actin and PrP signal indicating protein material may have denatured. Replacing papain with collagenase III in the isolation protocol results in EV pellets which show β-actin and PrP signal at levels similar to that of whole brain homogenate.

2.3.3 Mechanical disruption of tissue causes significant increase in sample yield without appreciable differences in markers of contamination

A position paper put forward by the International Society for Extracellular Vesicles (ISEV) has stated the opinion that EVs isolated by mechanical disruption of tissue can result in the release of intracellular vesicles [138]. To investigate whether CNS tissues processed with the current protocol yielded a relatively pure population of EVs, we tested three different methods of mechanical dissociation: fine mincing of tissue with a scalpel, minimal disruption of tissue by making one cut to produce 2 hemi-brains, and vigorous shaking of hemi-brains during the enzymatic dissociation step. The resultant exosome pellets from two different HuWTSOD1 transgenic and NonTg animals were compared to the exosome-depleted fraction (the supernatant

following the 100,000 x *g* centrifugation concentrated using a 10 kDa molecular weight cut-off filter) by immunoblot. When probed with EV-associated markers such as the lipid-raft protein flotillin-1, and the cytoskeletal marker β-actin [99], specific enrichment was observed in the exosome pellets relative to the supernatant fraction in all three methods of tissue processing **(Figure 2.3A).** PrP and SOD1 were present in both the exosome fractions and exosome-depleted fractions. This data indicated that EVs can be isolated by all three methods. BiP, an endoplasmic reticulum marker [144], was probed to determine if the exosome pellet was contaminated with intracellular constituents. BiP was present in the concentrated exosome-depleted fraction, but not in the exosome pellets, although trace amounts of BiP were observed in EVs isolated by mincing tissues **(Figure 2.3A).** HSP-70, a ubiquitously expressed chaperone known to be enriched in the intracellular space and on endosomal/lysosomal membranes [145], was similarly distributed. The lowest amount of BiP and HSP-70 was present in the whole hemi-brain fraction, indicating that the least amount of tissue processing resulted in the least amount of cell lysis and liberation of intracellular contents.

When sample yield was investigated by total protein assay, the amount of protein material isolated by mincing tissue was significantly higher than that for hemi-brains or hemi-brains with shaking **(Figure 2.3B).** Overall, the data indicate that although the lowest amount of intracellular contamination is present in the least disruptive method, the sample yield in these preparations is too low to be sufficient for downstream analysis. Mincing tissue did not cause large scale liberation of intracellular material as indicated by the low BiP signal in the concentrated supernatant **(Figure 2.3A)**. Therefore, for downstream application, we proceeded with the protocol that includes mincing of tissue.

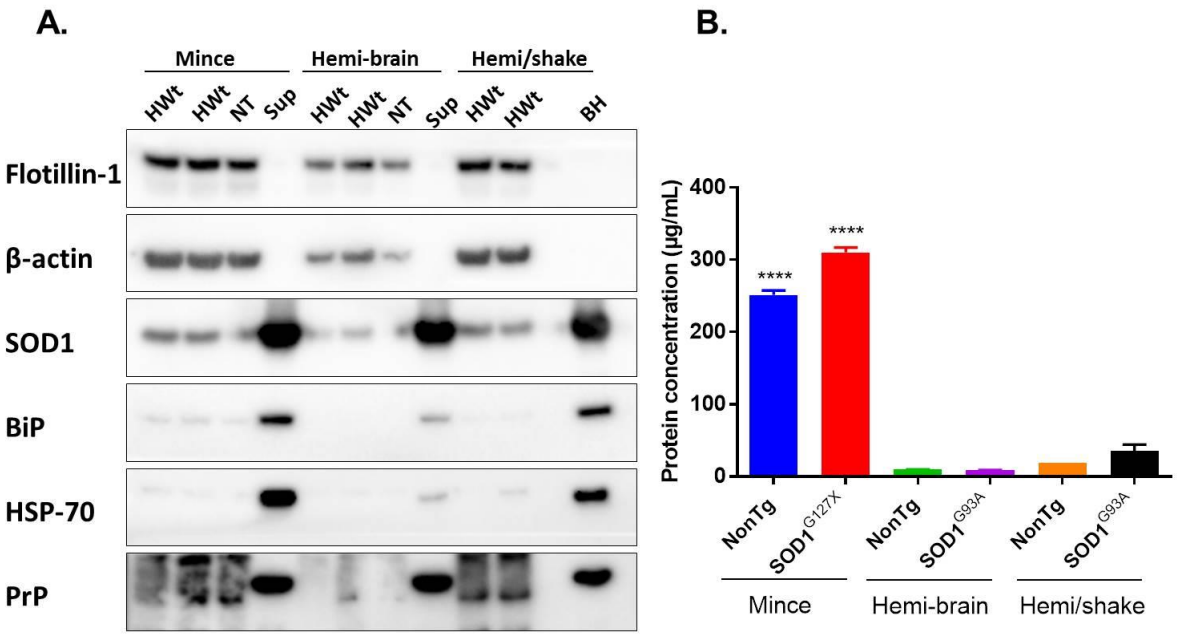

Figure 2.3 Mechanical dissociation of tissue displays low levels of intracellular contamination and high sample yield.

A. Mincing tissues, making a single cut to produce 2 hemi-brains, and hemi-brains with vigorous shaking all result in EV pellets that display a positive signal for EV-associated markers flotillin-1 and β-actin, as well as soluble markers SOD1, PrP. Material isolated from NonTg(NT) or HuWTSOD1 (HWt) animals, exosome-depleted supernatants (Sup), or whole brain homogenates (BH) were used in the analysis. The exosome-depleted supernatants do not display EV-associated markers flotillin-1 and β-actin. Lower amounts of intracellular markers BiP and HSP-70 are present in the hemi-brain preparation, indicating the least amount of contamination. **B.** Highest sample yield as measured by total protein concentration is seen in EV pellets isolated by mincing tissues. (N=2 brains per condition, ****p<0.0001 following analysis by one-way ANOVA and Holm-Sidak's multiple comparison test)

2.3.4 Sucrose purification is essential for clearance of debris and soluble protein in tissue-derived EV preparations

Next, using exosomes isolated with the optimized protocol, we examined whether sucrose purification was essential for the protocol since it requires significant time to perform, and some groups have shown data using cell culture supernatant-derived EVs isolated without sucrose purification. Therefore, we examined exosomes isolated with and without sucrose purification by TEM (refer to 2.2.4 for detailed protocol). At low magnification, the pellet collected without sucrose purification

showed a substantial amount of debris and extra-vesicular material that were present as irregular blobs without visible double membranes **(Figure 2.4)**. At higher magnification, it appeared that this material could be pieces of broken vesicles, protein, or other debris, with some intact vesicles dispersed throughout **(Figure 2.4, red arrows)**. This debris-like material was eliminated following sucrose purification, yielding a more homogenous population of vesicles as evident in the right hand panels of **(Figure 2.4)**. These results clearly demonstrate that sucrose-purification is essential for isolating a homogenous population of EVs from CNS tissues.

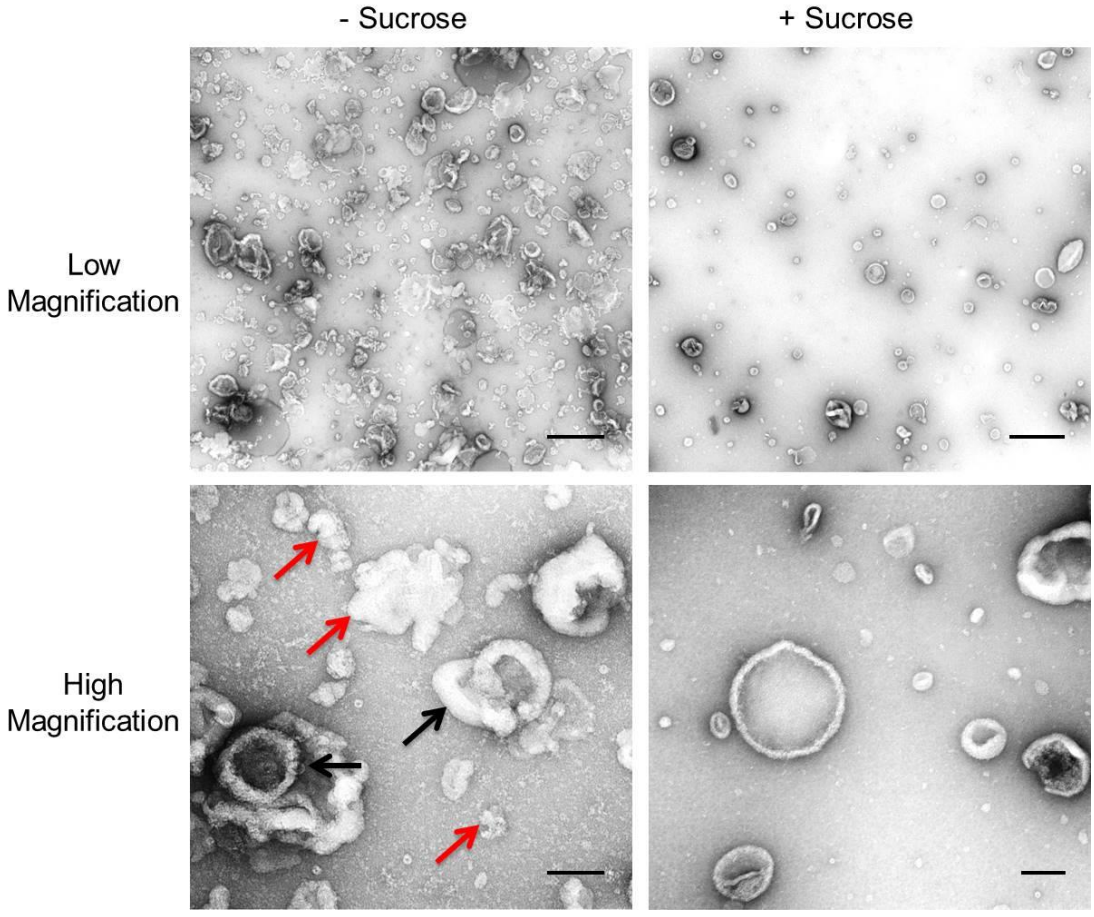

Figure 2.4 Sucrose purification is essential for clearance of debris in tissue-derived EV preparations.

TEM images of exosomes isolated without a sucrose purification step at lower magnification show a substantial amount of debris and non-vesicular material (top left). At higher magnification (bottom left), non-vesicular material and debris lack a visible double membrane(red arrows) while EVs in the preparation show cup-shaped morphology and a

double membrane (black arrows). Sucrose purification step yields a preparation clear of large debris with an enrichment of double membrane-enclosed vesicles (right hand panels). Low magnification scale bar=500nm, high magnification scale bar=100 nm.

2.3.5 EVs ISOLATED FROM ALS MOUSE MODELS MIGRATE TO EXPECTED SUCROSE DENSITIES

For downstream investigation of propagated SOD1 misfolding by *in vivo* EVs, we required mice overexpressing human $SOD1^{G127X}$, a naturally occurring mutation known to cause ALS in humans [17]. $SOD1^{G127X}$ transgenic mice present a typical murine ALS-like disease phenotype with foreleg onset, reduced motor function at ~150 days, and death from disease at ~250 days of age [56]. The $SOD1^{G127X}$ mouse model was chosen because the frameshift G127X mutation results in truncation of the wild-type C-terminal SOD1 sequence in the region containing the epitope for the misfolded SOD1-specific antibody 3H1 [83]. The absence of the 3H1 epitope in $SOD1^{G127X}$, and its presence and exposure in full-length misfolded HuWTSOD1, allows for the distinction of these two species of SOD1, enabling unambiguous detection of induced HuWTSOD1 misfolding initiated by G127X [83].

EVs were isolated from frozen whole brain tissues of 5 month old $SOD1^{G127X}$ mice or non-transgenic (NonTg) littermates. As previously mentioned, proteomic and meta-analyses have identified SOD1 and prion protein (PrP) as neuronal EV markers [130, 146], and we used these proteins to examine the flotation of CNS-derived EVs in a sucrose gradient. Vesicles from a 100,000 x *g* pellet migrated to 0.6-0.95 M or ~20-30% sucrose **(Figure 2.5A, fractions 5-7),** consistent with previously published findings for exosomes [99]**.** Vesicles that were pelleted at 10,000 x *g* (termed microvesicles) migrated to slightly higher densities of sucrose at 0.95-1.3M or ~30-40% sucrose **(Figure 2.5B, fractions 6-8).** There were no appreciable differences in the density of EVs isolated from $SOD1^{G127X}$ and NonTg mice, suggesting that the isolation technique yields consistent preparations of EV populations.

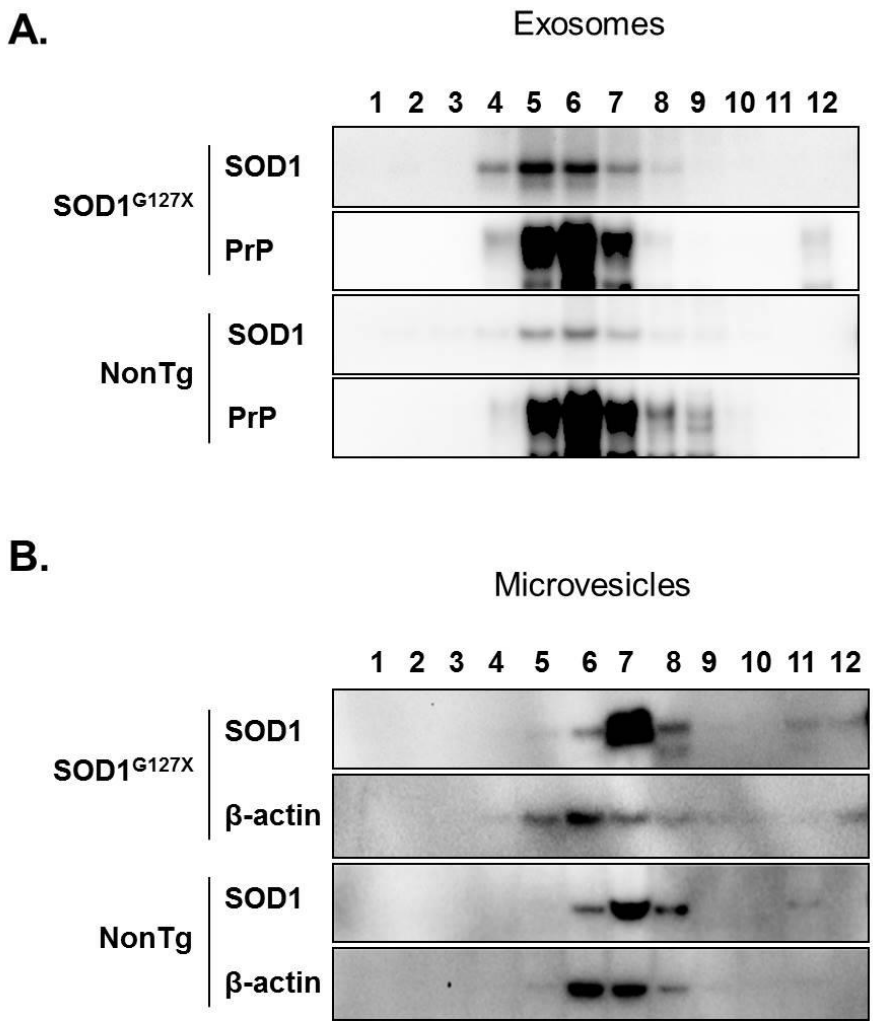

Figure 2.5 The 10,000xg and 100,000xg pellets migrate to sucrose density fractions consistent with densities for extracellular vesicles

A. The vesicle pellet pulled down at 100,000xg from both SOD1^{G127X} and NonTg mice migrates to ~20-30% sucrose fractions, as indicated by the markers SOD1 and PrP (fraction numbers 4-7), and is termed the exosome pellet. **B.** The 10,000xg pellet, termed microvesicles, from both genotypes migrates to sucrose fractions at a slightly higher density than exosomes at ~30-40% sucrose as indicated by the presence of SOD1 and β-actin bands in fraction numbers 5-8.

For subsequent characterization and experiments, EVs were purified on sucrose cushions of the identified molarities (0.95 M for exosomes and 1.3 M for microvesicles).

2.3.6 CNS TISSUE-DERIVED EVS DISPLAY CHARACTERISTIC CUP-SHAPED MORPHOLOGY

We then examined isolated CNS tissue-derived EVs by TEM to determine if they displayed structural features similar to those previously identified for EVs in literature. EVs have been shown to exhibit a circular cup-shaped morphology reminiscent of erythrocytes when visualized by TEM (**refer to Figure 1.6**) [98]. Such morphology is not indicative of intact vesicles under physiological conditions, but is an artifact of the membrane-drying process where vesicles collapse inward. When visualized with TEM, exosomes and microvesicles isolated using our protocol displayed the expected morphological characteristics for EVs, apparent as circular invaginated structures bounded by a double membrane **(Figure 2.6)**

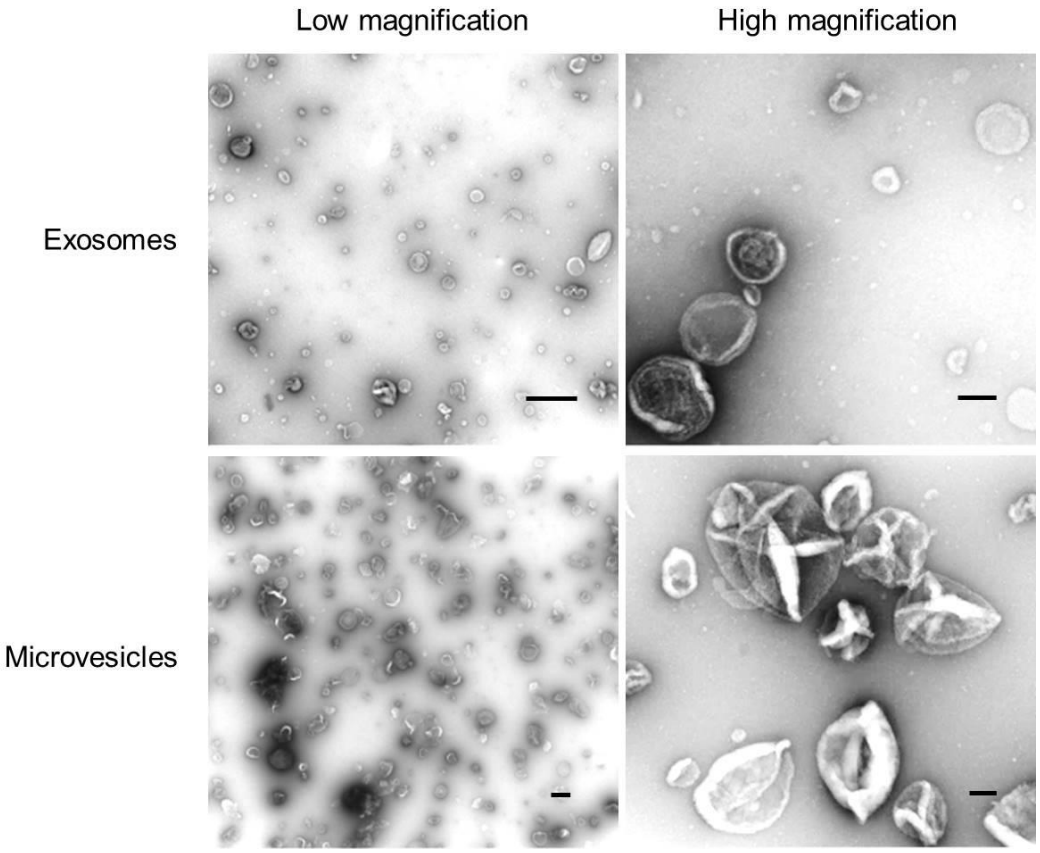

Figure 2.6 Neural tissue-derived extracellular vesicles display characteristic erythrocyte-like morphology

Representative TEM images of uranyl-acetate stained exosomes (top panel) at low magnification (top left, scale bar=500nm) and high magnification (top right, scale bar=100 nm), and the microvesicle pellet at low (bottom left, scale bar=500nm) and high magnification (bottom right, scale bar=100nm) demonstrate cup-shaped morphology typical of dehydrated extracellular vesicles visualized by TEM

2.3.7 PROTEIN MARKER PROFILE OF CNS TISSUE-DERIVED EVS

To further characterize CNS-derived exosome and microvesicle populations, we probed them for known EV-associated markers such as the tetraspanin CD9, lipid raft marker flotillin-1, SOD1, PrP and β-actin [99, 114]. Both the exosome and microvesicle pellets showed CD9, flotillin-1, β-actin, as well as SOD1 and PrP signal **(Figure 2.7A,B).** EVs derived from $SOD1^{G127X}$ animals displayed two SOD1 reactive bands representing the presence of both the truncated human $SOD1^{G127X}$ and full-length murine SOD1 protein in association with EVs **(Figure 2.7A,B)**; the truncated

SOD1^{G127X} runs at a slightly lower molecular weight than does full-length endogenous murine SOD1 via gel electrophoresis [83].

Interestingly, microvesicles displayed an additional band for both flotillin-1 and CD9 relative to exosomes, representing possible cleavage products in the microvesicle pellets **(Figure 2.7B)**. Markers typically used for detection of intracellular contamination such as BiP (ER) and GM130 (Golgi) were not present in the exosome pellet, indicating a high degree of purity in the preparation **(Figure 2.7A).** The microvesicle pellet did not contain GM130, but did contain BiP **(Figure 2.7B).** BiP signal could be due to the presence of some contamination in the microvesicle pellet, although the absence of GM130 insinuates otherwise. Alternatively, BiP may be naturally sorted to microvesicles but not to exosomes, consistent with another study which shows that a proportion of cellular BiP is localized to the plasma membrane and secreted into the extracellular space [147].

To further demonstrate that contamination of free soluble protein in the vesicular pellets was minimal, we concentrated the vesicle-depleted supernatant following the 100,000 x *g* centrifugation using a 10 kDa molecular weight cut-off filter, and compared it to the exosome pellet. The EV-specific markers flotillin-1 and β-actin were enriched in the exosome fraction, but were entirely absent in the soluble EV-depleted fraction **(Figure 2.7C).** The soluble proteins SOD1 and PrP were present in both the supernatant and the exosomes, although cleavage products of PrP were concentrated in the exosome fraction **(Figure 2.7C)**. BiP and HSP-70, markers of intracellular contents, were enriched in the soluble fraction but absent in exosomes**.** Together, the above data demonstrate that CNS EVs isolated from both SOD1^{G127X} and NonTg animals are enriched in EV-associated markers with minimal indicators of contamination by intracellular material.

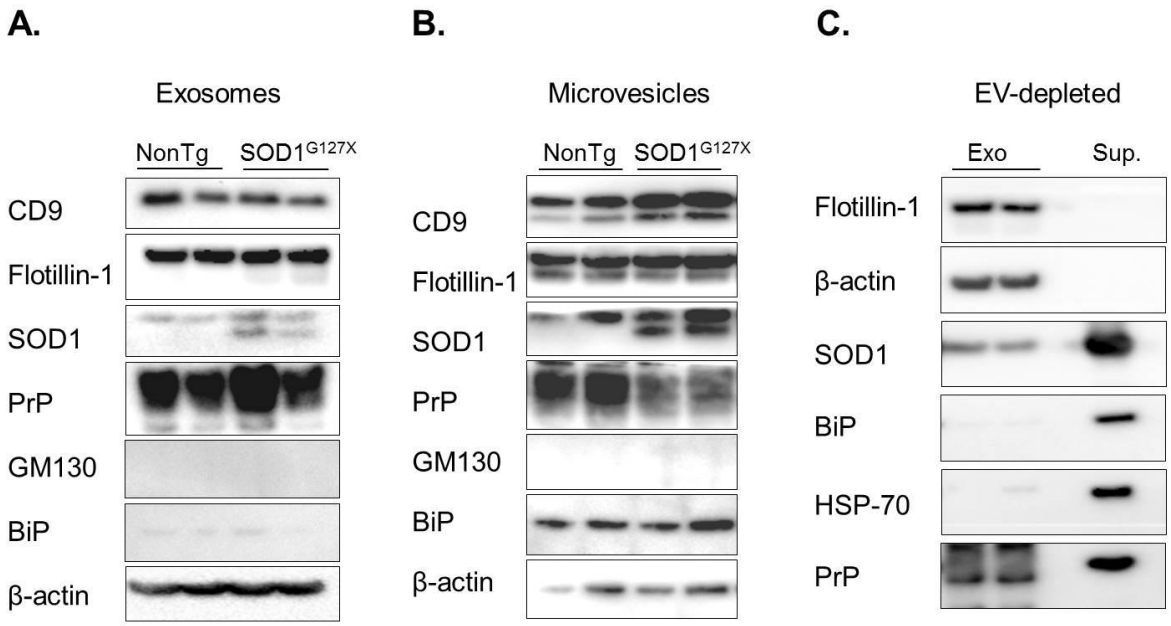

Figure 2.7 Protein marker profile of isolated EVs

A. EV-associated markers CD9, Flotillin-1, SOD1 and PrP are present in the sucrose-purified exosome pellet. Markers of cellular contamination, GM130 and BiP, are largely absent in the exosome pellet. **B.** The same vesicle-specific markers are also present in the microvesicle pellet. Endoplasmic reticulum marker BiP is present in the microvesicle pellet while the golgi marker, GM130, is absent. c. EV-associated marker proteins are specifically enriched in the exosome pellet relative to the concentrated EV-depleted fraction following 100,000 x g centrifugation. (representative blots from N=3 tests)

2.3.8 Extracellular vesicle size

As previously mentioned, one distinguishing characteristic of EVs is their discrete size range. Exosomes derived from cell-culture supernatants and biofluids are known to be ~ 50-150 nm in diameter, while microvesicles are typically larger in size (~150-1000 nm) [99]. Vesicles isolated in different experimental systems should adhere to similar size parameters in order to be identified as authentic EVs [138]. Nanoparticle tracking analysis (NTA) is a technique which uses Brownian-motion to enumerate the size of particles in a suspension [141]. We used NTA to characterize the size range of CNS tissue-derived EVs. Sample output plots of concentration versus particle size demonstrated that both NonTg and SOD1^{G127X} exosome populations had heterogeneous size profiles, with the existence of multiple subpopulations as indicated by several peaks in the plot **(Figure 2.8A)**. The

subpopulations observed in SOD1^{G127X} samples were slightly higher than those in NonTg samples. To gain an overall perspective of the particle diameter of isolated EVs, we graphed the mean and mode particle diameters for each sample. The exosome pellet contained particles with a mean diameter of ~150 nm, while the mode size, the size of particle most frequently occurring in the population, was ~115 nm **(Figure 2.8B)**, both of which are consistent with previously reported values for exosomes [99]. Microvesicles were more heterogeneous, and displayed a larger size range **(Figure 2.8A,B).** However, the mean and mode particle diameters of microvesicles were only slightly higher than that of exosomes at ~200 nm and ~130nm respectively. These data show that both exosomes and microvesicles isolated from CNS tissues of ALS mouse models and controls using the described protocol are within the range identified in published findings for EVs. However, the degree of overlap in vesicle size between exosomes and microvesicles suggests that some portion of the exosome population may potentially be isolated with microvesicles, or vice versa.

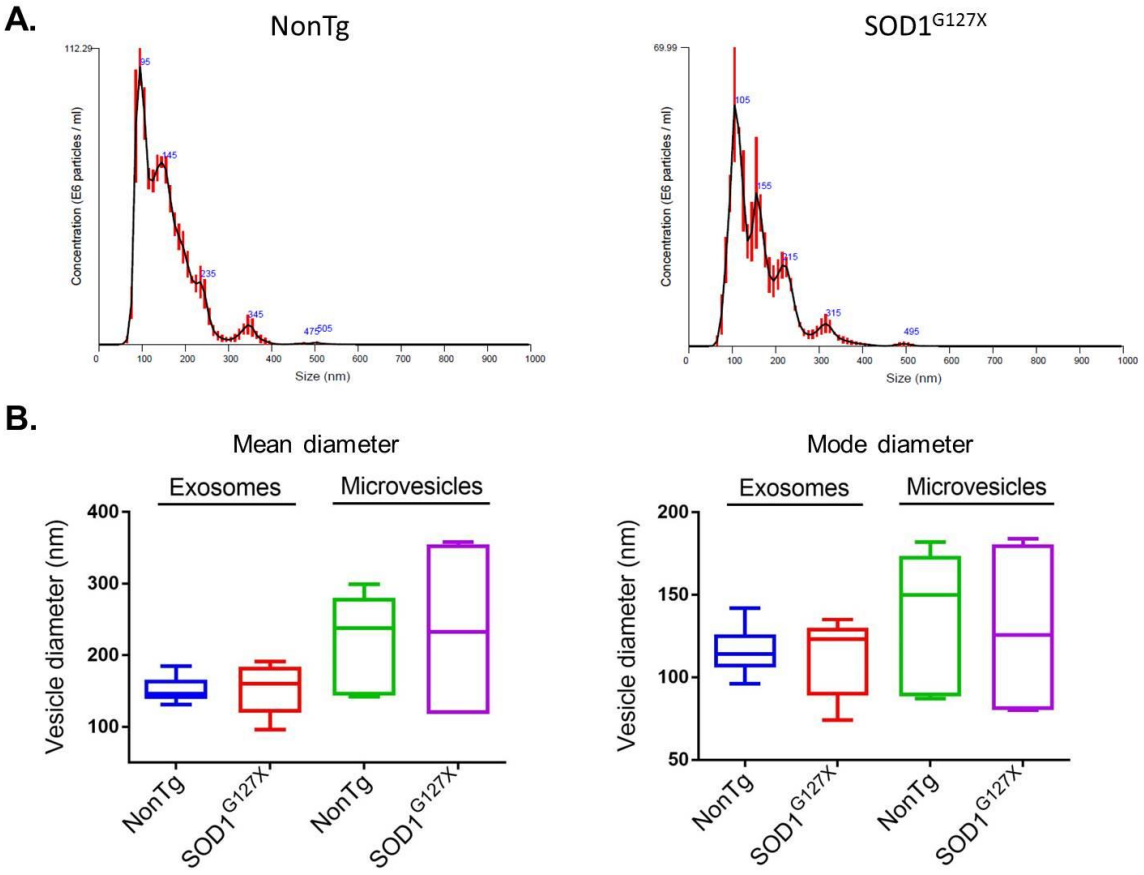

Figure 2.8 Size characterization of EV populations.

A. Mean vesicle diameter of CNS-derived EVs show a larger size range of particles is encompassed in the MV population compared to exosomes (N=7 brains for exosomes, N=4 brains for microvesicles). No significant differences were observed among groups. **B.** Mode vesicle diameter of brain-derived EVs indicates that the most frequently occurring particle size overlaps between exosomes and MVs (N=7 brains for exosomes, N=4 brains for microvesicles). Differences among groups were not significant following analysis by 2-way ANOVA and Tukey's multiple comparisons test.

2.3.9 Particle characteristics

We next characterized multiple parameters of the exosome and microvesicle populations at the individual particle level by correlating total protein content of vesicles to particle size and concentration. Since, to our knowledge, there are no other studies in literature which characterize both tissue-derived exosomes and

microvesicles, identifying particle characteristics in these populations would add useful information for future investigations on these EV subpopulations.

The gross sample pellet obtained from the microvesicle isolation step at 10,000 x *g* was visibly larger than exosome pellets prepared from the same volume of CNS tissue, and unsurprisingly, its total protein content was also significantly higher than that of exosomes **(Figure 2.9A)**. There were no significant differences in amount of total protein content between EVs isolated from $SOD1^{G127X}$ mice relative to NonTg mice, in both EV populations **(Figure 2.9A)**. This indicates that the isolation protocol produces consistent preparations of EVs with comparable yield between genotypes.

However, NTA showed that exosome samples contained higher numbers of particles per unit volume with 60 and 45 x 10^{11} particles/mL for NonTg and $SOD1^{G127X}$ exosomes, relative to microvesicles at 20 and 19 x 10^{11} particles/mL for NonTg and $SOD1^{G127X}$ samples **(Figure 2.9B)**. The difference in particle concentration between NonTg exosomes and both NonTg and $SOD1^{G127X}$ microvesicles were significant **(Figure 2.9B)**. Within each EV population, there was no significant difference between genotypes. This data demonstrate that although a larger amount of protein material is present in microvesicles, exosomes have a higher number of individual particles in the same volume of sample.

Consistent with the above findings, exosome samples showed a significantly higher amount of particles per mg of total protein in comparison to microvesicles **(Figure 2.9C).** When the inverse relationship of protein per particle was explored, microvesicles displayed a higher mg protein content per particle **(Figure 2.9D).** These results suggest that higher numbers of vesicles are present in the exosome fraction, but that each individual vesicle in the microvesicle sample contains a larger quantity of protein. Some caution should be taken in attributing protein content to

individual vesicles however, since potential extra-vesicular soluble protein in the preparation would also be detected by total protein quantitation.

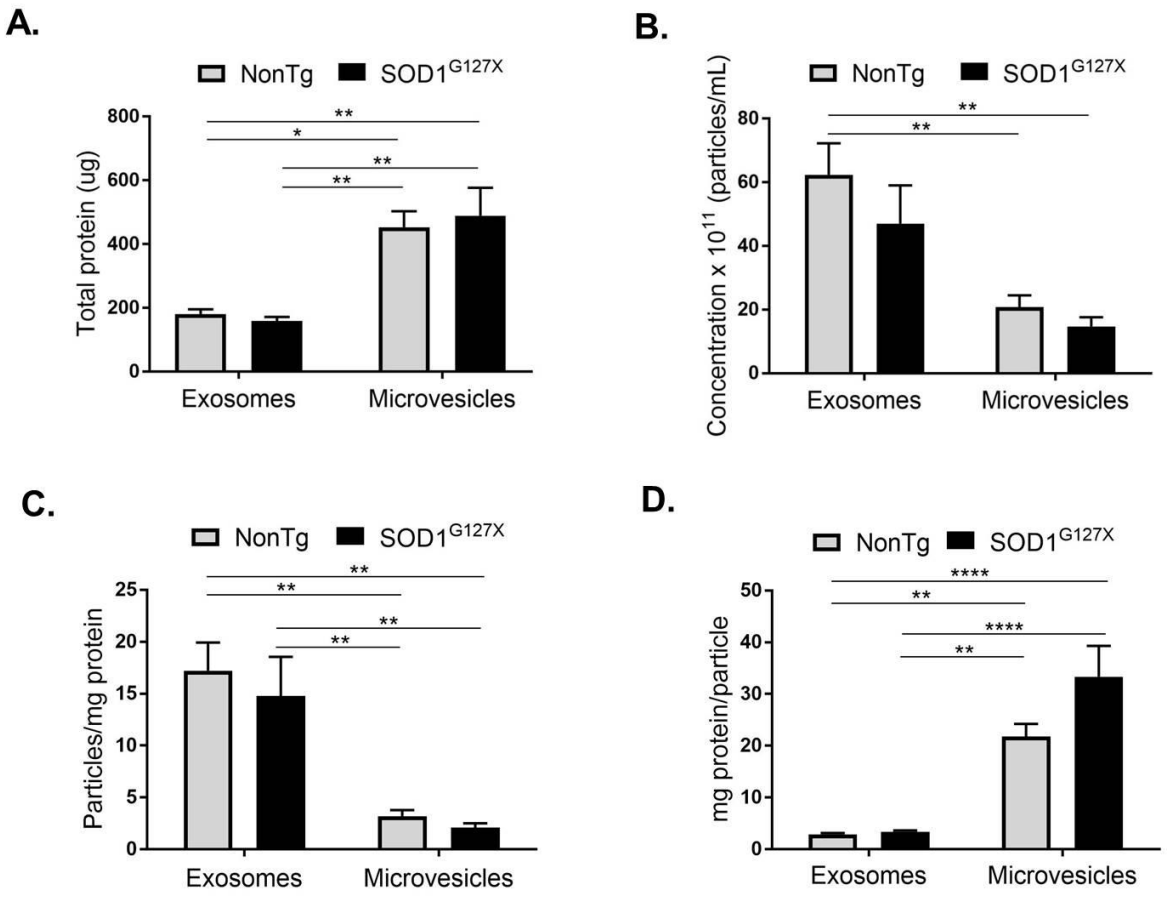

Figure 2.9 Correlation between total protein content and particle concentration of EV populations

A. The total protein yield for exosome and microvesicle pellets did not differ significantly between SOD1^{G127X} and NonTg animals. The microvesicle pellets isolated from both SOD1^{G127X} and NonTg animals are significantly higher (**p<0.005, *p<0.05) in protein content than the exosome pellets (N=9 exosomes, N=11 microvesicles) **B.** Exosome samples contain higher numbers of particles per unit volume relative to microvesicles (**p<0.006) (N=7 exosomes, N=8 NonTg microvesicles, N=6 SOD1^{G127X} microvesicles). Within each EV population, there was no significant difference between genotypes. **C.** Exosomes demonstrate a significantly higher amount of particles/mg of total protein relative to microvesicles (**p<0.008). **B.** Microvesicles have a higher amount of total protein per particle relative to exosomes (**p<0.05, ****p<0.0001). There was no significant differences between genotypes. Statistical analysis of **A-D** conducted with 2-way ANOVA followed by Tukey's multiple comparisons test.

2.3.10 Enrichment of beta-actin

The ability to distinguish between EV subtypes is important when studying differences in various EV populations, and currently there is a lack of established protein or nucleic acid markers which reliably do so [114]. In our hands, when probing for protein markers and using β -actin as a loading control, we observed that β-actin was consistently enriched in exosome samples. Indeed, when equal amounts of total protein content were loaded and microvesicles and exosomes were compared side-by-side, exosomes displayed enrichment of β-actin relative to microvesicles and whole-brain homogenate **(Figure 2.10).** This data suggest that β-actin could potentially be used as a marker for distinguishing between CNS tissue-derived exosomes and microvesicles. It also indicates that β-actin should not be used as a loading control in EV preparations, at least in tissue-derived EVs, since it may not accurately reflect the total protein content of exosomes. SOD1 or a similar soluble protein marker should be used instead.

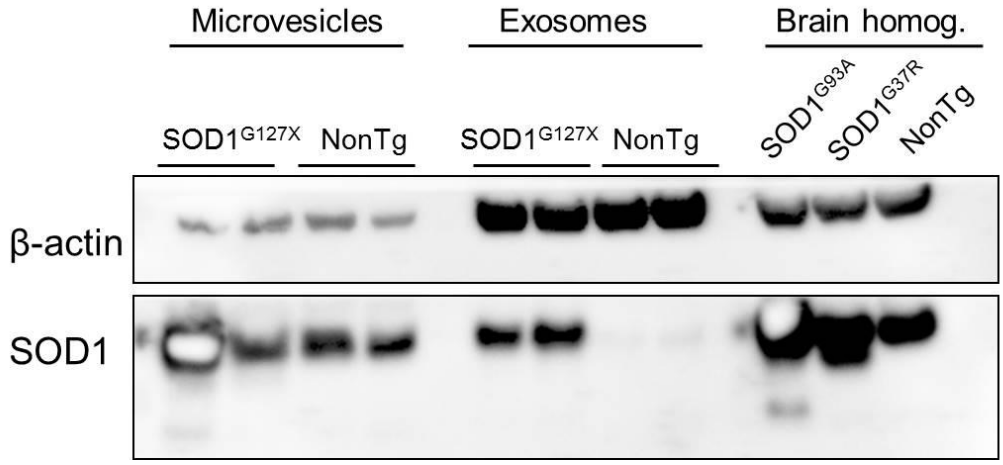

Figure 2.10 Exosomes and microvesicles show differential enrichment of β-actin.

Exosomes isolated from $SOD1^{G127X}$ and NonTg brain tissues show higher levels of β-actin relative to microvesicles and whole-brain homogenate when 30 ug of total protein is loaded. Similar levels of SOD1 are seen in both exosomes and microvesicles, although NonTg exosomes do not show a SOD1 signal.

2.4 DISCUSSION

In addition to the active release of EVs, cells passively release protein aggregates, membrane complexes, and RNA material, especially when undergoing cell death [148]. Other vesicle types originating from within the cell are also released during cell membrane lysis. These contaminating materials can co-sediment with EVs during the centrifugation process. Sucrose density purification has been shown to separate these components from cell culture-derived EVs; exosomes have been shown to reach equilibrium at 1.12 to 1.19 g/mL sucrose, endoplasmic reticulum vesicles at 1.18 to 1.25 g/ml, Golgi-derived vesicles at 1.05 to 1.12 g/ml, and protein aggregates at 1.22 g/ml [148-150]. From our findings, it is apparent that sucrose purification of tissue-sourced EV preparations is essential for removing non-vesicular material. When analyzing our crude EV pellets before the sucrose density step by TEM, we observe the presence of extravesicular material and debris **(Figure 2.4)**. These components are largely reduced following sucrose density purification, and a more homogeneous population of spherical, cup-shaped structures are visible by TEM.

We also demonstrated that our optimized isolation protocol can be used to obtain two different CNS-derived EV subpopulations (exosomes and microvesicles) characterized by the presence of known EV-associated protein markers, and with morphology and size range consistent with published findings for EVs **(Figure 2.6, Figure 2.7,Figure 2.8)**. One of the major challenges in EV-related work is the inability to discriminate reliably between exosomes and microvesicles, and the entire field is at an early stage in the process of being able to consistently define the two populations based on intrinsic characteristics such as size, morphology, buoyant density, or protein and nucleic acid cargo [99]. Some groups have found different morphologies and distribution of RNA, genomic DNA, and lipid content among these groups, indicating that differential sorting mechanisms might be at play in subpopulations of EVs [131, 151, 152]. However, the broad application of these

findings to distinguish EVs originating from many different cell types is yet to be tested.

The protein markers we probed for and detected in tissue-derived EVs did not vary widely between exosomes and microvesicles **(Figure 2.7A,B)**. The same is true for morphology, and mean and mode size **(Figure 2.6, Figure 2.8)**, indicating that, overall, exosomes and microvesicles isolated from CNS tissues have a high degree of overlap. This finding suggests that the biology of the two EV subtypes do not differ significantly from each other. Microvesicles isolated with this protocol could therefore potentially be used interchangeably with exosomes under certain parameters. This is of significance since a major barrier in the EV field is the limited amount of exosome sample obtained from isolation protocols. As we have shown, the microvesicle population is both higher in protein content **(Figure 2.9A)** and in the size range of isolated vesicles **(Figure 2.8B)**, indicating not only a higher abundance of protein in the microvesicle pellet, but also that microvesicles may contain physiological important subpopulations of vesicles that are potentially excluded in the exosome pellet.

There are currently very few markers which specifically distinguish exosomes from microvesicles, and the ability to separate EV subtypes based on cargo is important for studies that explore differences in EV populations [114]. We have found here that CNS tissue-derived exosomes from mice are enriched in β-actin relative to microvesicles and whole brain homogenate **(Figure 2.10)**. Recent work has shown that cortactin, an actin-binding protein, plays a role in late-endosomal trafficking and exosome secretion, consistent with the finding that actin is specifically enriched in exosomes [153].

It has become increasingly apparent that the methodology used to isolate EVs should be carefully considered when analyzing EV-associated protein content. High-

throughput proteomic studies on EVs have identified several thousand EV cargo proteins, which are catalogued in a database termed EVpedia (http://evpedia.info)[121, 154]. Although there is a common set of EV-associated cargo proteins, the protein content detected by different research groups and from different studies varies widely [155]. There are several possible explanations for this, including a cell-type specificity of EV cargoes, and the active versus resting state of the secreting cell [99]. Recently, many groups have also found that the isolation technique can heavily influence proteomics studies [155]. In support of this finding, we detected digestion of EV-associated proteins with the use of papain, the enzyme used in the original published protocol by Perez Gonalez *et al.* [135]. We subsequently used a milder digestive enzyme, collagenase III, which caused relatively less digestion of EV-associated proteins β-actin and PrP **(Figure 2.2)**. Based on this information, we suggest that future work conducted on tissue-derived EVs test out several different digestion enzymes, especially for applications such as mass spectroscopy, since it is possible that false negatives are given because of enzymatic digestion of EV-associated proteins.

Finally, our results indicate that there are no significant differences between $SOD1^{G127X}$ and NonTg EVs in all EV-associated criteria investigated here, including particle concentration **(Figure 2.9B)**. There is some evidence that in neurodegenerative diseases like ALS, there is an increased release of exosomes [130, 156]. In our hands, we don't see this effect in mouse models of ALS. However, ALS mouse models display muscle wasting as a symptom inherent to their condition, and our protocol uses whole brains or spinal cords from both NonTg and diseased animals. For a fair comparison, future results should be normalized to tissue weight.

An implication of this work is that EVs isolated from affected neural tissues, as opposed to cerebrospinal fluid (CSF) or other biofluids, can be used to pre-screen potential biomarkers of disease. Exosomes isolated from urine and plasma have been shown to carry tumour-specific cargoes in several different cancer types, and

many researchers in the field hypothesize that EVs carrying misfolded proteins can be used to identify neurodegenerative diseases [90, 157-159]. Isolating EVs directly from affected tissues or tissues with disease pathology makes it less likely that non-pathological EVs would dilute or obscure disease effects. Therefore, screening for the appearance of pathological markers in tissue-sourced EVs may help identify diagnostic or disease-specific markers which can subsequently be probed for in CSF, plasma, or other biofluids.

In summary, we demonstrate a protocol for isolating EVs from whole neural tissues, adapted from a published study and optimized for the isolation of two subpopulations of EVs from ALS mouse models and corresponding NonTg controls. To our knowledge, this is the first study which characterizes both exosomes and microvesicle populations isolated from solid tissues, and as such, provides a more detailed and expanded understanding of these EV subtypes. Future studies should be conducted to fully characterize EVs isolated from spinal cord tissues to determine if they are similar to brain-tissue derived EVs. Since the anatomic region most affected in ALS and the one presenting the most pathology is the spinal cord, it would be interesting to determine if any disease-specific differences exist in spinal cord EV populations.

CHAPTER 3. MISFOLDED SOD1 CARGO IN EXOSOMES AND MICROVESICLES FROM ALS MOUSE MODEL TISSUES

3.1 INTRODUCTION

Although SOD1 is located predominantly in the cytosol, there is evidence to show that a portion of total SOD1 is present in the extracellular space, and has potential functional roles in cell signaling and other pathways [160]. Extracellular SOD1 has been shown in a number of different cell types including the mouse motor neuron-like NSC-34 cells, primary spinal cord cultures, the neuroblastoma cell line Neuro2A, human embryonic kidney (HEK) cells, and cultured primary astrocytes [83, 156, 161-163]. SOD1 has also been detected in cerebrospinal fluid (CSF) from ALS patients with and without SOD1 mutations, indicating that extracellular SOD1 may be relevant to all subtypes of ALS [164, 165]. However, it is unclear whether extracellular SOD1 is beneficial to cells by eliminating extraneous protein and exerting neuroprotective effects, or whether it is deleterious and has toxic effects such as seeding prion-like propagation of protein misfolding [86, 160, 161, 166, 167]. Some groups show microgliosis and motor neuron death when SOD1 is secreted in association with chromogranins [161, 162]. Others have demonstrated that exogenous mutant SOD1 is not directly toxic to motor neurons, but mediates neurodegeneration via glial activation [72, 168]. An impaired secretion of mutant SOD1 relative to wild-type was also shown [161]. These reports demonstrate the need for a better understanding of extracellular SOD1 in ALS, as well as in normal physiology.

The pathway through which SOD1 is secreted from cells is unknown. SOD1 lacks a signal peptide targeting it for secretion via the classical ER-Golgi secretory pathway. However, there is some evidence of a fraction of SOD1 being secreted via the ER-Golgi pathway in a brefeldin A-sensitive manner [161]. Others argue that brefeldin-A also interferes with alternative secretory pathways, and that SOD1 trafficking bears

resemblance to secretion of interleukin 1β, fibroblast growth factor, and other proteins which also lack signal peptides via an ER-independent unconventional secretory pathway [169].

Parallels to extracellular SOD1 can be drawn from studies conducted on α-synuclein, a pivotal player in the pathology of Parkinson's disease (PD), and whose biology and secretion mechanisms have been heavily investigated [170]. Like SOD1, it is a soluble cytosolic protein known to be secreted from healthy and diseased cells alike, and is increased in stress conditions such as lysosomal, mitochondrial and endoplasmic reticulum dysfunction, or oxidative stress [170]. Consistent with transport through a non-ER pathway, extracellular α-synuclein has been found localized to exosomes [171]. Because of the similarity between α-synuclein and SOD1, it is reasonable to hypothesize that EVs are a potential pathway for SOD1 release as well. Consistent with this hypothesis, two different reports showed that wild-type SOD1 is secreted in association with exosomes [84, 130]. More recently, using an *in vitro* model of ALS expressing mutant SOD1, Grad *et al.* demonstrated that released exosomes possess surface misfolded SOD1 protein [84, 172]. Basso *et al.* subsequently showed that astrocytes overexpressing $SOD1^{G93A}$, a FALS-associated SOD1 mutant, had an increased release of exosomes relative to astrocytes derived from non-transgenic animals, indicating potential functional implications for EV-associated SOD1 [156]. Despite these reports in cell culture models, foundational studies into the *in vivo* relevance of extracellular mutant SOD1 in EVs have yet to be conducted.

In this study, we probed vesicles derived from an *in vivo* environment, the extracellular space of the ALS mouse model CNS, for the presence of mutant misfolded SOD1. We then further investigated the uptake and toxicity of SOD1-bearing extracellular vesicles on recipient cells. The results of this chapter aid our understanding of the role EVs play in trafficking of SOD1 from cells both in disease

and healthy states, and provide insight into the potential use of EV-associated SOD1 as a biomarker and therapeutic target in ALS.

3.2 METHODS

3.2.1 EV ISOLATION

Frozen brain or spinal cord tissues from mice were finely sliced in Hibernate A medium (Brain Bits, Springfield, IL), added to a pre-warmed solution of Hibernate A containing 125 U/mL Collagenase III to digest the extracellular matrix, and incubated with shaking at 37°C for 15 minutes. Enzymatic digestion was stopped by adding ice-cold Hibernate A containing Protease Inhibitors (EDTA-free protease inhibitor cocktail; Roche Diagnostics, Switzerland). The mixture was centrifuged at 300 x *g* and subsequently at 2000 x *g* to remove cells and cellular debris. Microvesicles were isolated by centrifuging the supernatant at 10,000 x *g* for 30 min. Exosomes were isolated by centrifuging the resultant supernatant at 100,000 x g for 90 min. All ultracentrifugation steps were performed using the Beckman Coulter Type 70Ti Rotor (Break, CA) at 4°C. A sucrose cushion was then used to purify the pelleted EVs. 0.95 M sucrose for exosomes or 1.3 M sucrose for microvesicles was layered on top of 2M sucrose in a 1.5mL ultracentrifuge tube (Beckman, CA). The EV pellet from the ultracentrifugation step was diluted in PBS, top-loaded onto the cushion, and centrifuged for 2 h at 20,000 x *g* for the MV pellet, or 150,000 x *g* for the exosome pellet. The 700 µL fraction at the interphase between the 2 sucrose densities was collected into a fresh tube, and spun down for 1 h at 10,000 x *g* for microvesicles and 100,000 x *g* for exosomes to isolate the purified vesicle pellet.

3.2.2 CELL CULTURES

Human embryonic kidney cells (HEK293FT; ATCC, Manassas, VA) were cultured in complete medium (Dulbecco's Modified Eagle Medium (DMEM) with 10 % FBS, 10 U/ml penicillin, 10 U/ml streptomycin and 2 mM L-glutamine (Life Technologies,

Carlsbad, CA)). NSC-34 cells stably expressing HuWTSOD1 were cultured in complete media with 300 µg/mL G418 sulphate (Millipore) to induce expression of the HuWTSOD1 gene. Biological repeats were performed on separate days on different passages of cells and using EVs isolated from different animals.

3.2.3 IMMUNOPRECIPITATION

Cells were washed twice with PBS, harvested in PBS, and transferred into a microcentrifuge tube and centrifuged at 3000 x *g* to pellet cells. Cells were lysed in 400 µL of lysis buffer (PBS, 0.5% sodium deoxycholate (DOC), 0.5% Triton X- 100, and complete EDTA-free protease inhibitor mixture; Roche Diagnostics) for 2 min on ice. 100 µL of each cell lysate and 10 µL of antibody-coupled M-280 Tosyl-activated magnetic Dynabeads (ThermoFisher Scientific) were mixed and incubated for 3 h at room temperature with constant rotation. Beads were washed three times in 150 µL of RIPA buffer (150 mM NaCl, 50 mM Tris-HCl (pH 8.0), 1% Nonidet P-40, 0.5% DOC, and 0.1% SDS) and boiled in SDS sample buffer containing 1% β-mercaptoethanol for 5 min. As a pre-IP control, 1 µL of cell lysate was prepared in SDS sample buffer as described.

3.2.4 MISFOLDED SOD1 ELISA

96-well Nunc ELISA plates (ThermoFisher Scientific) were coated with 36.9 µg/mL of the anti-misfolded SOD1 monoclonal antibody 3H1 overnight at 4°C. Plates were washed with wash buffer (Tris-buffered saline (TBS) containing 0.05% Tween-20), and blocked with TBS + 1% BSA for 1 h at room temperature. Samples were prepared by measuring total protein concentration using the Pierce BCA Assay Kit (ThermoFisher Scientific). Equal protein concentrations of intact EVs, EVs lysed in PBS + 1% Triton-X 100, or cell lysates were added to the plate and incubated for 1 h at room temperature. Plates were washed with wash buffer and incubated with rabbit polyclonal anti-SOD1 antibody at room temperature for 1 h. Finally, the plate was washed and incubated with horseradish peroxidase (HRP)-linked anti-rabbit IgG

antibody for 1 h at room temperature, followed by a final wash, and incubated with SuperSignal™ ELISA Femto chemiluminescent substrate (ThermoFisher Scientific) for 5 min at room temperature. Total chemiluminescence at all wavelengths was read using a SpectraMax M2 microplate reader (Molecular Devices, CA).

3.2.5 PKH67 LABELING OF EVS

CNS tissue-derived EVs were labeled using the PKH67 green fluorescent cell linker kit (Sigma-Aldrich) according to manufacturer's instructions. Briefly, EVs were re-pelleted at 150,000 x *g* for 60 min and resuspended in 500 µL of Diluent C. In a separate microcentrifuge tube, 4 µL of PKH67 dye was diluted in 500 µL of Diluent C and mixed well. The contents of the two tubes were then mixed together by pipetting up and down, and incubated for 5 min at room temperature. The mixture was subsequently incubated with 500 µL of 3% BSA and centrifuged at 150,000 x *g* for 60 min. The resulting supernatant was washed by resuspending the pellet in PBS and centrifuging once more at 150,000 x *g* for 60 min. The final washed pellet was resuspended in 50 µL of PBS, and the protein concentration determined by BCA assay (ThermoFisher Scientific). HEK293 cells or NSC-34 cells stably expressing HuWTSOD1 were incubated with 0.1 µg/mL labeled EVs for 24 h, fixed, and analyzed by confocal microscopy.

3.2.6 CONFOCAL MICROSCOPY

Confocal images were captured with a Leica TCS SP8 scanning confocal microscope (Leica Microsystems, Wetzlar, Germany) using LAS-X software. Images were focused using the DAPI signal, and by making minor focal modification to capture signal emitted at 488 nm (PKH67 signal) [143].

3.2.7 Cytotoxicity assay (lactate dehydrogenase)

The levels of lactate dehydrogenase (LDH) in the supernatant were assayed using a LDH assay kit (Thermo Fisher). Cells treated with 1% Triton X-100 were used as a positive control for maximum LDH release, and untreated cells for background LDH release.

3.2.8 Cell viability assay (alamar blue)

Viable cell numbers were determined by a resazurin reduction assay termed Alamar Blue (ThermoFisher Scientific). HEK or NSC-34 cells were seeded onto 24 well plates and allowed to reach ~60% confluency. EVs were added at the doses indicated, and incubated for 24 h at 37 °C in 5% CO2. Alamar Blue reagent was added according to manufacturer's instructions. Cells were incubated with reagent for 30 min at 37 °C and fluorescence readings were taken at 590 nm using a microplate reader (Tecan, Mannedorf, Switzerland). Samples were assayed in triplicates.

3.2.9 Immuno-electron microscopy

Suspensions of EVs were diluted 200-fold in 2% PFA in filtered PBS to lightly fix, and 5 µl pipetted onto formvar-coated 200-mesh nickel grids (EM Sciences). Material was allowed to adhere to the grids for 20 min before excess liquid was wicked off. The following was performed in a humidity box at room temperature using paper-filtered PBS or water: grids were blocked in 1% milk in PBS for 10 min; incubated in 3H1 primary antibody 20 µg/ml in 1% milk PBS for 2 h; washed x 3 briefly in PBS; incubated in anti-mouse secondary antibody conjugated to 15 nm gold bead (EM Sciences), 1:30 in 1% milk PBS with 0.05% polyethylene glycol, for 1 h; washed x 3 briefly in PBS; post-fixed with 1% glutaraldehyde in PBS for 5 min; washed x 2 in PBS; washed x 3 in distilled filtered water; counterstained in filtered

1% aqueous uranyl acetate for 5 min, and allowed to dry. Grids were viewed on a Tecnai G2 Spirit Transmission Electron Microscope (FEI, Hillsboro, OR).

3.2.10 Statistical analysis

All data were analyzed using GraphPad Prism version 6.00 for Windows (GraphPad Software, La Jolla, CA). Statistical analysis performed is indicated in figure captions. One-way ANOVA was performed followed by Kruskal-Wallis or Mann-Whitney-U tests. Two-way ANOVA was performed followed by Tukey's or Sidak's post-tests. All data is presented as mean ± SEM.

3.3 Results

3.3.1 CNS tissue-derived EVs are immunopositive for misfolded SOD1

We first looked at surface levels of misfolded SOD1 on intact CNS tissue-derived EVs using monoclonal antibodies (3H1 and 10C12) directed against conformation-specific epitopes on misfolded SOD1 protein. 3H1 and 10C12 antibodies bind distinct epitopes on the misfolded SOD1 protein which are only exposed when the protein is misfolded **(Figure 3.1)**. They do not recognize natively folded endogenous SOD1 protein, and have been characterized in work previously published by our group [83].

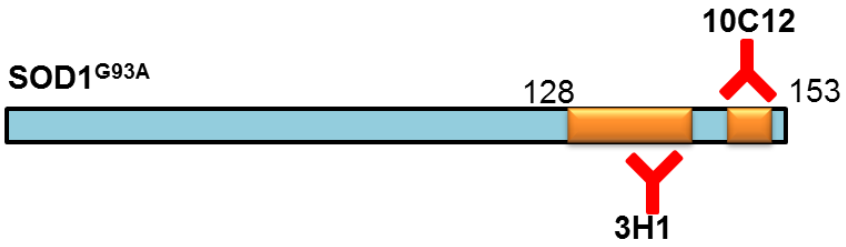

Figure 3.1 Conformation-specific antibodies identify full-length misfolded SOD1.

SOD1^{G93A} transgenic animals express a full-length FALS-associated mutant SOD1 protein which contains epitopes for the monoclonal antibodies 3H1 and 10C12. 3H1 and 10C12 recognize aberrantly folded conformations of full-length SOD1, such as the mutant SOD1-G93A sequence.

Using 3H1 and 10C12, we performed immunoprecipitations on brain tissue-derived exosomes from SOD1^{G93A} animals which express a full-length FALS-associated mutant SOD1 protein, as well as NonTg control animals. We found that SOD1^{G93A} tissue-derived exosomes displayed immunopositivity for misfolded SOD1 with both 3H1 and 10C12 antibodies, but not with the mouse IgG2a isotype control **(Figure 3.2A)**. To quantify the results, the amount of misfolded SOD1 was normalized to the total immunoprecipitable SOD1 (pan-SOD1 signal in **Figure 3.2A**) by densitometry analysis. The % immunoprecipitable SOD1 was significantly higher with both 3H1 and 10C12 antibodies in SOD1^{G93A} exosomes relative to NonTg **(Figure 3.2B)**. Similar results were observed with spinal cord tissue-derived EVs **(Figure 3.2C,D)**. However, quantitation analysis showed that SOD1^{G93A} spinal cord-derived exosomes had a slightly lower proportion of 3H1 and 10C12 signal than did brain tissue-derived exosomes **(Figure 3.2D)**.

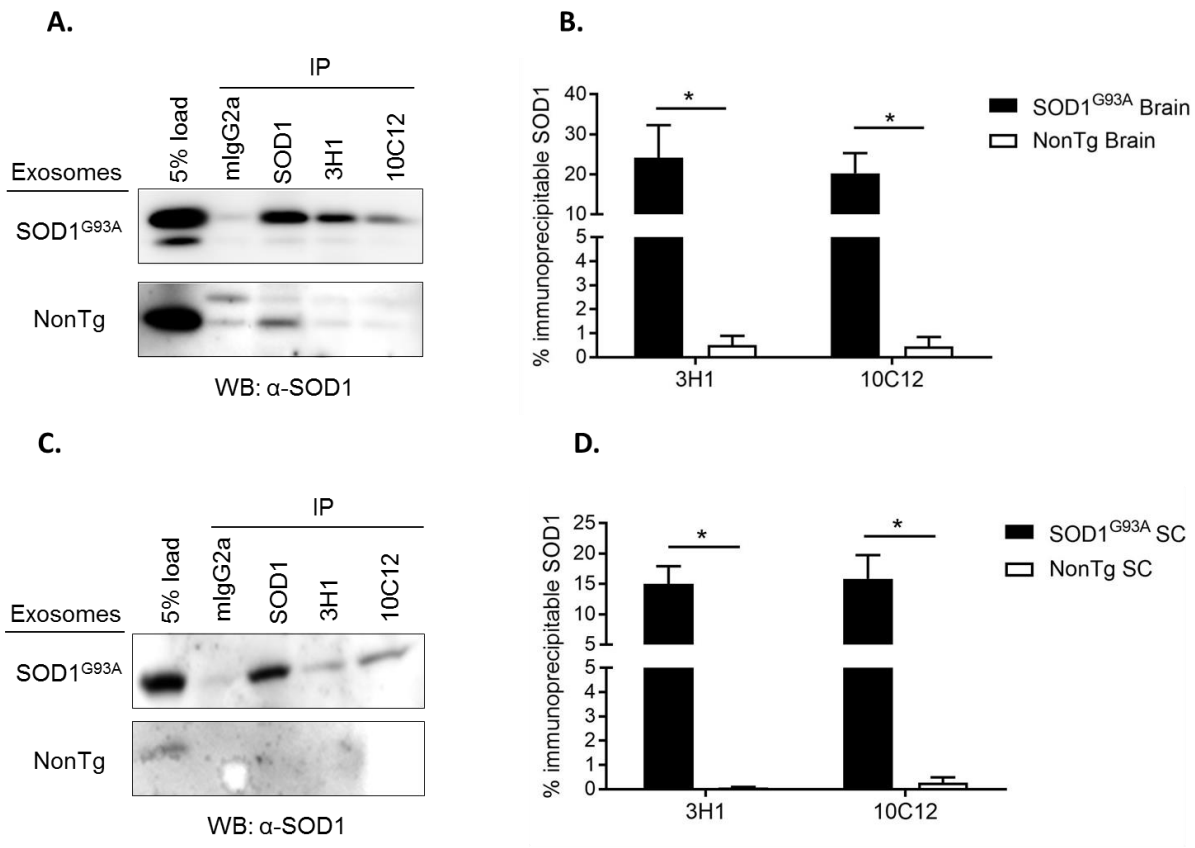

Figure 3.2 SOD1^{G93A} CNS tissue-derived EVs are positive for misfolded SOD1 by immunoprecipitation with 3H1 and 10C12.

Lysates of cells treated with SOD1^{G93A} exosomes were immunoprecipitated with 3H1 and 10C12. **A.** A representative immunoblot shows positive signal for both 3H1 and 10C12 in SOD1^{G93A}-treated cells, as well for a pan-SOD1 antibody. 5% Pre-IP load shows that similar amount of NonTg EV-treated cells were immunoprecipitated, but that these cells showed no signal for either 3H1 or 10C12. **B.** Quantification of multiple immunoprecipitation experiments shows that significantly higher levels of misfolded SOD1 are present in SOD1^{G93A} brain-derived exosomes relative to NonTg. (N=3, $p<0.04$) **C.** Results similar to the experiments with brain-tissue derived exosomes are observed in cells treated with spinal-cord tissue-derived exosomes, but to a lesser extent. 3H1 and 10C12 immunopositivity are observed in SOD1^{G93A} spinal cord exosome-treated cells, but not NonTg. **D.** Quantification of multiple experiments shows significantly higher misfolded SOD1 levels in SOD1^{G93A} spinal-cord exosome-treated cells relative to cells treated with NonTg exosomes. (N=3, $p<0.07$). All data in graphs were analyzed using a student's two-tailed t-test. Error bars ± SEM. (Experiment designed by Drs. Judith Silverman and Leslie Grad, performed by Dr. Leslie Grad)

3.3.2 THE SURFACE OF SOD1^{G93A} TISSUE-DERIVED EVS IS DECORATED WITH MISFOLDED SOD1

Since our CNS tissue-derived exosome preparations were shown to also contain some portion of soluble non-EV material **(Figure 2.7)**, we wanted to determine whether misfolded SOD1 was directly associated with EVs rather than with the soluble fraction. Previous work by our group demonstrated the presence of misfolded SOD1 on the surface of exosomes isolated from NSC-34 cells expressing FALS-associated SOD1 mutants [84]. To investigate surface misfolded SOD1 on CNS tissue-derived EVs, we performed immuno-EM using the misfolded SOD1-specific antibody 3H1.

Using this technique, we detected 3H1 immunopositivity in brain-derived microvesicles from SOD1^{G93A} mice, as evidenced by immunogold labeling on the outside edges of intact EVs. Following immunoEM, 62% of vesicles visualized in the SOD1^{G93A} microvesicle sample demonstrated 3H1 positivity, whereas none from the NonTg samples did. However, each vesicle only showed low amounts of surface labeling, ~1 bead/vesicle. Taken together, the above data demonstrate that individual SOD1^{G93A} microvesicles are immunopositive for surface misfolded SOD1.

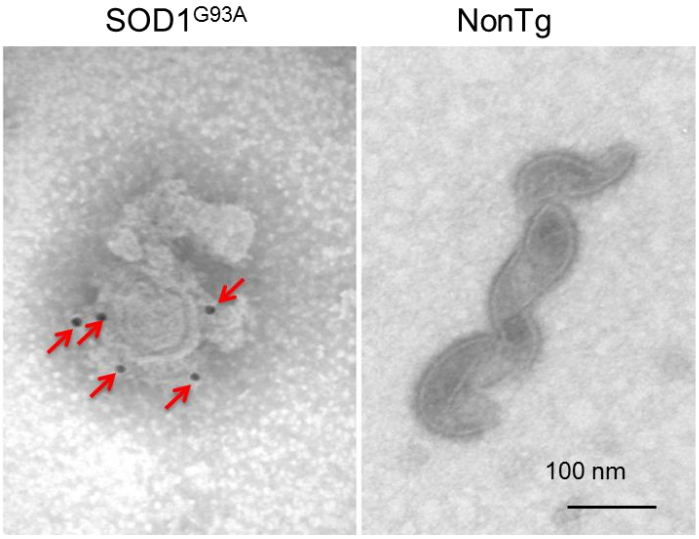

Figure 3.3 Individual CNS tissue-derived microvesicles from SOD1^{G93A} mice possess surface misfolded SOD1 cargo.

Immunopositive misfolded SOD1 labeling (red arrows) can be detected on the vesicle surface of a SOD1^{G93A} sample, but not NonTg, when immunogold labeled with 3H1 antibody and visualized with transmission electron microscopy. Images are representative of N=3 experiments. Scale bar=100 nm

3.3.3 A PROPORTION OF EV MISFOLDED SOD1 CARGO IS NON SURFACE-ASSOCIATED

We next performed shaving experiments to determine whether all or most of the misfolded SOD1 signal arising from CNS tissue-derived EVs is surface-associated. To do so, we digested the protein content of intact EVs and EVs lysed with Triton-X100, with proteinase K (PK). Following direct-immunoblot with 3H1 antibody of PK-treated and untreated control samples, we detected a portion of misfolded SOD1 remaining in EVs treated with PK alone **(Figure 3.4A)**. Triton-digested EVs showed total abrogation of 3H1 signal **(Figure 3.4A).** Direct-immunoblot of the same samples with β-tubulin showed that equal amounts of protein content were present in all samples. This data suggested that a greater proportion of misfolded SOD1 may be in the luminal compartment of SOD1^{G93A} CNS tissue-derived EVs relative to the surface.

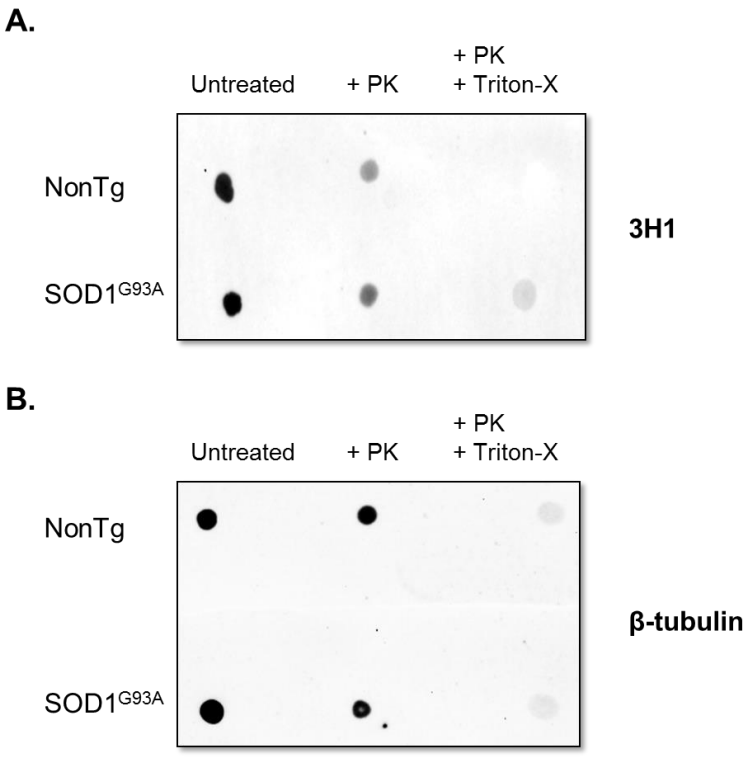

Figure 3.4 A proportion of EV misfolded SOD1 is non surface-associated.

A. Intact EVs and EVs lysed with Triton-X100 were treated with proteinase K (PK) to digest protein content. PK-treated and untreated control samples were immunoblotted with 3H1 antibody. PK-treated intact EVs (without Triton-X lysis) displayed lower levels of 3H1 signal relative to the untreated samples, suggesting that a portion of misfolded SOD1 is contained in the lumen of EVs and is protected from PK treatment. Triton-X treatment resulted in total, or near-total, loss of 3H1 signal in samples. **B.** Direct-immunoblot with β-tubulin, a luminal protein, of the same samples investigated in A. shows that equal amounts of protein content were present in samples, and that all signal is abrogated when the lumen is exposed. Images are representative of N=2 experiments.

3.3.4 The luminal compartment of SOD1^{G93A} CNS tissue-derived EVs is enriched with misfolded SOD1 cargo

In order to quantitatively assess relative levels of surface and luminal misfolded SOD1 in CNS tissue-derived EVs we used a sandwich ELISA system with 3H1 antibody as the capture and pan-SOD1 as the detection antibody. Using the 3H1 ELISA, we probed exosomes and microvesicles for misfolded SOD1 in the presence and absence of 1% Triton-X100, with Triton-X 100 being utilized to rupture the vesicle membrane. Exosomes from SOD1^{G93A} mice showed significantly higher levels of luminal misfolded SOD1 following Triton-X100 treatment, as detected with

3H1, compared to EVs from NonTg animals **(Figure 3.5A; p=0.0069)**. The same finding was true for microvesicles **(Figure 3.5B; p<0.02)**. Almost no misfolded SOD1 was detectable on the surface of $SOD1^{G93A}$ exosomes and microvesicles by the ELISA system; the large majority of the misfolded protein being in the vesicle lumen, and detectable only following lysis of the vesicular membrane.

Due to limitations in the abundance of exosome sample obtained via the isolation protocol, half the amount of exosomes relative to microvesicles was used in the ELISA. When we normalized the results to total protein concentration, and performed a side-by-side comparison, exosomes and microvesicles showed similar levels of luminal misfolded SOD1 **(Figure 3.5C)**. Taken together, our data demonstrate that both exosomes and microvesicles from the $SOD1^{G93A}$ mouse model contain luminal misfolded SOD1, with relatively low levels of the misfolded protein present on the vesicle surface.

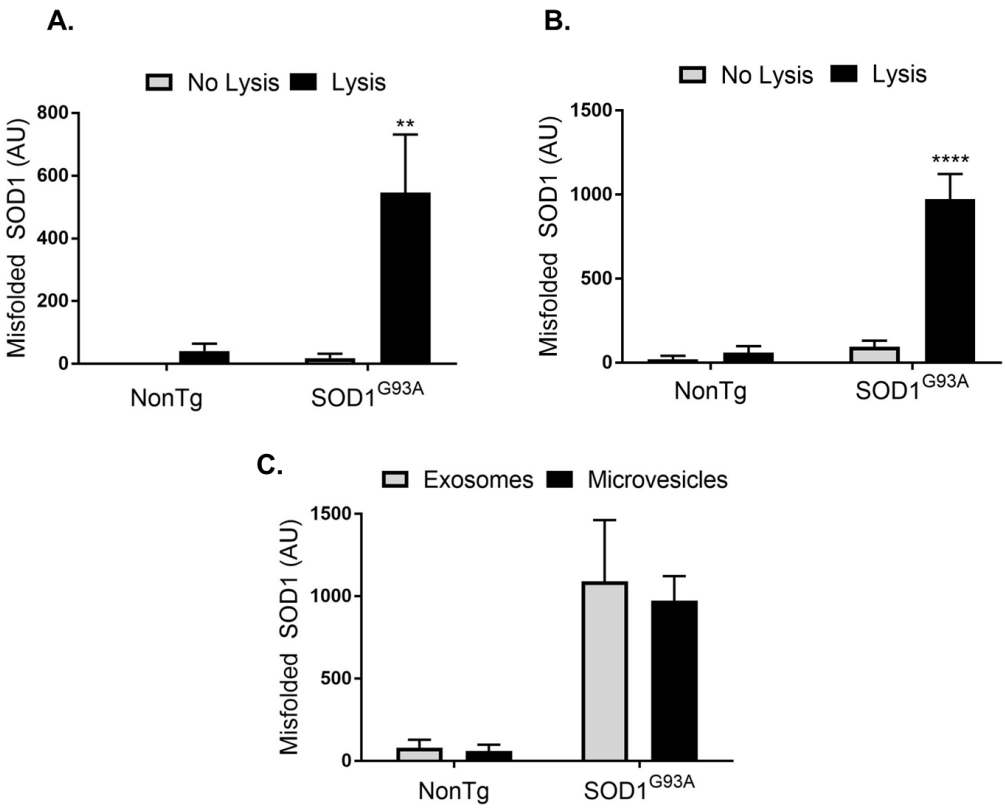

Figure 3.5 CNS tissue-derived exosomes and microvesicles SOD1^{G93A} mice contain luminal misfolded SOD1 cargo.

A. ELISA with 3H1 antibody shows presence of misfolded SOD1 in the lumen of SOD1^{G93A} exosomes, detectable following vesicle lysis with 1% Triton-X100, but not before (N=4 biological replicates, p=0.0084) **B.** Microvesicles from SOD1^{G93A} CNS tissue also carry luminal misfolded SOD1 detectable following vesicle lysis, at levels significantly higher than do NonTg microvesicles (N=6 biological replicates, p<0.0001) **C.** Following normalization to protein content loaded, detergent-lysed exosomes and microvesicles display similar levels of misfolded SOD1 (N=4-6 biological replicates). All data were analyzed by two-way ANOVA followed by Tukey's multiple comparisons test. Data showed as ± SEM.

3.3.5 CNS TISSUE-DERIVED EVS ARE EFFICIENTLY TAKEN UP BY CELLS

To determine if CNS tissue-derived EVs isolated from ALS mouse models and NonTg animals are functional and show uptake by recipient cells, we labeled exosomes with the membrane dye PKH67 and treated HEK cells and the murine neuroblastoma-spinal cord hybrid NSC-34 cells with labeled EVs. When incubated with exosomes for 24 hours, fixed, and visualized by single-focus-plane confocal microscopy, both HEK and NSC-34 cells treated with exosomes and microvesicles

showed similar patterns of uptake as indicated by the presence of green fluorescence in treated cells but not dye-only controls (**Figure 3.6**).

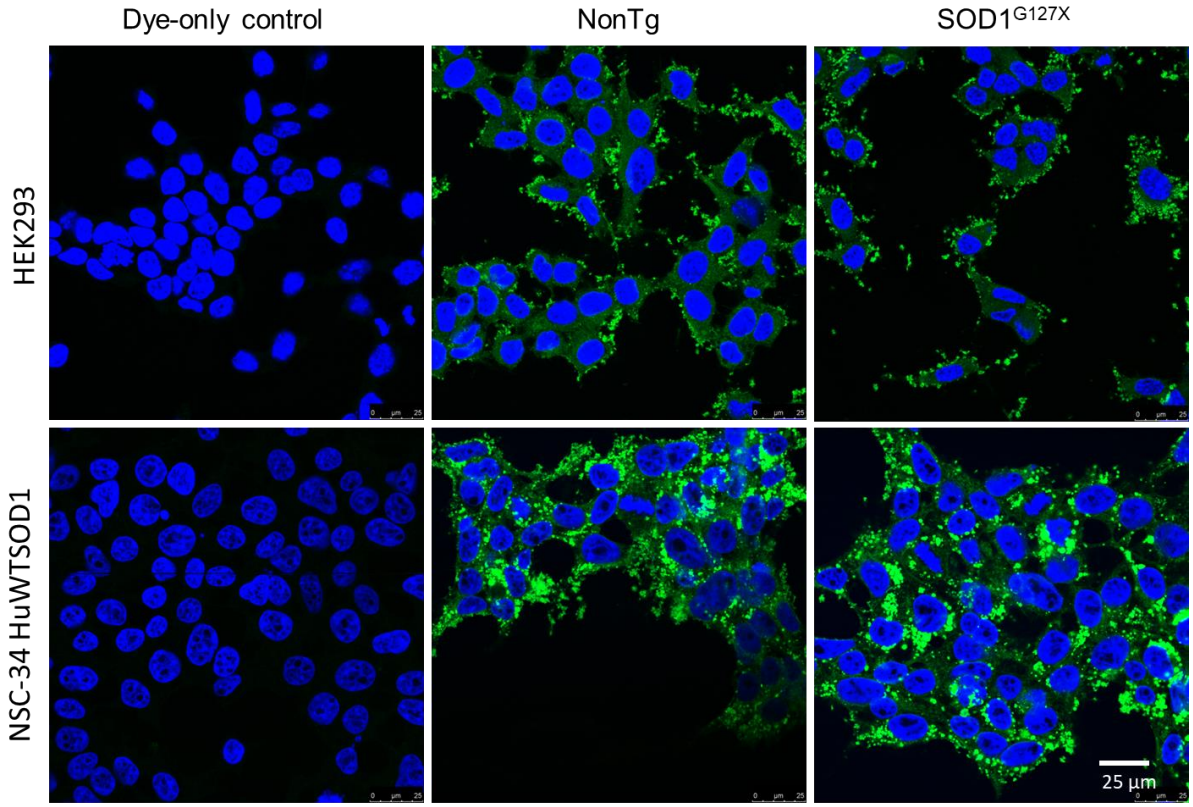

Figure 3.6 CNS tissue-derived EVs are efficiently taken up by cultured cells.

Human embryonic kidney (HEK293) and the mouse neuroblastoma-like cell line NSC34 show efficient uptake of PKH67-labeled tissue-derived microvesicles from both NonTg and SOD1^{G127X} transgenic animals as indicated by the presence of fluorescent green puncta in the area surrounding DAPI-positive nuclei when a single plane was visualized with confocal microscopy. Images representative of N=2 experiments.

At higher magnification, HEK cells treated with both PKH67-labeled NonTg and SOD1^{G127X} exosomes showed round, punctate green fluorescent labeling limited to the cell peripheries **(Figure 3.7)**. In contrast, EV-treated NSC34 cells showed intense punctate green fluorescence both at the cell periphery and within the apparent cell boundaries. In addition to the punctate signal indicative of intact vesicles or aggregates of vesicles, both HEK and NSC34 cells showed low levels of diffuse fluorescence with labeled EV treatment **(Figure 3.7)**. Diffuse labelling may be due fusion of CNS tissue-derived EVs with the recipient cell plasma membrane,

or alternatively, due to leakage of PKH67 dye onto the cell membrane. Both PKH67-labeled NonTg and SOD1^{G127X} exosomes showed relatively similar levels of interaction with recipient cells.

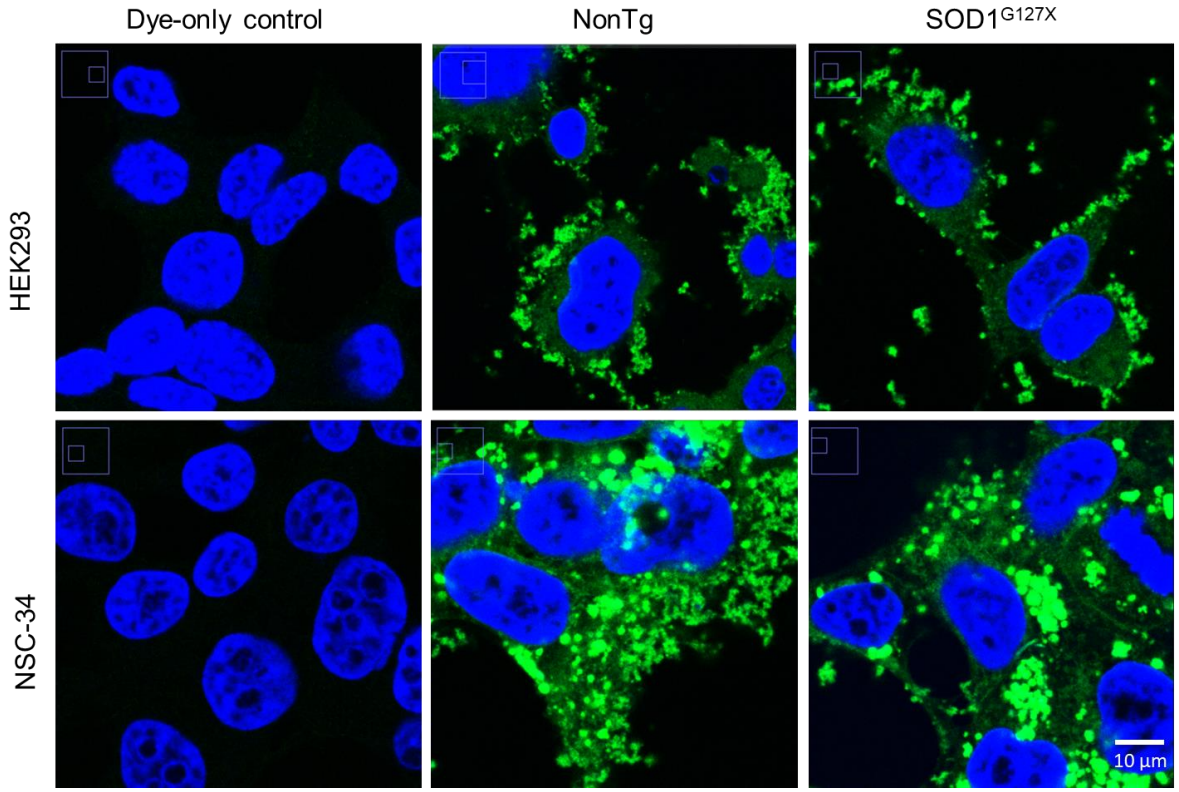

Figure 3.7 Higher magnification images show differential pattern of PKH67 labeling in HEK and NSC-34 cells

HEK cells treated with PKH67-labeled NonTg and SOD1^{G127X} exosomes show punctate green fluorescent labeling at cell peripheries, while cells treated with dye alone show no fluorescence **(top panels)**. Conversely, the mouse neuroblastoma-spinal cord hybrid NSC-34 cells show intense green fluorescent labeling of internalized PKH67-labeled exosomes in cell bodies as well as the periphery **(bottom panels)**.

3.3.6 CNS TISSUE-SOURCED EVS DO NOT CAUSE SIGNIFICANT DEATH IN RECIPIENT CELLS AND INCREASE CELL VIABILITY

The biological basis for selective motor neuron death in ALS is not currently understood. Many investigations into the selective toxicity of motor neurons, and other cell types, to different species of mutant and wild-type SOD1 have been conducted with varying results [73, 88, 173]. Here we sought to determine if EV-bound mutant SOD1 is toxic to HEK and spinal cord hybrid NSC-34 cells. To do so,

we treated both cell types with exosomes or microvesicles from SOD1^{G93A} and NonTg animals, and looked for toxicity and cell viability by lactate dehydrogenase (LDH) and Alamar blue assays, respectively. As a control, we also treated cells with equivalent protein amounts of the concentrated EV-depleted fractions from NonTg and SOG1^{G93A} animals remaining after EV isolation.

When analyzed by LDH, we did not detect significant levels of cell death in HEK or NSC34 cells treated with 100 µg/mL of NonTg or SOD1^{G93A} tissue-derived microvesicles **(Figure 3.8)**. In contrast, the same cells treated with concentrated EV-depleted fractions from both NonTg and SOD1^{G93A} EV preparations showed high levels of cytotoxicity. There were no differences between genotypes for either microvesicles or EV-depleted fractions with respect to toxicity on recipient cells. These results show that CNS tissue-derived EVs from SOD1^{G93A} animals bearing mutant misfolded SOD1 are not toxic to HEK and NSC-34 cells at a concentration upto 5 x higher than is typically used in literature for treatment of cells with exosomes [174-177]. Due to sample size constraints, dose-dependent cytotoxicity of EVs at multiple concentrations was not investigated in this study. However, in future investigations, several samples should be pooled, and a dose-response curve performed to determine concentration-dependent toxicity of EV-associated mutant SOD1 on cells.

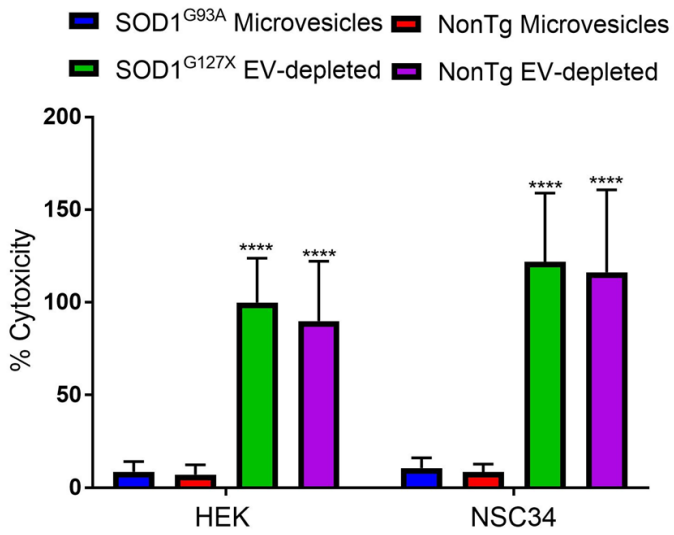

Figure 3.8 CNS tissue-derived EVs do not cause significant cytotoxicity in cultured cells.

HEK and NSC34 cells were treated with 100 µg/mL of SOD1^{G93A} or NonTg tissue-derived microvesicles, and levels of cell death in recipient cultures investigated by lactate dehydrogenase (LDH) assay. HEK and NSC34 cells treated with both NonTg or SOD1^{G93A} microvesicles showed ~10% cytotoxicity in HEK and NSC-34 cells by LDH. In contrast, the same cells treated with concentrated EV-depleted fractions from either NonTg or SOD1^{G93A} EV preparations showed significantly higher levels of cytotoxicity. N=4 brains per condition. ****p<0.001 Results were analyzed by 2-way ANOVA followed by Dunnett's multiple comparisons test.

To further these observations, we performed a cell viability assay using Alamar blue on HEK and NSC-34 cells treated with 50 µg/mL or 100 µg/mL of NonTg and SOD1^{G127X} CNS tissue-derived microvesicles. Alamar blue contains a cell-permeable, non-toxic, blue compound that is converted to a fluorescent signal in the presence of living cells. Surprisingly, HEK cells treated with both NonTg and SOD1^{G127X} microvesicles showed a significantly higher level of fluorescence by Alamar blue relative to untreated cells, indicating an increase in viability or proliferation in cultured cells **(Figure 3.9A)**. Similar findings were observed in microvesicle-treated NSC-34 cells **(Figure 3.9B)**. Consistent with our observations, some literature reviews have suggested that exosomes can trigger oncogenesis and tumour growth due to their ability to transfer nucleic acid and protein content between cells and cause cell proliferation [178]. Taken together, these results suggest that both NonTg and SOD1^{G127X} EVs do not cause significant cell death at

the treated doses, but instead cause some degree of increase in cell viability, and/or proliferation, of HEK and NSC-34 cells in culture.

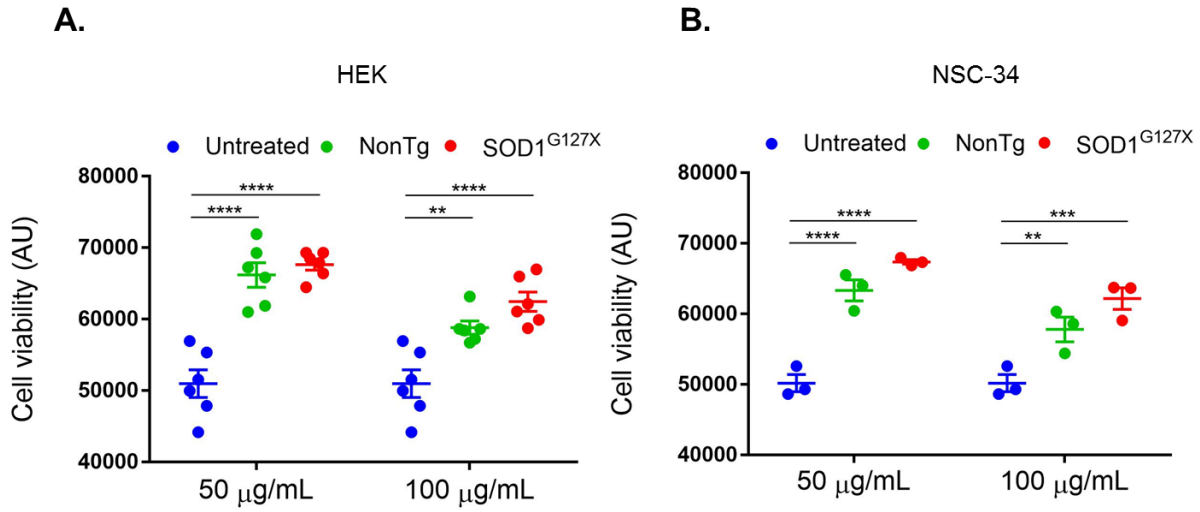

Figure 3.9 CNS tissue-derived EVs increase cell viability in recipient cultures.

A. When assayed by Alamar blue cell viability assay, HEK cells treated with 50 µg/mL or 100 µg/mL of NonTg and SOD1^{G127X} CNS tissue-derived microvesicles showed significantly higher levels of cell viability relative to untreated cells. (N=6, ****p<0.0001, **p<0.003) **B.** Similar results were observed in EV-treated NSC-34 cells relative to control untreated cells. (N=3, ****p<0.0001, **p<0.005). All data were analyzed by two-way ANOVA followed by Tukey's multiple comparisons post-test. Data is represented ± SEM.

3.4 DISCUSSION

Previously, Grad *et al.* demonstrated that exosomes secreted from cells expressing mutant SOD1 were decorated with surface misfolded SOD1 [84]. In support of, and further to this observation, we demonstrate here that EVs isolated from an *in vivo* environment of an ALS mouse model possess misfolded SOD1 cargo on the surface and within the luminal compartment. Brain and spinal cord tissue-derived exosomes from SOD1^{G93A} animals possessed surface misfolded SOD1 detectable by immunoprecipitation with 3H1 and 10C12 antibodies **(Figure 3.2)**. The misfolded SOD1 signal was confirmed to be EV-associated by immuno-EM of individual SOD1^{G93A} microvesicles with 3H1 antibody **(Figure 3.3)**. These results demonstrate that 3H1 and 10C12 antibodies are capable of detecting misfolded SOD1 within CNS tissue-derived EVs are a potentially viable means of specifically detecting

disease-associated EVs. Future studies on patient tissue-derived EVs are needed to determine the application of this finding to human ALS.

ELISA analysis of lysed CNS tissue-derived EVs in this study also showed that although misfolded SOD1 is present on the surface of intact EVs, a relatively greater amount is present in the lumen of both exosomes and microvesicles from the FALS mouse model $SOD1^{G93A}$ **(Figure 3.5)**. This finding strongly suggests that misfolded SOD1 is actively sorted into EVs. Several groups have demonstrated that EVs can rid the cell of extraneous material when the misfolded protein burden surpasses a certain threshold [128, 179] . To this end, EVs may be employed by the cell to secrete excess mutant misfolded protein. However, a possible unwanted physiological by-product of this process may be the spreading of misfolded protein from cell to cell via EV carriers [172, 180]. Based on reports that show EV-associated α-synuclein is increased under conditions of cell stress [181], some in the field have hypothesized that misfolded or damaged proteins may be targeted for removal by the cell and selectively sorted into EVs [170]. It is possible that a similar mechanism is used for removal of misfolded SOD1 from cells under pathological or stress conditions. Alternatively, or perhaps simultaneously, misfolded SOD1 within EVs may be used to communicate stress signals to neighbouring cells since stress-modified exosomes have been shown to cause an *in vivo* immune response in recipient animals [182].

Our study does not identify the proportion of natively-folded SOD1 that reside in EV populations. The increased levels of misfolded protein seen in transgenic mouse models could thus be due to the expression of exogenous protein in these mice. Protein overexpression may result in hijacking of the EV pathway to rid the cell of unwanted extra protein. However, our later finding that spinal cord EVs from ALS patients also possess misfolded SOD1 argues against the presence of SOD1 cargo within mouse-model EVs being exclusively an artifact of protein overexpression.

A further implication of the finding that EVs from ALS mouse model tissues contain luminal misfolded SOD1 is the potential for using EV-associated misfolded SOD1 as a biomarker. The process of understanding pathology and developing therapeutics for ALS is hampered by the lack of specific biomarkers to identify disease onset and progression. Disease-relevant biomarkers such as tau in Alzheimer's disease are found in picogram amounts in the CSF, and at ten times lower amounts in blood [159]. Therefore, methods which enrich for disease-specific proteins while depleting irrelevant high-abundant proteins such as albumin are needed to develop sensitive biomarkers for neurodegeneration. EVs are gaining traction for this purpose as several groups have shown that EVs are an enriched source of CNS-specific biomarkers [123, 183, 184].

In this work we have also shown that EVs isolated from the extracellular spaces of frozen CNS tissues are efficiently taken up by cultured cells. Both HEK and NSC-34 cells showed patterns of fluorescence consistent with the uptake of dye-labeled EVs from $SOD1^{G127X}$ and NonTg animals **(Figure 3.6).** However, higher magnification images showed differential patterns of EV localization within recipient HEK and NSC-34 cells **(Figure 3.7)**. *In vivo* studies showed that the biodistribution of EVs depends at least partially on the EV-secreting cell type, with differential distribution observed EVs originating from different cell types [185, 186]. Consistent with this, CNS-sourced EVs in our study showed differential distribution in the spinal cord neuroblastoma hybrid cell line, NSC-34, relative to the kidney cell line HEK.

Despite proficient uptake of EVs by both cell types, we did not observe significant levels of cell death in HEK or NSC-34 cells treated with a dose of EVs higher than that routinely used in literature **(Figure 3.8)**. However, the true physiological concentration of EVs in the CNS of either mice or humans is not yet established, and higher doses may be required observe toxicity. Future studies with pooled EV samples should be conducted to determine the upper limit of cytotoxicity in these cell types, as well as in cultured motor neurons. Furthermore, certain studies have found

that exogenous mutant SOD1 is only toxic to motor neurons when co-incubated with conditioned media from microglia or astrocytes [72, 168, 187]. Thus, it is possible that CNS-sourced EVs exert toxicity specifically on neuronal cells either directly or in the presence of glial populations, and warrants further investigation in a system with these cell types.

We also observed an increase in cell viability in HEK and NSC-34 cells by Alamar blue assay when treated with 100 µg/mL of microvesicles from either SOD1^{G127X} or NonTg animals **(Figure 3.9)**. Since there were no significant differences between genotypes, these results suggest a general effect of CNS tissue-derived EVs on recipient cells. As previously mentioned, some have suggested that exosomes can trigger proliferation of cancer cells and tumour growth due to their ability to transfer nucleic acid and protein content between cells [178]. Indeed, bladder cancer cell-derived exosomes have been shown to cause proliferation of cells *in vitro* [188]. Another investigation showed that exosomes isolated from cells expressing mutant KRAS which is associated with colorectal cancer caused increased three-dimensional growth of non-transformed wild-type KRAS-expressing cells [189]. These studies demonstrate that extracellular vesicles with mutant cargo can trigger cell growth and proliferation, consistent with our observations on EVs carrying mutant SOD1.

Previous studies by our group had shown that SOD1 can be secreted from cells both as naked aggregates, and in association with exosomes [84]. However, whether one of these species is preferentially taken up by cells is not yet known. Danzer and colleagues found that α-synuclein was more toxic to cells when secreted with exosomes relative to free soluble protein [171]. Thus, it is possible that exosome-associated misfolded SOD1 has pathogenic effects at sub-toxic levels. Future studies should investigate whether naked or EV-bound SOD1 is preferentially taken up by cells, and the relative toxicity and transmissibility of each of these fractions.

CHAPTER 4. PRION-LIKE PROPAGATION OF PROTEIN MISFOLDING VIA SOD1-CONTAINING EXTRACELLULAR VESICLES

4.1 INTRODUCTION

A hallmark of neurodegenerative diseases is the presence of aggregated proteins within intra- and extracellular inclusions in specific cell types characteristic to each disease [190]. Some proteins found in inclusions have been shown to be misfolded, and can propagate pathology from cell to cell [191]. Insights into the pathogenicity and intercellular transmissibility of these proteins can be gleaned from prions – infectious proteins that can transmit between cells and confer their aberrant conformation onto wild-type protein [191]. Currently, a prion-like mechanism of propagation has been demonstrated *in vivo* for tau and amyloid-β (Aβ) in Alzheimer's disease and α-synuclein in Parkinson's disease, and *in vitro* for the latter, as well as for TDP-43 and Huntingtin proteins [191].

There are clues that suggest a similar prion-like mechanism is at play for ALS. Post-mortem ALS patient tissues show a radial gradient of pathology from a localized site, suggesting that pathology begins focally and spreads along anatomically contiguous tracts through the central nervous system (CNS) [4]. Several different proteins can be found within pathological inclusions of ALS patients that are potentially involved in a prion-like cascade: TDP-43, FUS, and SOD1, among others [191]. Although some studies have demonstrated seeded protein aggregation by TDP-43 *in vitro* [54, 55], so far, definitive prion-like propagation has not been shown for either TDP-43 or FUS. Using *in vitro* and cell culture systems, Grad *et al.* have shown that mutant SOD1 has the capability to convert human wild-type SOD1 (HuWTSOD1) into a misfolded conformation, and the subsequent spreading of SOD1 misfolding from cell culture to cell culture successively [83, 84]. Moreover, two studies have shown that HuWTSOD1 induced to misfold by TDP43 also acquires a prion-like property of

intercellular transmission [29, 85]. Indeed, the number of *in vitro* studies implicating misfolded SOD1 as the toxic agent which is spread in this manner is growing [73, 84, 86-89]. More recently, Ayers *et al.* provided the first *in vivo* demonstration of SOD1 transmissibility by injecting brain homogenates from diseased $SOD1^{G93A}$ transgenic mice into mice transgenic for a GFP-tagged version of G85R ($SOD1^{G85R-GFP}$), another FALS-associated SOD1 mutation [86]. $SOD1^{G85R}$ mice normally never develop disease phenotype, but injection of $SOD1^{G93A}$ brain homogenates caused ALS-like symptoms and death in the recipient $SOD1^{G85R-GFP}$ mice within a timeframe of months [86]. Together, these reports demonstrate that there is solid rationale for treating ALS as a prion-like disease and SOD1 as a potential culprit in the spread of pathology from one region to another within a patient.

The mechanisms that mediate the intercellular transfer of SOD1 misfolding are still uncertain. Possible routes of transmission include transfer of whole aggregates released from cells and taken up by recipient cells via micropinocytosis [84, 167, 192, 193]. An alternate mode for intercellular spreading of misfolded protein seeds is via extracellular vesicles (EVs). Exosomes, a subclass of EVs, have been shown to transfer their cargo to neighbouring cells, and are involved in several physiological processes such as immune responses, neuronal communication, and tissue repair [194]. EVs can also have detrimental effects. In neurodegenerative diseases, for example, exosomes have been shown to spread toxic forms of aggregated proteins such as α-synuclein, β-amyloid, and prion protein, and contribute to disease pathogenesis [124, 171, 195, 196].

Our group has previously demonstrated the presence of misfolded SOD1 on the surface of exosomes *in vitro* [84], and it was hypothesized that EVs may be a major route of SOD1 propagation in living cells. However, evidence for this mechanism from *in vivo* EVs had not, until now, been brought forward. In this study, we demonstrate for the first time that CNS tissue-sourced exosomes and microvesicles from the $SOD1^{G127X}$ ALS mouse model propagate SOD1 misfolding to primary spinal

cord mixed neuron and glial cultures. We further show that induced misfolded SOD1 is present in cells with neuronal and astrocytic morphology. Together, this work contributes evidence for a role of EVs in the propagation of SOD1 pathology seen in ALS.

4.2 MATERIALS AND METHODS

4.2.1 EV ISOLATION

As described in Chapter 3 Materials and Methods (3.2.1, pg 62).

4.2.2 PRIMARY SPINAL CORD CELL CULTURES

Experiments involving animals were approved by the Animal Care Committee of the University of British Columbia (Approval ID: A10-0212), and were conducted according to guidelines set by the Canadian Council on Animal Care. Pregnant C57 BL/6 (B6SJL-Tg(SOD1)2Gur/J strain, stock no. 002297; Jackson Laboratories) or HuWTSOD1 (B6SJL-Tg(Sod1-hWT)2Gur/J; Jackson Laboratories) female mice were sacrificed at embryonic day 12-14, and primary cerebral cortical cultures were prepared from harvested embryos. Cervical, thoracic, and lumbar regions of the spinal cord were dissected in Ca^{2+}/Mg^{2+}-free Hanks Balanced Salt Solution (GIBCO BRL, Grand Island, NY). After removal of the meninges, the tissue was transferred to 0.25% trypsin (GIBCO BRL, Grand Island, NY) and digested at 37 °C for 15 min. The tissue was then resuspended in DMEM plus 10% (vol/vol) fetal bovine serum (GIBCO BRL) and triturated 4-6 times through a fire-polished tip. The supernatant was centrifuged at 200 × g for 45 s. Pelleted neural cells were resuspended in Neurobasal media (GIBCO BRL), B27 (GIBCO BRL), 2 mM L-glutamine (Sigma, St. Louis, MO) and seeded at a density of 2×10^5 cells/well onto poly-D-lysine (Sigma) coated #1.5 coverslips in 24-well plates. Cultures were maintained in serum-free Neurobasal B27 medium, and one-half of medium was replaced on days 3 or 4 with equal volume of fresh medium. Cells were treated with CNS tissue-derived EVs at 14 days in vitro.

4.2.3 IMMUNOPRECIPITATION

Cells were washed twice with PBS, harvested in PBS, and transferred into a microcentrifuge tube and centrifuged at 3000 x *g* to collect the cell pellet. Cells were lysed in 400 µL of lysis buffer (PBS, 0.5% sodium deoxycholate (DOC), 0.5% Triton X- 100, and complete EDTA-free protease inhibitor mixture; Roche Diagnostics) for 2 min on ice. 100 µL of each cell lysate and 10 µL of antibody-coupled M-280 Tosyl-activated magnetic Dynabeads (ThermoFisher Scientific) were mixed and incubated for 3 h at room temperature with constant rotation. Beads were washed three times in 150 µL of RIPA buffer (150 mM NaCl, 50 mM Tris-HCl (pH 8.0), 1% Nonidet P-40, 0.5% DOC, and 0.1% SDS) and boiled in SDS sample buffer containing 1% β-mercaptoethanol for 5 min. As a pre-IP control, 1 µL of cell lysate was prepared in SDS sample buffer as described.

4.2.4 IMMUNOCYTOCHEMISTRY

Primary spinal cord neuronal and mixed glial cells were cultured on glass cover-slips in 24-well plates for immunocytochemical studies. After 24 h incubation with EVs, cells were washed twice with ice-cold phosphate buffer saline (PBS), and fixed in 4% paraformaldehyde in PBS for 15 min at room temperature. Fixed cells were washed once with PBS, permeabilized in 0.3% Triton X-100 in PBS for 10 min, and blocked with 10% normal goat serum in PBS (blocking buffer) for a further 30 min. Coverslips were then incubated with 7.4 µg/ml misfolded SOD1-specific mouse monoclonal antibody, 3H1 diluted in blocking buffer for 1 h at room temperature. Cell were washed thrice in PBS, and incubated with anti-mouse secondary antibody conjugated to Alexa Fluor- 647 fluorescent dyes (Life Technologies, Carlsbad, CA; 1:1000 dilution) for 1 h at room temperature in the dark. Following a further washing step, nuclei were counterstained using 2 µg/ml Bis-benzimide H33342 trihydrochloride (Hoechst 33342) for 5 min. Cells were then washed twice more in PBS and mounted on glass slides using ProLong Gold Antifade mountant (ThermoFisher Scientific).

4.2.5 Confocal microscopy

Confocal images were captured with a Leica TCS SP8 scanning confocal microscope (Leica Microsystems) using LAS-X software. Images were focused using the Hoechst signal, and by making minor focal modification to capture signal emitted at 647 nm (3H1 signal). Two coverslips per biological replicate were analyzed, and a minimum of 10 random fields from each coverslip were captured at 10 x magnification. All images within an experiment were acquired at the same settings as to be comparable among treatment groups. % Area of 3H1-positive staining was quantified by first setting a threshold manually, subsequently applying the selected threshold setting to all images within that experiment, and analyzing the % area positive for signal using the batch processing function in Fiji software [143].

4.2.6 Statistical analysis

All data were analyzed using GraphPad Prism version 6.00 for Windows (GraphPad Software, La Jolla, CA). Statistical analysis performed is indicated in figure captions. One-way ANOVA was performed followed by Kruskal-Wallis or Mann-Whitney-U tests. Two-way ANOVA was performed followed by Tukey's or Sidak's post-tests. All data is presented as mean ± SEM.

4.3 Results

4.3.1 Antibody system for identifying SOD1 misfolding induced by CNS tissue-derived EVs

We used mice overexpressing human $SOD1^{G127X}$, a FALS-associated SOD1 mutation, to investigate the role of CNS tissue-derived EVs in transmission of SOD1 misfolding to cells [17]. As mentioned previously, $SOD1^{G127X}$ transgenic mice present a typical murine ALS-like disease phenotype with foreleg onset, reduced

motor function at ~150 days, and death from disease at ~250 days of age [56]. The frameshift G127X mutation results in a C-terminal truncation of the wild-type SOD1 sequence, the region encompassing epitopes for 3H1 and 10C12 antibodies specific for misfolded SOD1 **(Figure 4.1)** [83]. The presence and exposure of these epitopes in full-length HuWTSOD1 allows for unambiguous detection of induced HuWTSOD1 misfolding initiated by G127X without detection of the G127X seed (Fig 4.1) [83].

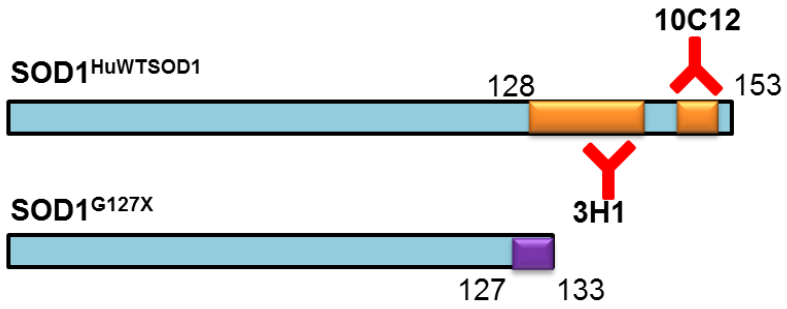

Figure 4.1 Monoclonal antibodies 3H1 and 10C12 specifically detect full-length misfolded SOD1.

The anti-misfolded SOD1 antibodies 3H1 and 10C12 detect epitopes on the full-length human SOD1 protein expressed by $SOD1^{HuWTSOD1}$ transgenic mice. Epitopes for these antibodies are absent in the truncated G127X mutant protein expressed by $SOD1^{G127X}$ transgenic mice.

4.3.2 Transmissible agent in the $SOD1^{G127X}$ EV-containing fraction is denaturation sensitive

We first indirectly demonstrated that transmission of SOD1 misfolding via EVs is heat and reduction-labile, suggesting that the transmissible agent is proteinaceous. We transfected HEK cells with $SOD1^{G127X}$ DNA, allowed expression of the G127X construct for 24 h, and subsequently centrifuged the conditioned cell culture media at 100,000 x *g* to isolate the $SOD1^{G127X}$ EV-containing fraction **(Figure 4.2A)**. We then treated naïve HEK cells with the $SOD1^{G127X}$ EV-containing fraction, or the same fraction pre-treated with heat or reduction (DTT-denaturation) **(Figure 4.2A)**. Full-length endogenous HuWTSOD1 in HEK cells provides the necessary substrate for

template-directed misfolding to occur in the presence of an initiating misfolded-SOD1 seed such as $SOD1^{G127X}$ as described previously in our work [84]. After 24 h, we collected the treated cell lysates, and probed them by immunoprecipitation for signs of HuWTSOD1 misfolding. When the untreated $SOD1^{G127X}$ EV-containing fraction was applied to HEK cells, the cell lysates showed an induction of endogenous HuWTSOD1 misfolding indicated by increased levels of immunoprecipitable SOD1 with 3H1 and 10C12 antibodies **(Figure 4.2B)**. Heat or DTT-treating the EV-containing fraction before layering onto naïve cells abrogated the transmission effect **(Figure 4.2B)**.

Quantification of the results by densitometric analysis of bands corresponding to immunoprecipitated protein showed that the robust induction of endogenous wild-type protein misfolding initiated by $SOD1^{G127X}$ was entirely absent when the EV-containing fraction was first boiled or boiled and reduced **(Figure 4.2B)**. These results indicate that the inductive agent in $SOD1^{G127X}$ EV fraction is denaturation sensitive, and suggest that it is potentially proteinaceous.

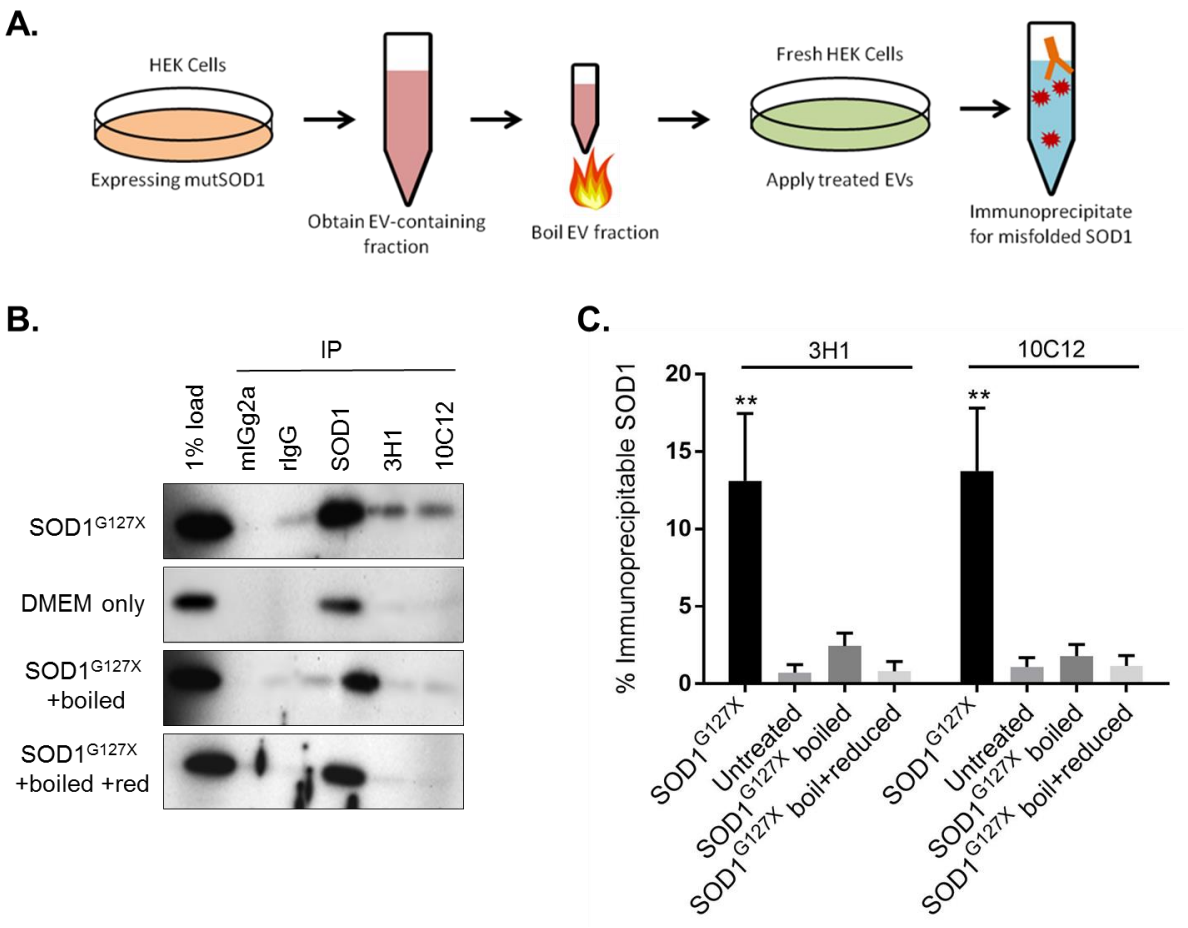

Figure 4.2 Transmissible agent in the SOD1G127X EV-containing fraction is denaturation sensitive.

A. HEK cells overexpressing SOD1G127X were ultracentrifuged to obtain the EV-containing fraction, which was then treated by boiling or reducing with DTT, and applied onto naïve HEK cells. After 24 hours, the cell lysates of treated HEK cells were immunoprecipitated with 3H1 and 10C12 antibodies to probe for the presence of misfolded SOD1. **B.** 3H1 and 10C12 signals are detectable in naïve cells layered with the untreated EV-containing fraction of SOD1G127X expressing HEK cells. No 3H1 and 10C12 is detectable in cell lysates from the negative control were media alone was applied (DMEM only), or in the conditions where boiled, or boiled and reduced, EV-containing fractions were applied. **C.** Quantification of results from multiple immunoprecipitation experiments shows that the robust 3H1 signal is present in cells treated with $SOD1^{G127X}$ EV-containing fraction is abrogated to levels comparable to untreated cells when that fraction is first heat-denatured (boiled), or boiled and reduced (N=6, **p<0.01). Similar results are observed for 10C12 (N=6,**p<0.01). All data was analyzed by 2-way ANOVA followed by Sidak's multiple comparisons test.

4.3.3 SOD1^{G127X} CNS TISSUE-DERIVED EVS PROPAGATE MISFOLDING TO HEK CELLS

Next, to assess whether CNS tissue-derived EVs from an ALS mouse model can initiate misfolding of cell-endogenous HuWTSOD1, we again used HEK cells. We treated cells with SOD1^{G127X} and NonTg CNS tissue-derived exosomes, and performed immunoprecipitation with 3H1 and 10C12 antibodies on cell lysates. Following immunoprecipitation, we detected higher levels of misfolded SOD1 by both 3H1 and 10C12 antibodies in HEK cells treated with SOD1^{G127X} exosomes, as shown in a representative immunoblot **(Figure 4.3A)**. A low level of 3H1 signal was also detected in the NonTg sample, but this signal was not above background IgG2a isotype control signal obtained **(Figure 4.3A)**.

When quantified by densitometry analysis, we detected statistically higher levels of 3H1 signal in SOD1^{G127X} exosome-treated cells relative to NonTg-treated cells **(Figure 4.3B)**. The difference between treatments was not significant by 10C12 immunoprecipitation **(Figure 4.3C)**. Together, these data show that SOD1^{G127X} CNS tissue-derived EVs can propagate SOD1 misfolding to HEK cells, although the level of induction appears to be at the threshold of detection by immunoprecipitation.

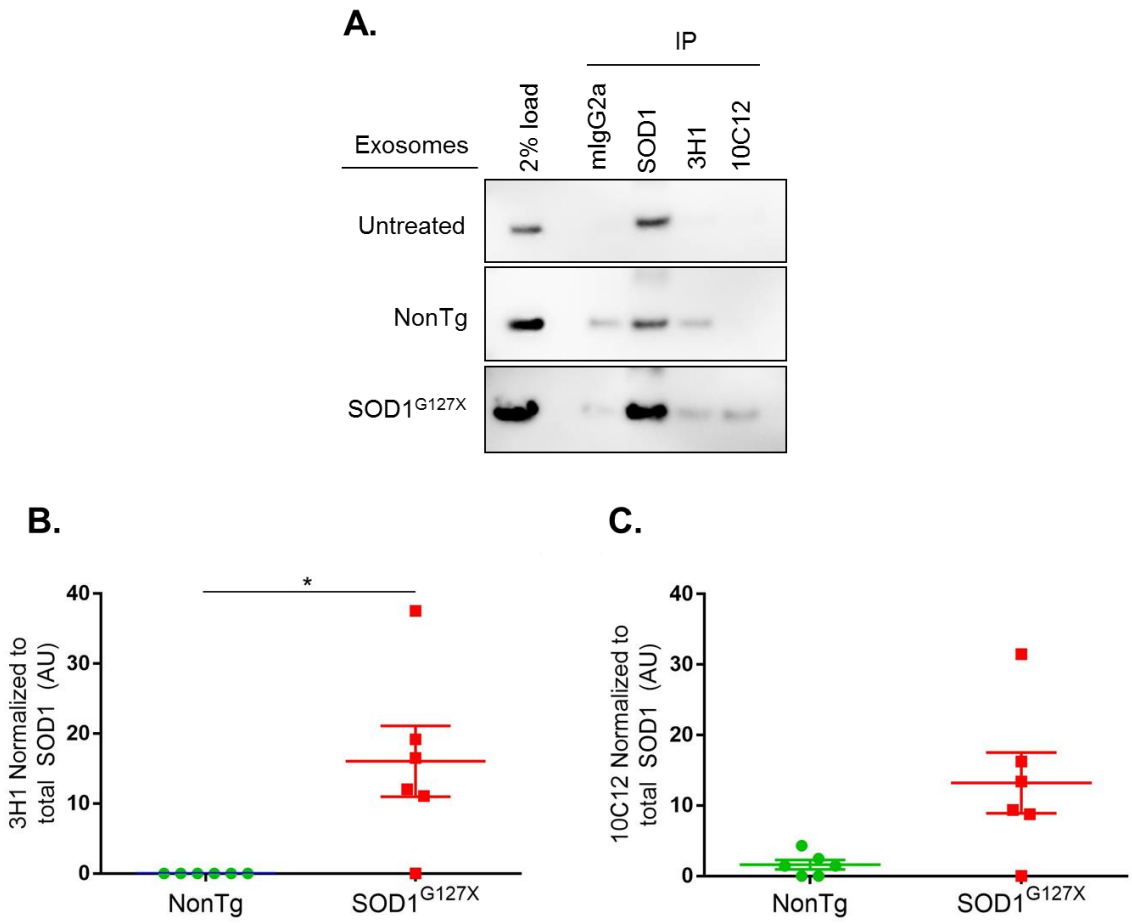

Figure 4.3 Induced misfolded SOD1 is detectable in HEK cells treated with CNS tissue-derived EVs from SOD1G127X mice.

A. 3H1 and 10C12 signals are detectable in HEK cells treated with exosomes isolated from SOD1^{G127X} transgenic mice in a representative immunoblot. Strong total SOD1 signal as well as pre-IP (2% load) signal is present in these cells. No 3H1 or 10C12 is detectable in HEK cells treated with PBS alone (Untreated). NonTg EV-treated cells show 3H1 signal that is comparable to mIgG2a isotype control background levels. **B.** When immunoprecipitation results are quantified, SOD1^{G127X} exosome-treated HEK cells show statistically higher levels of misfolded SOD1 as detected by 3H1 (N=6, $p<0.02$) . **C.** SOD1^{G127X} exosome treated HEK cells show higher levels of 10C12 signal relative to NonTg exosome-treated cell lysates, but results are not significant. (N=6, $p=0.06$). Paired student's t-tests were used for analysis. Error bars represent ± SEM

4.3.4 Propagation via CNS EVs in HEK cells is undetectable by less sensitive assays

Due to the high variability of detected 3H1 signal by immunoprecipitation of HEK cells treated with SOD1^{G127X} EVs, we attempted to verify our findings using

additional assays. We used HEK, and NSC-34 cells expressing HuWTSOD1, for this purpose, and probed cells for the presence of EV-induced SOD1 misfolding.

We first assessed endogenous SOD1 expression in these cell types by immunoblot, and detected human SOD1 in both HEK and NSC-34 cells **(Figure 4.4A**). Although both cell types show expression of SOD1, higher levels were detected in HEK cells. We then treated HEK and NSC-34 cells with CNS tissue-derived EVS from $SOD1^{G127X}$ or NonTg animals for 24 h, collected cell lysates, and assessed induced SOD1 misfolding levels in cells by 3H1 ELISA. Following ELISA analysis, there were no significant differences between $SOD1^{G127X}$ and NonTg EV-treated HEK cells detectable using this system **(Figure 4.4B)**. The same finding was observed in treated NSC-34 cells **(Figure 4.4C**). These results indicated that propagated SOD1 misfolding was either not occurring, or occurring at levels below the detectable threshold of the assay.

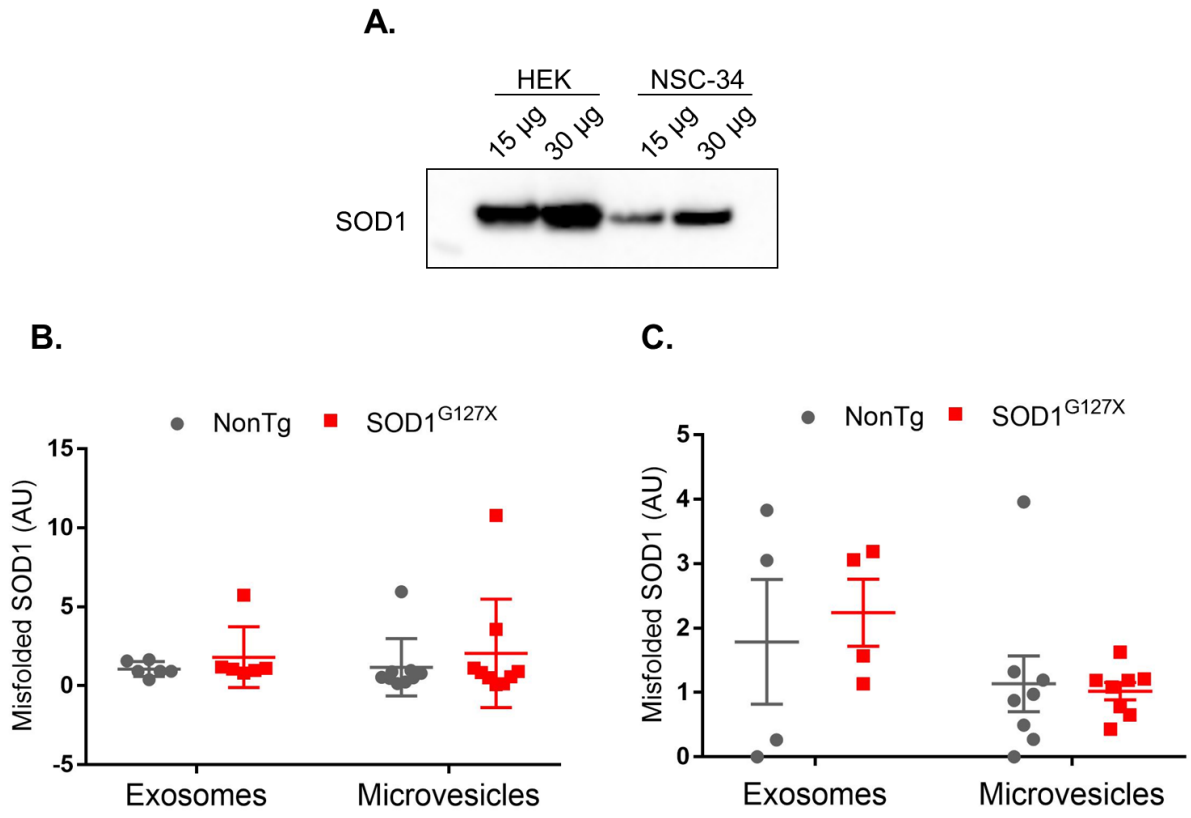

Figure 4.4 Propagation of SOD1 misfolding to HEK and NSC-34 cells is undetectable by 3H1 ELISA.

A. HEK and NSC-34 cells display endogenous SOD1 expression. Higher levels of endogenous SOD1 are present in HEK relative to NSC-34 cells when equal total protein amounts are loaded. **B.** HEK cells treated with SOD1G127X exosomes or microvesicles have levels of misfolded SOD1 similar to cells treated with NonTg EVs (N=7 exosomes N=9 microvesicles). **C.** NSC-34 cells treated with SOD1G127X exosomes or microvesicles also do not show induced misfolded SOD1 at higher levels relative to the same cells treated with NonTg EVs (N=4 exosomes, N=8 microvesicles). All data was analyzed by 2-way ANOVA followed by Tukey's multiple comparisons test.

Finally, we assessed propagation by direct immunocytochemistry and confocal microscopy of cells. We did not detect observable differences between treatment groups **(Figure 4.5).**

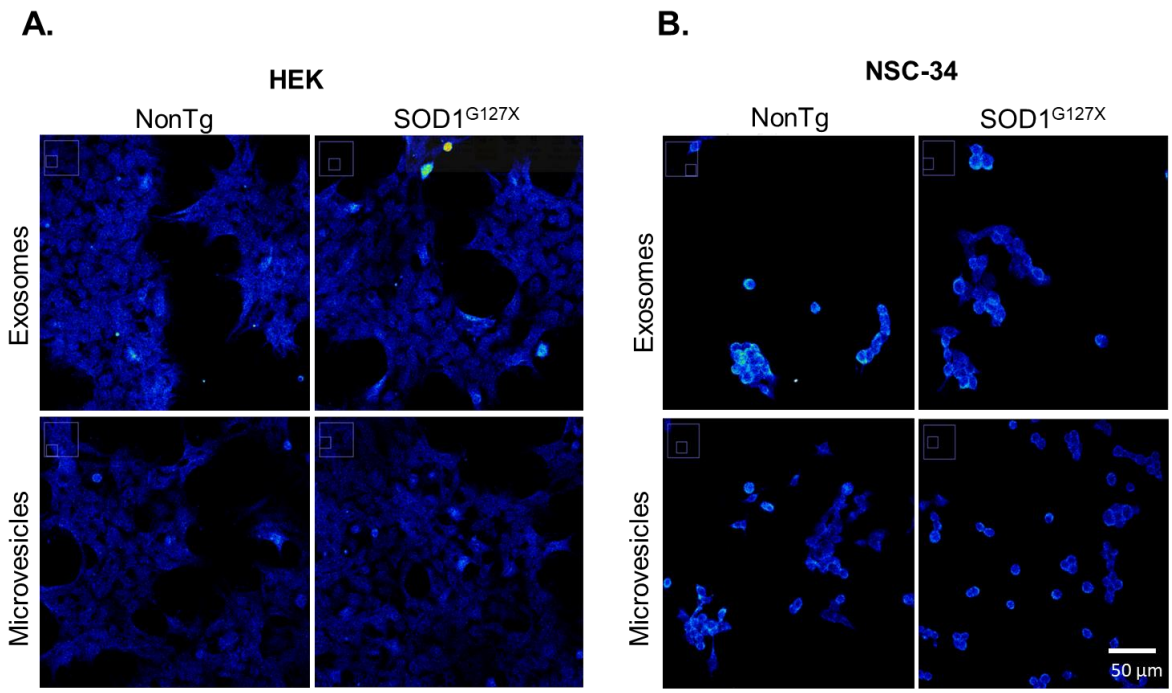

Figure 4.5 Similar patterns of signal is detected by 3H1 immunocytochemistry in cells treated with both NonTg and SOD1^{G127X} EVs.

A. HEK cells treated with exosomes and microvesicles isolated from SOD1^{G127X} and NonTg CNS tissues show similar patterns of low diffuse background signal comparable to untreated control cells (not shown) by 3H1 immunocytochemistry followed by confocal microscopy. **B.** Similar results were observed in treated NSC-34 cells. Images representative of N=3 experiments.

Taken together, the above data show that induced misfolded SOD1 is below the detectable limit of several different assays of varying sensitivity, and suggest that propagation of SOD1 misfolding to HEK cells by SOD1^{G127X} CNS tissue-derived EVs may be occurring at very low levels, or not at all. The former is likely since SOD1 misfolding was observed after immunoprecipitation, a relatively more sensitive method of detection.

4.3.5 CNS-DERIVED EVS FROM SOD1^{G127X} MICE PROPAGATE SOD1 MISFOLDING TO PRIMARY MIXED SPINAL CORD CULTURES FROM HUWTSOD1 TRANSGENIC MICE

Our previous experiments suggest that HEK and NSC-34 were not a suitable system to assess propagation of misfolding by tissue-derived EVs; possible explanations for this are many-fold, including the key point that the source of EV material is CNS-derived while the recipient cells were not. The cell-type specificity of pathology observed in spinal cord motor neurons of ALS patients indicates that there may be cell-type differences in the pathogenesis of disease. With these points in mind, we chose to move forward with a more physiologically-relevant cell system, primary spinal cord mixed neurons and glia, to determine if CNS-derived EVs carrying mutant SOD1 are sufficient to seed propagation of wild-type SOD1 misfolding. The HuWTSOD1 protein expressed in these cells can be converted to a misfolded conformer in the presence of an inducing agent (mutant SOD1 or mislocalized TDP-43 and FUS) as previously demonstrated [29, 83-85].

We layered CNS tissue-derived EVs from SOD1^{G127X} and NonTg mice onto mouse primary spinal cord mixed neuron and glia cultures, fixed cells, and performed immunocytochemistry with 3H1 antibody. As a control for non-specific induction of SOD1 misfolding, we also treated NonTg primary cultures that lack HuWTSOD1 expression with the same tissue-derived EVs. Notably, the Cashman group also previously demonstrated that mouse SOD1 is not a substrate for human mutant SOD1 or TDP43/FUS induced SOD1, which we have mapped to the Trp32 of human SOD1 lacking in mouse SOD1[83, 85]. When visualized with confocal microscopy at low magnification, NonTg cells treated with exosomes from NonTg control animals as well as SOD1^{G127X} animals showed little to no 3H1 staining **(Figure 4.6)**, indicating that misfolding of murine SOD1 had not occurred in these cells. HuWTSOD1-expressing primary neurons and glia treated with NonTg exosomes also show relatively low levels of immunoreactivity, with levels comparable to EV-treated NonTg cells, indicating no induction of SOD1 misfolding had occurred via NonTg EVs **(Figure 4.6).** In contrast, HuWTSOD1-expressing primary cells treated

with SOD1^{G127X} exosomes showed high levels of 3H1 immunoreactivity, representing a robust induction of SOD1 misfolding. We observed similar results in primary cultures treated with microvesicles **(Figure 4.6)**

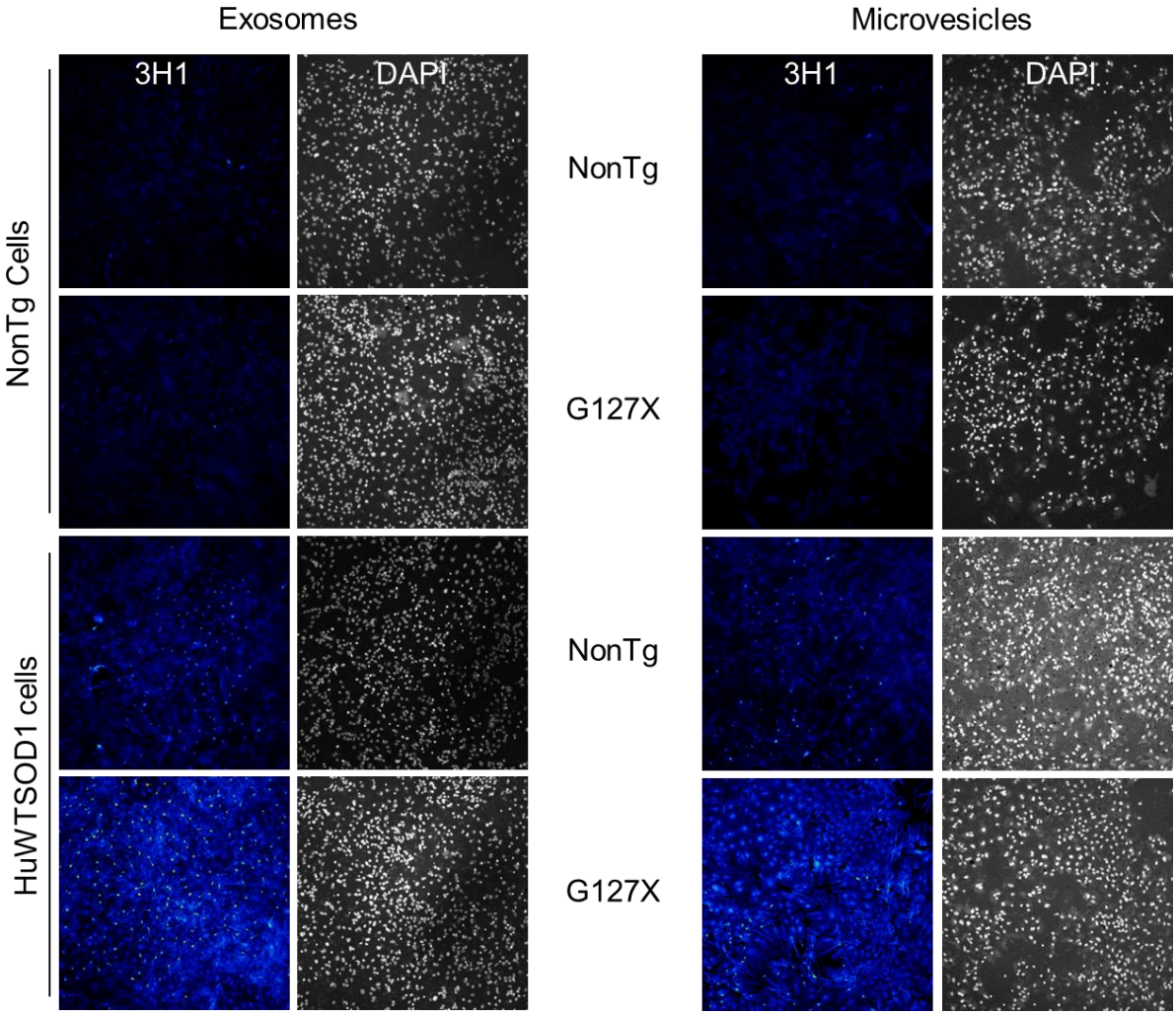

Figure 4.6 Exosomes and microvesicles from SOD1G127X mice propagate SOD1 misfolding to primary neuronal cultures overexpressing HuWTSOD1.

Representative thresholded images of primary spinal cord mixed neuronal and glial cells treated with EVs and immunolabeled with 3H1. Recipient NonTg or HuWTSOD1 cells treated with CNS tissue-derived exosomes and microvesicles from NonTg animals do not display high levels of 3H1 staining. Visibly higher levels of 3H1 staining can be seen in mouse primary spinal cord neuronal cells overexpressing HuWTSOD1 treated with SOD1^{G127X} EVs relative to NonTg cells treated with same.

Quantification of the % area labeled with 3H1 showed that HuWTSOD1-overexpressing cells treated with SOD1^{G127X} exosomes had significantly higher

levels of misfolded SOD1, 25.2%, relative to the same cells treated with NonTg exosomes, 3.3% **(Figure 4.7A, p=0.007**). Similar results were observed in the microvesicle treatment group (25.8% 3H1 positivity in HuWTSOD1-overexpressing cells relative to 4.67% for the same cells treated with NonTg EVs) **(Figure 4.7, p= 0.007)**. For both exosome and microvesicle populations, there was no significant difference between HuWTSOD1-expressing cells treated with NonTg EVs, and NonTg cells treated with either $SOD1^{G127X}$ or NonTg EVs, indicating the absence of transmission in all three control conditions in comparison to HuWTSOD1 cells receiving $SOD1^{G127X}$ EVs **(Figure 4.7A,B)**. There was no significant difference in numbers of cells analyzed between exosome treatment groups as indicated by quantification of DAPI-positive nuclei per image **(Figure 4.7C).** Lower average cell numbers were analyzed in NonTg cells relative to HuWTSOD1 cells treated with NonTg microvesicles **(p=0.0253)**, but no significant differences of average cell number exist among other EV-treated groups analyzed **(Figure 4.7D)**.

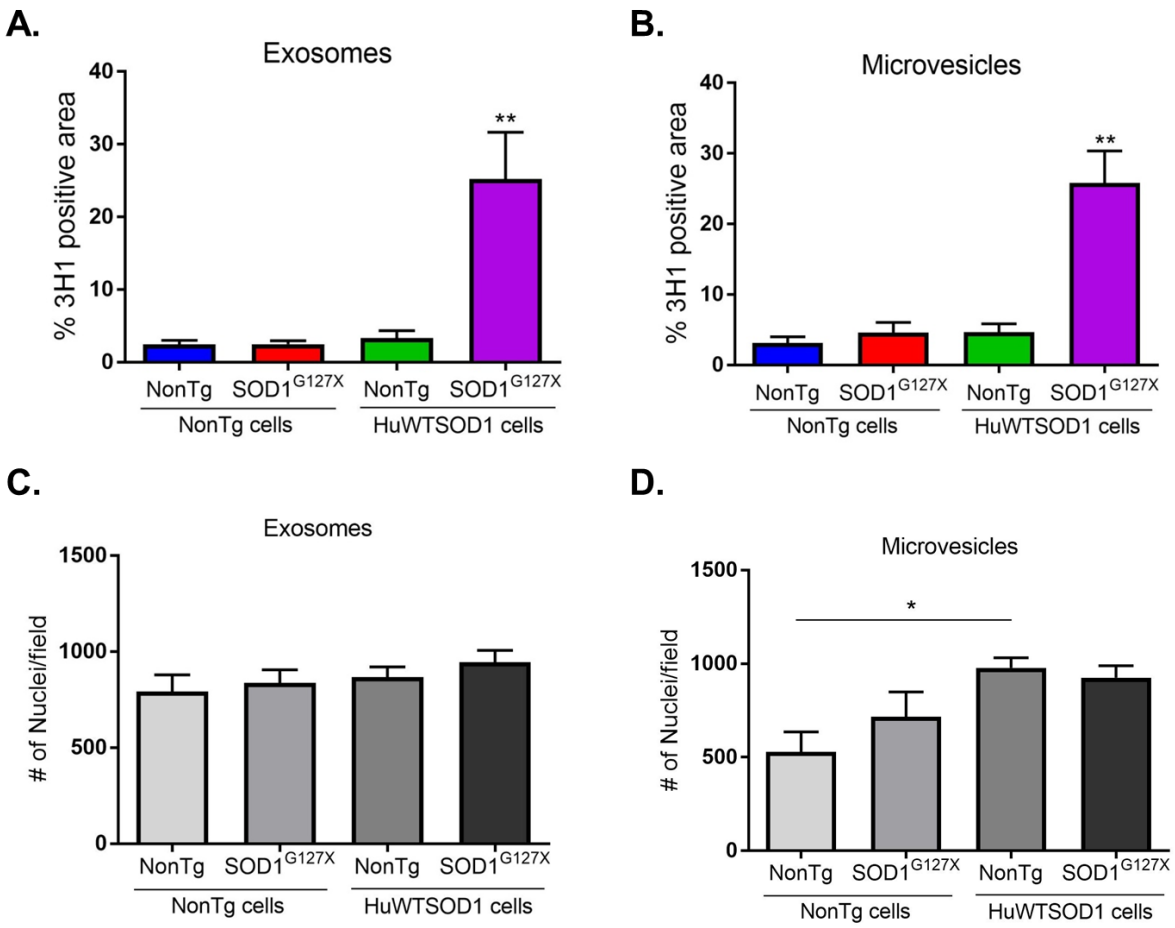

Figure 4.7 Exosomes and microvesicles from SOD1G127X mice propagate SOD1 misfolding to primary neuronal cultures overexpressing HuWTSOD1.

A. Quantification of immunostaining results shows significantly higher levels of misfolded SOD1 in HuWTSOD1 cells treated with $SOD1^{G127X}$ exosomes (N=5-6, **p<0.05) relative to HuWTSOD1 cells treated with NonTg exosomes as detectable with % 3H1-positive area. **B.** Quantification of microvesicle-treated cultures display similar results with highest levels of 3H1 positivity in HuWTSOD1 cells treated with $SOD1^{G127X}$ microvesicles (N=5-6,**p<0.05). **C.** There is no significant difference in the average number of cells counted per image between treatment groups in exosome-treated cells as indicated by DAPI-positive nuclei per field **D.** Slightly lower numbers of NonTg cells were analyzed relative to HuWTSOD1 cells treated with NonTg microvesicles (p=0.0253), but no significant differences of average cell number exist among other EV-treated groups analyzed. All data were analyzed with one-way ANOVA followed by Dunn's multiple comparisons test.

Furthermore, NonTg and HuWTSOD1 primary cultures showed similar patterns of interaction with PKH67-labeled exosomes and microvesicles from both NonTg and $SOD1^{G127X}$ CNS tissues by single-plane confocal microscopy **(Figure 4.8)**. This

suggests that the observed differences in misfolded SOD1 are not due to differences in uptake of EVs by cells. Taken together, these findings demonstrate that both a mutant SOD1 seed and a HuWTSOD1 substrate are required for propagation of misfolding to occur, and the provision of that required seed via SOD1^{G127X} CNS tissue-derived EVs.

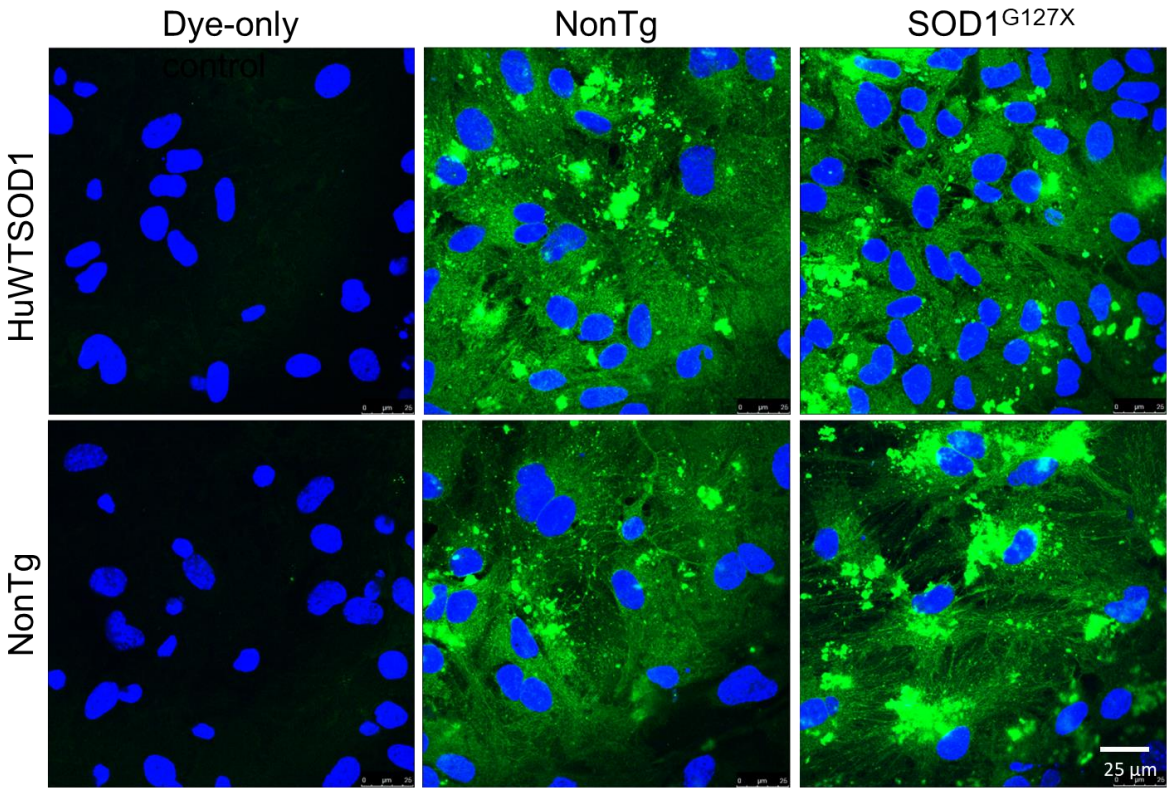

Figure 4.8 Primary spinal cord mixed neuronal and glial cultures treated with NonTg and SOD1G127X EVs show similar pattern of interaction.

HuWTSOD1-expressing primary cultures treated with PKH67-labeled NonTg and SOD1^{G127X} exosomes show punctate green fluorescent labeling at cell peripheries, while the same cells treated with dye alone show no fluorescence (top panels). NonTg primary mixed cultures also show intense green fluorescent labeling of internalized PKH67-labeled NonTg and SOD1^{G127X} exosomes in cell bodies and periphery (bottom panels).

We then looked at higher magnification images to observe if there were any differences in 3H1 signal in neurons and astrocytes visible by confocal microscopy. Single-plane high magnification views of treated primary cultures revealed qualitative

differences in 3H1 immunoreactivity in addition to the qualitative differences observed previously. SOD1^{G127X} EV-treatment of recipient cultures showed high 3H1 immunoreactivity in cells with neuronal morphology (indicated by arrows), including cell bodies and neurites **(Figure 4.9A,B).** Large flat cells consistent with astrocyte profiles also showed 3H1 at relatively lower levels. In contrast, HuWTSOD1 cells exposed to NonTg EVs, or non-transgenic cultures receiving either SOD1^{G127X}- or NonTg-derived EVs showed little to no immunoreactivity in both neuronal and astrocyte cell types. These observations are consistent with propagation of SOD1 misfolding in both neuronal and astrocyte cell types via SOD1^{G127X} CNS EVs.

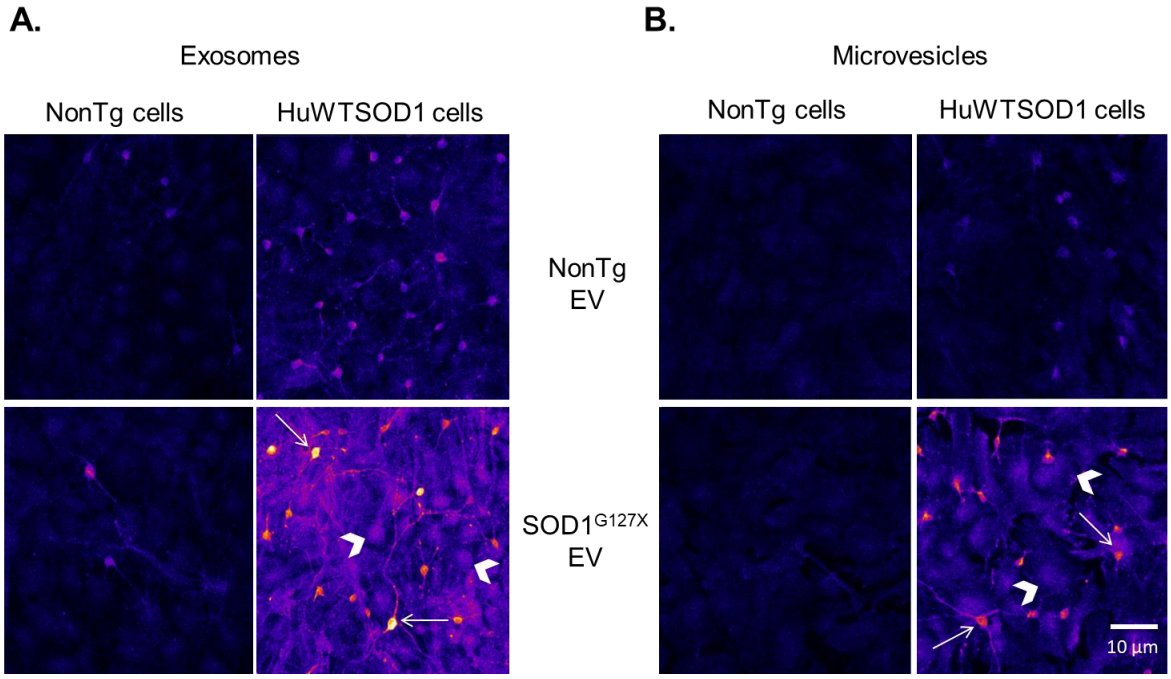

Figure 4.9 Higher magnification images of EV-treated mixed neuronal and glial cell cultures show misfolded SOD1 in astrocytes and neurons.

A. Representative thresholded images of primary spinal cord cells stained with 3H1 antibody show little to no immunoreactivity in NonTg cells treated with exosomes from NonTg or SOD1^{G127X} animals (top left and bottom left panels). HuWTSOD1 cells treated with NonTg exosomes show slight levels of immunoreactivity in structures with neuronal morphology (top right). Highest levels of 3H1 immunoreactivity are seen in HuWTSOD1-expressing cells treated with SOD1^{G127X} exosomes with intense staining visible in neuronal cell bodies (arrows) and in flat structures resembling astrocytes (arrowheads). **B.** Microvesicle-treated primary spinal cord cells show a similar pattern to exosome-treated cell cultures with 3H1 immunostaining visible in structures with astrocytic (arrow heads) and neuronal (arrows) morphology.

4.4 DISCUSSION

Clinical and neuropathological observations suggest that ALS disease progression is propagative, nonaccelerating, and orderly, consistent with the hypothesis of a toxic entity being replicated and spread systematically throughout the neuroaxis [4, 197]. Better understanding the mechanisms of ALS pathology has important implications for therapy, as well as for providing insight into possible initiating events. SOD1 protein exhibits prion-like characteristics, and is a potential candidate to underpin systematic spread of pathology observed in ALS. *In vitro* studies using recombinant mutant SOD1, or oxidized and metal-free versions of wild-type SOD1, have shown that SOD1 undergoes nucleation-dependent polymerization, a process by which prions replicate [58, 198, 199]. Cell culture studies have also shown the ability of misfolded SOD1 conformers to propagate from cell to cell [84, 167]. However, the mechanism(s) by which SOD1 does so are currently unclear. In this thesis chapter, we demonstrate new evidence that exosomes and microvesicles directly isolated from CNS tissues of the FALS mouse model $SOD1^{G127X}$, can seed and propagate SOD1 misfolding to primary mixed neuronal and glial spinal cord cultures expressing HuWtSOD1. Our findings indicate that EVs from an *in vivo* mutant SOD1 environment are sufficient to induce misfolding of full-length wild-type protein in recipient cells, and represent a potential mechanism for systematic spread of ALS pathology.

3H1 immunopositivity in primary cells with neuronal and astrocytic morphology suggests that $SOD1^{G127X}$ EVs propagate misfolding to both cell types **(Fig 7a,b).** SOD1 misfolding may be induced initially in one cell type and subsequently propagated to another, or alternatively, be directly induced in both cell types simultaneously. Additional experiments are needed to demonstrate which of these scenarios occur. There is a body of evidence indicating an essential role of glial cells in the pathogenesis of ALS, as observed in mutant SOD1 experimental models [72, 133, 200]. More recently, Basso et al. demonstrated an increased release of exosomes from cultured astrocytes expressing mutant SOD1, and that these

exosomes induced selective death in recipient motor neurons [156]. Thus, exosomes (and microvesicles) may play an essential role in mediating the toxicity of astrocytes in the context of ALS, and warrants further investigation.

Although we observed robust induction of SOD1 misfolding in primary spinal cord cultures, we did not detect such an induction in HEK cells by 3H1 immunocytochemistry, or by a number of other assays; immunoprecipitation being the only method by which minute levels of induced SOD1 misfolding were detected. In Chapter 3 of this thesis, we showed that CNS tissue-derived EVs from both NonTg and SOD1^{G127X} animals were efficiently taken up by HEK and NSC-34 cells, indicating that observed differences in induction were not due to insufficient or inefficient uptake of EVs **(Figure 3.7)**. However, comparative side-by-side analysis of EV uptake by HEK and primary cultured neuronal cells were not conducted, making it a possibility that HEK cells take up less quantities of EVs than do primary cultured cells.

Another reason for lack of SOD1 misfolding in HEK cells may be due to lower levels of the wild-type SOD1 expression in these cells relative to HuWTSOD1-expressing primary cultures. However, in previous studies, our group had demonstrated robust induction of misfolding in both HEK and HuWTSOD1-expressing mouse neural primary cells transfected with SOD1^{G127X} DNA, and in the same cells treated with conditioned media from SOD1^{G127X}-transfected HEK cells [83]. HEK cells have thus been demonstrated to show a detectable level of endogenous SOD1 misfolding in response to certain inducing “seeds”, and are demonstrably capable of such an induction. An alternate possibility is that HEK cells process CNS-sourced EVs differently than they do EVs originating from other HEK cells. Properties such as particle size and surface charge of exosomes are known to vary with the secreting cell type, and are postulated to effect the pharmacokinetics of exosomes [201]. Studies have also shown that exosomes can be differentially distributed when injected into live mice, consistent with differential cell-type processing [201]. Thus,

primary cells cultured from the CNS may differentially process CNS tissue-derived EVs, making induction of SOD1 misfolding by these EVs more efficient in primary cells.

Finally, the presence of glial cell populations in primary cultures may contribute to SOD1 pathology mediated by EVs in these cells. Astrocytes from FALS and SALS patients have been shown to be toxic to cultured motor neurons [202]. Others showed that astrocytes expressing mutant SOD1 secrete toxic factors that selectively kill motor neurons [72, 187]. Thus, glia appear to be important contributors to toxicity in motor neurons, and the presence of glia in our primary cultures may potentially accelerate disease phenotype, including SOD1 misfolding, in co-cultured neurons. A recent landmark study demonstrated that exosomes secreted from astrocytes specifically transfer microRNAs targeting a tumour-suppressor to metastatic tumour cells, and that the blockade of astrocyte exosome secretion suppresses brain metastasis [203]. Therefore, the potential specificity of a glial response to EVs in the CNS is of exceptional interest as it relates to ALS, and should be investigated in future studies using *in vivo*-sourced EVs.

The finding that $SOD1^{G127X}$ EVs induce misfolding of wild-type SOD1 in primary cells also brings to the forefront the question of what drives secretion and uptake of these EVs. As previously mentioned, SOD1 lacks the signal sequence that targets it for trafficking through the classical ER-Golgi secretory pathway, and is normally present in the cytosol [204]. Instead, SOD3 is the isoform of the superoxide family that is usually present extracellularly [204]. However, many have shown that a portion of SOD1 is also present in the extracellular space, and that this amount is increased in SOD1 mutants or under acute cell stress conditions [132, 166, 168, 169]. Classically, proteins are secreted via the ER-Golgi via large dense-core vesicles (LDCVs), synaptic vesicles, or microvesicles [205]. The docking, fusion and exocytosis of these vesicle types are mediated by the N-ethylmaleimide-sensitive factor attachment protein receptor (SNARE) family proteins [205]. In ALS patients,

the expression of certain SNARE family members was shown to be reduced, suggesting potential impairment of this pathway in disease [206]. Chromogranin A, which normally resides in LDCVs, was also shown to be differentially distributed in SALS [207]. These studies, among others, support an ER-Golgi disturbance in ALS. However, it is confounding how SOD1 can be secreted via the ER-Golgi pathway when it does not have an obvious signal peptide.

Others have shown that EV-associated α-synuclein, a cytosolic soluble protein similar to SOD1, is more oligomeric and aggregation-prone than free α-synuclein in the extracellular milieu, and therefore, potentially more pathogenic [170, 195]. Under certain stress conditions such as dysfunction of protein clearance pathways or oxidative stress, translocation of α-synuclein to vesicles is increased, resulting in more oligomeric forms of α-synuclein being released under these conditions [208-210]. Based on these reports, some have hypothesized the existence of a cellular mechanism that recognizes oligomeric misfolded or aggregated forms of α-synuclein and sort them into vesicles for release by exocytosis [170]. It is plausible that a similar mechanism exists for sorting of misfolded SOD1 into EVs.

Finally, it would be of high importance to determine which species of SOD1 causes the most efficient propagation of misfolding: SOD1 aggregates or EV-bound SOD1. Munch et al showed that preparations of mutant SOD1 aggregates were able to penetrate a 0.4 µm mesh filter to seed persistent aggregation in co-cultured neuronal cells, and that these were taken up by macropinocytosis [167]. However, it is unclear whether the aggregate preparations they used contained extracellular vesicles. Some have postulated the possibility that these aggregates were encapsulated within exosomes [128]. Consistent with this, we have shown that the size range of vesicles investigated in this study were well below 0.4 µm. In addition, because EV's carry surface proteins that specifically target it for uptake by certain cells, it is possible that EVs cause uptake of SOD1 (aggregated or oligomeric) by targeted cell types. Therefore, further investigating the exact molecular species in such

preparations, and the relative propagation competencies of EV-bound and naked SOD1 species could answer interesting questions we have about the role EVs play in the propagation of protein misfolding.

CHAPTER 5. HUMAN CNS TISSUE-DERIVED EXTRACELLULAR VESICLES: PRELIMINARY FINDINGS

5.1 INTRODUCTION

Extracellular vesicles (EVs) have been implicated in the propagation of disease pathology in a number of neurodegenerative diseases, including Alzheimer's, Huntington's, and Parkinson's diseases [128, 211]. As previously mentioned, extracellular vesicles isolated from *in vitro* models have been shown to contain tau, Aβ, SOD1, and huntingtin proteins [130, 171, 196, 212-214]. More recently, *in vivo* work in an Alzheimer's disease mouse model has also offered evidence for the involvement of extracellular vesicles in the propagation of tau pathology, a characteristic typically seen in Alzheimer's disease pathology [215]. However, the application of these findings to human patients is hampered by the lack of studies using EVs isolated from human material. Some work has been performed on EVs isolated from blood and other biofluids from human patients [216, 217], but their relevance to diseases of the CNS is not well established. The only biofluid in direct contact with the CNS, cerebrospinal fluid (CSF), is in limited supply, thus making it impractical to isolate sufficient quantities of extracellular vesicles from it for the purpose of investigating disease biology, although some studies have investigated this potential. Thus, the applicability of findings in the EV field to human neurodegenerative diseases remains uncertain.

In this chapter, we investigated the relevance of our findings in murine models (possession of misfolded SOD1 cargo and SOD1 propagation competency via EVs) to human ALS. For these studies, we isolated EVs from spinal cord and brain tissues of ALS patients and healthy controls, characterized them, and performed investigations using experimental setups similar to those used in our studies on $SOD1^{G127X}$ and $SOD1^{G93A}$ mouse models. The preliminary findings depicted in this chapter offer insight into the exciting potential of tissue-derived EVs to inform our understanding of human ALS pathobiology.

5.2 METHODS

5.2.1 EV ISOLATION FROM HUMAN CNS TISSUES

0.5-1g of Frozen brain or spinal cord tissues from post-mortem patients were finely sliced in Hibernate A medium (Brain Bits, Springfield, IL), added to a pre-warmed solution of Hibernate A containing 125U/mL Collagenase III to digest the extracellular matrix, and incubated with shaking at 37°C for 15 minutes. Enzymatic digestion was stopped by adding ice-cold Hibernate A containing Protease Inhibitors (EDTA-free protease inhibitor cocktail, Roche Diagnostics). The mixture was centrifuged at 2000 x *g* to remove cells and cellular debris. Microvesicles were isolated by centrifuging the supernatant at 10,000 x *g* for 30 min. Exosomes were isolated by centrifuging the resultant supernatant at 100,000 x *g* for 90 min. All ultracentrifugation steps were performed using the Beckman Coulter (Break, CA) Type 70Ti Rotor at 4°C. EV pellets were then re-suspended in either 0.95 M sucrose (exosomes) or 1.3 M sucrose (microvesicles), and layered on top of 2 M sucrose in a 1.5 mL ultracentrifuge tube (Beckman). Tubes were centrifuged for 2 h at 20,000 x *g* for the microvesicle pellet, or 150,000 x g for the exosome pellet. The 700 μL fraction at the interphase between the 2 sucrose densities was aliquoted into a fresh tube, resuspended in PBS, and spun down for 1 h at 10,000 x *g* for microvesicles and 100,000 x *g* for exosomes to isolate the purified vesicle pellet. Complete EDTA-free protease inhibitor mixture (Roche Diagnostics) was added to the final resuspension at 1x final concentration before immediate use, or before freezing at -80°C for later use.

5.2.2 TRANSMISSION ELECTRON MICROSCOPY

A 3 μL sample of exosomes or microvesicles was applied to glow discharged 200 mesh formvar/carbon coated TEM grids (Ted Pella Inc., Redding, CA), and negatively stained with 2% aqueous uranyl acetate. A Hitachi H7600 TEM (Hitachi High-Technologies Corp., Tokyo, Japan) instrument operated at 80kV with a side

mounted 1K AMT Advantage digital camera (Advanced Microscopy Techniques, Corp. Woburn, MA) were used to observe samples and capture images.

5.2.3 Nanoparticle tracking analysis

The NanoSight LM10-HS instrument (Malvern Instruments Ltd., Malvern, UK) equipped with the NTA 2.0 analytical software was used to characterize the diameter of particles in EV samples. Samples were diluted 1:3000 in distilled water, and injected with constant output via syringe-pump into a 405 nm laser chamber. Three recordings were performed for each sample, followed by use of the batch process function in the NTA software to integrate readings to obtain a mode and mean size for each sample.

5.2.4 Immunoprecipitation

EV samples were resuspended in 100 µL of PBS, mixed with 10 µL of antibody-coupled M-280 Tosyl-activated magnetic Dynabeads (ThermoFisher Scientific), and incubated for 3 h at room temperature with constant rotation. Beads were washed three times in 150 µL of RIPA buffer (150 mM NaCl, 50 mM Tris-HCl (pH 8.0), 1% Nonidet P-40, 0.5% DOC, and 0.1% SDS) and boiled in SDS sample buffer containing 1% β-mercaptoethanol for 5 min. As a pre-IP control, 1 µL of cell lysate was prepared in SDS sample buffer as described.

5.2.5 Immunoblotting

Immunoprecipitation samples prepared in SDS sample buffer containing 1% β-mercaptoethanol as described above were run on 4% Bis-Tris gels (LifeTechnologies, Carlsbad, CA), and transferred to a PVDF membrane. Membranes were incubated for 1 h at room temperature in blocking buffer (TBS, 0.1% Tween-20 (TBST), 5% skim milk powder), and subsequently incubated with 1

µg/ml rabbit SOD100 antibody (Assay Designs, Ann Arbor, MI) for 1 h at room temperature. Membranes were then washed twice in TBST and incubated with anti-rabbit IgG horseradish peroxidase-linked whole antibody (GE Healthcare, Buckinghamshire, UK) diluted 1:10,000 in blocking buffer for 1 h at room temperature. SuperSignal West Femto chemiluminescence substrate (ThermoFisher Scientific, Waltham, MA) was used for protein antibody detection, and visualized using a VersaDoc Imager (Bio-Rad Laboratories, Hercules, CA).

5.2.6 Misfolded SOD1 ELISA

96-well Nunc ELISA plates (ThermoFisher Scientific) were coated with 36.9 µg/mL of the anti-misfolded SOD1 monoclonal antibody 3H1 overnight at 4°C. Plates were washed with wash buffer (Tris-buffered saline (TBS) containing 0.05% Tween-20), and blocked with TBS + 1% BSA for 1 h at room temperature. Samples were prepared by measuring total protein concentration using the Pierce BCA Assay Kit (ThermoFisher Scientific). Equal protein concentrations of intact EVs or EVs lysed in PBS + 1% Triton-X 100 were added to the plate and incubated for 1 h at room temperature. Plates were washed with wash buffer and incubated with rabbit polyclonal anti-SOD1 antibody at room temperature for 1 h. Plates were then washed and incubated with horseradish peroxidase (HRP)-linked anti-rabbit IgG antibody for 1 h at room temperature, followed by a final wash, and incubated with SuperSignal™ ELISA Femto chemiluminescent substrate (ThermoFisher Scientific) for 5 min at room temperature. Total chemiluminescence at all wavelengths was read using a SpectraMax M2 microplate reader (Molecular Devices, CA).

5.2.7 Immuno-electron microscopy

Suspensions of EVs were diluted 200-fold in 2% PFA in filtered PBS to lightly fix, and 5 µL pipetted onto formvar-coated 200-mesh nickel grids (EM Sciences). Material was allowed to adhere to the grids for 20 min before excess liquid was wicked off. The following was performed in a humidity box at room temperature

using paper-filtered PBS or water: grids were blocked in 1% milk in PBS for 10 min; incubated in 3H1 primary antibody 20 µg/ml in 1% milk PBS for 2 h; washed x 3 briefly in PBS; incubated in anti-mouse secondary antibody conjugated to 15 nm gold bead (EM Sciences), 1:30 in 1% milk PBS with 0.05% polyethylene glycol, for 1 h; washed x 3 briefly in PBS; post-fixed with 1% glutaraldehyde in PBS for 5 min; washed x 2 in PBS; washed x 3 in distilled filtered water; counterstained in filtered 1% aqueous uranyl acetate for 5 min, and allowed to dry. Grids were viewed on a Tecnai G2 Spirit Transmission Electron Microscope (FEI, Hillsboro, OR).

5.2.8 IMMUNOCYTOCHEMISTRY

Primary spinal cord-derived neuronal and mixed glial cells were cultured on glass cover-slips in 24-well plates for immunocytochemical studies. After 24 h incubation with EVs, cells were washed twice with ice-cold phosphate buffer saline (PBS), and fixed in 4% paraformaldehyde in PBS for 15 min at room temperature. Fixed cells were washed once with PBS, permeabilized in 0.3% Triton X-100 in PBS for 10 min, and blocked with 10% normal goat serum in PBS (blocking buffer) for a further 30 min. Next, coverslips were incubated with 7.4 µg/ml misfolded SOD1-specific mouse monoclonal antibody 3H1 diluted in blocking buffer for 1 h at room temperature. Cell were washed thrice in PBS, and incubated with anti-mouse secondary antibody conjugated to Alexa Fluor- 647 fluorescent dyes (Life Technologies, Carlsbad, CA; 1:1000 dilution) for 1 h at room temperature in the dark. Following a further washing step, nuclei were counterstained using 2 µg/ml Bis-benzimide H33342 trihydrochloride (Hoechst 33342) for 5 min. Cells were then washed twice more in PBS and mounted on glass slides using ProLong Gold Antifade mountant (ThermoFisher Scientfic, USA).

5.2.9 Confocal microscopy

Confocal images were captured with a Leica TCS SP8 scanning confocal microscope (Leica Microsystems) using LAS-X software. Images were focused using the Hoechst signal, and by making minor focal modification to capture signal emitted at 647 nm (3H1 signal). 2 coverslips per biological replicate were analyzed, and a minimum of 10 random fields from each coverslip were captured at 10x magnification. All images within an experiment were acquired at the same settings so as to be comparable among treatment groups. % area of 3H1-positive staining was quantified by first setting a threshold manually, subsequently applying the selected threshold setting to all images within that experiment, and analyzing the % area positive for signal using the batch processing function in Fiji software [143].

5.3 Results

5.3.1 Isolation and characterization of human CNS tissue-derived EVs

Using the same protocol outlined in Chapter 2, we isolated EVs from frozen post-mortem human tissues from ALS patients and age-matched healthy controls. We first characterized the morphology of isolated material. When visualized by TEM, exosomes isolated from human CNS tissues displayed the expected morphological characteristics for EVs (circular invaginated structures bounded by a double membrane) **(Figure 5.1A).** Particles in the isolated EV samples had a mean diameter of ~150 nm and a modal size of ~115 nm, consistent with published findings for extracellular vesicles, reported to be ~90-160 nm for exosomes derived from cell culture supernatants [174, 218]. These results suggest that the material we isolated from human CNS tissues using the indicated protocol were likely extracellular vesicles.

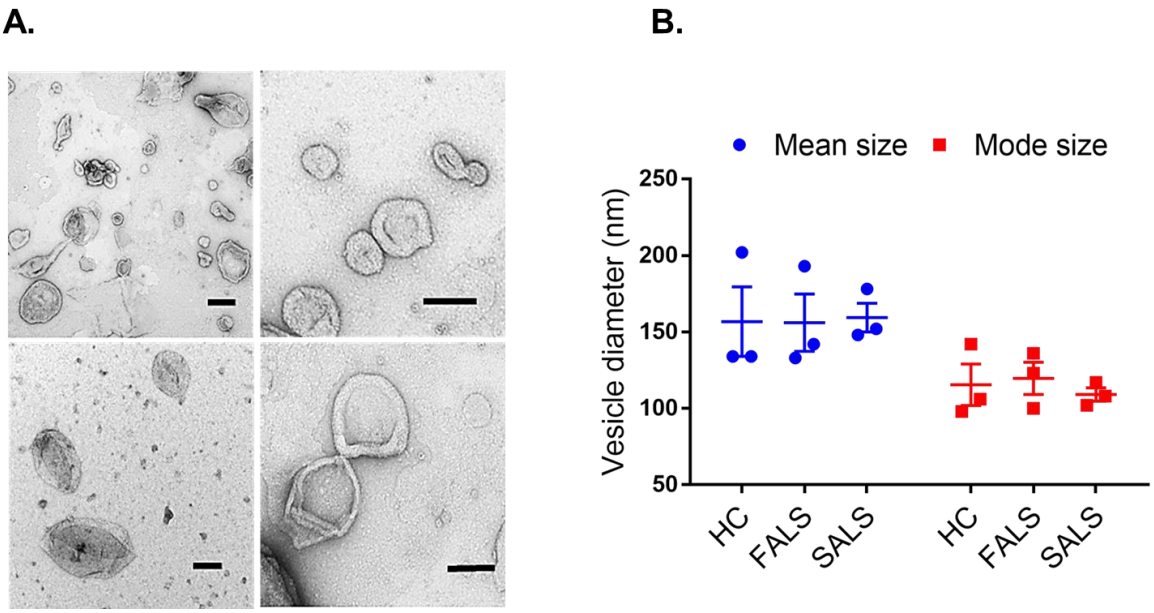

Figure 5.1 CNS EVs isolated from human ALS patients conform to EV-specific criteria.

A. A heterogeneous population with varying vesicle sizes and morphologies can be seen in a low magnification TEM view of exosomes isolated from a healthy control patient (top left). Higher magnification views show the presence of vesicles with a cup-shaped morphology consistent with extracellular vesicles. scale bar=100 nm **B.** Patient CNS tissue-derived exosomes have a mean diameter of ~150 nm. The diameter of vesicle most frequently occurring in the population, mode diameter, is ~115 nm. There were no significant differences among patient groups. Data was analyzed using two-way ANOVA followed by Tukey's multiple comparisons post-test. Data is presented ± SEM.

5.3.2 Surface misfolded SOD1 in EVs from human ALS patients

We were first interested in determining surface levels of misfolded SOD1 on intact CNS tissue-derived EVs from human ALS patients. To do so, we used the misfolded SOD1-specific monoclonal antibodies, 3H1 and 10C12, which were characterized in a previous publication by our group [83] and first described in Chapter 3 **(Figure 3.1).** When immunoprecipitations with 3H1 and 10C12 were performed on spinal cord tissue-derived exosomes from FALS and SALS patients and healthy controls, we observed higher levels of 3H1 and 10C12 signal in the FALS patient exosome sample relative to healthy controls as shown in the representative immunoblot **(Figure 5.2A).** When results from multiple experiments were quantified, we observed higher 3H1 signal in FALS and SALS samples relative to control **(Figure 5.2B)**. However, these results were not statistically significant with the number of

samples analyzed. Conversely, immunoprecipitation with 10C12 antibody showed a significantly higher level of misfolded SOD1 signal in the FALS spinal cord exosome sample relative to both SALS and healthy control samples **(Figure 5.2B)**.

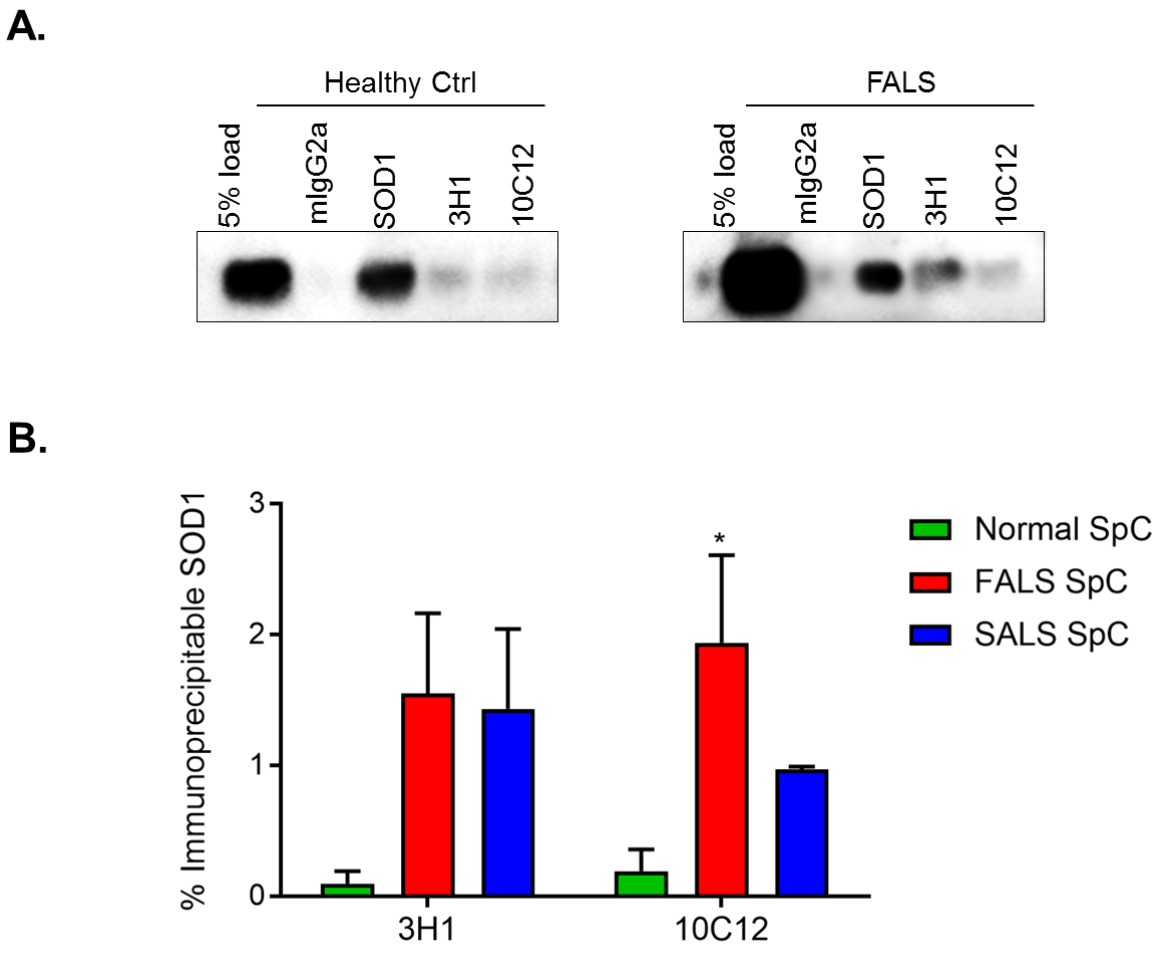

Figure 5.2 Spinal cord exosomes from FALS patients possess surface misfolded SOD1.

A. Immunoprecipitation with misfolded SOD1-specific monoclonal antibodies 3H1 and 10C12 shows higher levels of signal in a representative blot of spinal cord EVs isolated from a FALS patient relative to a healthy control patient. **B.** Quantification of immunoprecipitation experiments on multiple samples shows significantly higher levels of 10C12 in the FALS spinal cord EVs relative to both SALS and healthy control (normal) spinal cord EVs. 3H1 immunoprecipitation showed higher levels of signal in both FALS and SALS samples relative to healthy control, but results were not statistically significant. N=3 experiments. Data was analyzed using two-way ANOVA followed by Tukey's multiple comparisons post-test. Data is presented ± SEM. Experiment designed by Drs. Judith Silverman and Leslie Grad, and performed by Dr. Leslie Grad.

To ensure that misfolded SOD1 identified in our EV samples was specifically associated with vesicles, rather than with the soluble non-EV material within the preparation, we performed 3H1 immunogold labeling on microvesicles from patient groups and healthy controls, and visualized individual EVs by TEM. We detected low levels of immunogold labeling (~1-2 beads/vesicle) in EVs within the FALS and SALS samples, as well as some EVs from healthy control patients (**Figure 5.3**). We also detected individual EVs from the same samples that did not display surface labeling with 3H1 antibody, indicative of both misfolded-SOD1 positive and negative EVs being present within the CNS tissue-derived microvesicle populations investigated.

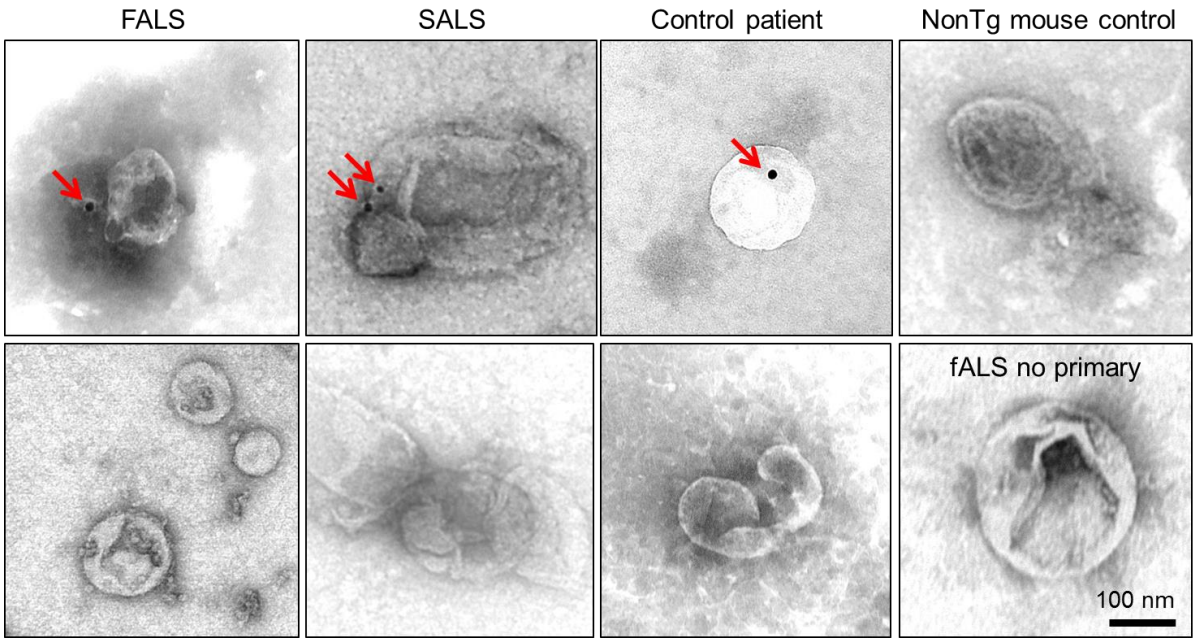

Figure 5.3 Individual microvesicles from ALS patients show low levels of surface 3H1 labeling.

EV samples were immunogold-labeled with 3H1 antibody and visualized by TEM. Individual EVs from FALS, SALS as well as a healthy control patient demonstrate modest labeling with 3H1 anitbody, but not NonTg mouse controls or FALS samples (top panels) with no primary antibody added (bottom right). Not all EVs within a population are labeled with 3H1, and EVs from each patient group has unlabeled EVs within the sample (bottom panels).

Taken together, these results suggest that exosome and microvesicle samples from human ALS patients display modest amounts of surface misfolded SOD1 labeling.

Further experiments with additional healthy control and patient samples are required to conclusively determine if EV surface-associated misfolded SOD1 is specific to ALS patients.

5.3.3 The luminal compartment of human ALS spinal cord-derived EVs is enriched with misfolded SOD1 cargo

In order to quantitatively assess relative levels of surface and luminal misfolded SOD1 in CNS tissue-derived EVs we used a sandwich ELISA system with 3H1 as the capture antibody and a pan-SOD1 antibody as detection. Using the 3H1 ELISA, we probed human spinal cord tissue-derived microvesicles from ALS patients, Alzheimer's disease (AD) patients, and healthy controls for misfolded SOD1 in the presence and absence of 1% Triton-X100. Triton-X 100 was used to rupture the vesicle membrane and liberate luminal protein into solution. Using this experimental setup, we detected statistically significant levels of misfolded SOD1 in the lumen of FALS and SALS patient EVs relative to both healthy control and AD patient EV samples (**Figure 5.4**). When vesicles were not treated with Triton-X100, and were presumably intact, there were no detectable differences in misfolded SOD1 among patient groups (**Figure 5.4**). These results indicated that spinal cord EVs from ALS patients contained higher detectable levels of luminal misfolded SOD1 protein when compared with both healthy controls and Alzheimer's disease patients.

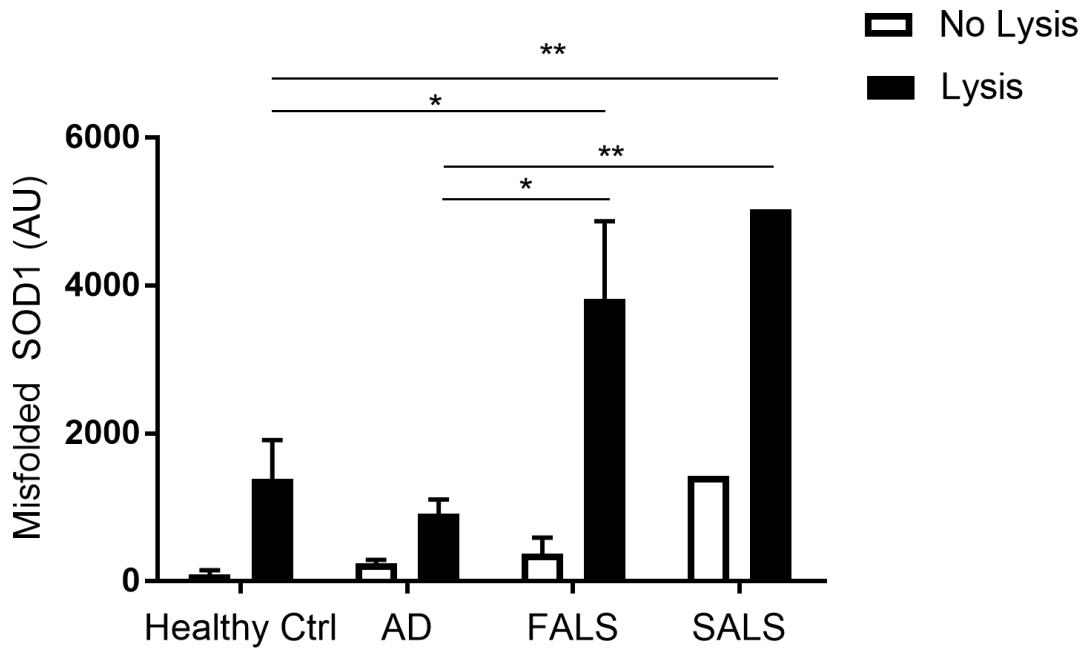

Figure 5.4 Spinal cord tissue-derived microvesicles from ALS patients possess luminal SOD1 cargo.

ELISA with 3H1 antibody shows higher levels of misfolded SOD1 in the lumen of FALS and SALS spinal cord tissue-derived microvesicles, relative to healthy control and Alzheimer's disease (AD) spinal cord microvesicle samples. No significant differences between ALS patient groups were observed in the samples with no detergent lysis (N=3 per group, N=1 for SALS **p<0.009, *p<0.02). Data was analyzed with two-way ANOVA followed by Tukey's multiple comparisons test. Results are presented ± SEM.

5.3.4 Frontal cortex EVs from ALS patients do not carry significant levels of misfolded SOD1

The above results were consistent with the fact that neurodegeneration and disease pathology is seen predominantly in the spinal cord and motor cortex of ALS patients. We next investigated EVs from an unaffected region, the frontal cortex, in order to determine whether EVs from this region also possess misfolded SOD1. When probed with the 3H1 ELISA in a manner similar to that used for spinal cord tissue-derived EVs, we observed misfolded SOD1 in frontal cortex exosomes of 1 FALS and several SALS patients at levels up to 7-fold lower than in spinal cord EVs from ALS patients (**Figure 5.5A**). Similar results were observed for microvesicles in even lower amounts (**Figure 5.5B**). Overall, these results suggest that misfolded SOD1 within EVs is relatively specific to anatomical regions with disease pathology

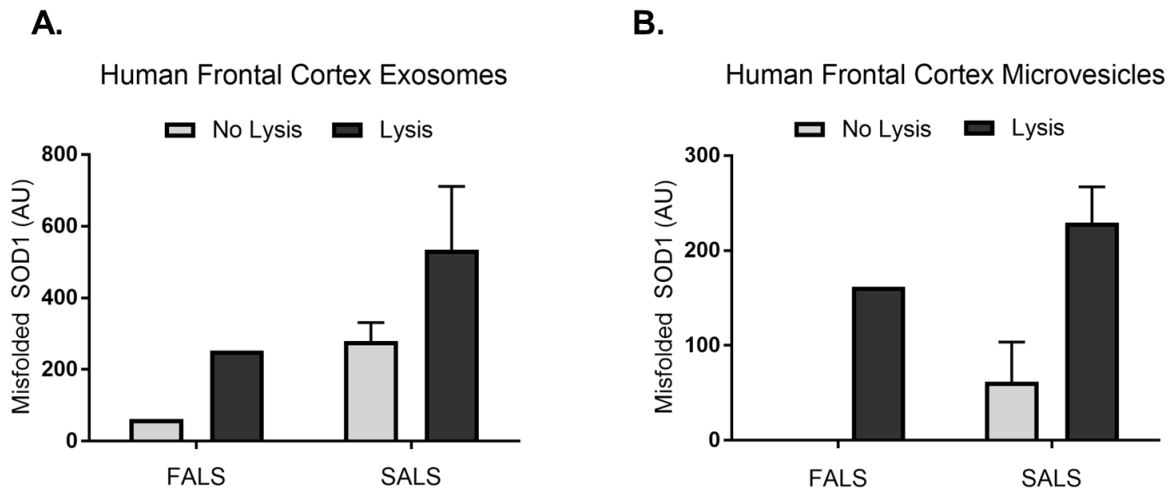

Figure 5.5 Frontal cortex EVs from ALS patients do not show significant levels of luminal misfolded SOD1.

A. ELISA with 3H1 antibody shows detectable levels of misfolded SOD1 in the lumen of FALS and SALS frontal cortex-derived exosomes. **B.** Similar results were observed for microvesicles. N=1 for FALS, N=2 for SALS. There were no significant differences between FALS and SALS samples. Results were analyzed by two-way ANOVA. Data presented as ± SEM.

5.3.5 Human CNS-derived EVs can propagate SOD1 misfolding to primary cultures expressing HuWTSOD1

Finally, we were interested in determining whether the propagation of SOD1 misfolding observed via EVs derived from an *in vivo* murine environment had physiological relevance to human ALS. To this end, we treated primary cultures of mixed neurons and glia derived from mouse spinal cord expressing HuWTSOD1 with microvesicles derived from post-mortem spinal cord tissue from ALS patients, fixed those cells, and performed immunocytochemistry with 3H1 antibody. As negative controls, we treated the same cells with microvesicles from healthy control patients. We also treated NonTg cells, expressing only endogenous murine SOD1, with microvesicles from all patient groups; as previously mentioned, mouse SOD1 is not a substrate for misfolding via human mutant SOD1 [83, 85].

When visualized with fluorescence microscopy, we observed higher intensity 3H1 staining in structures resembling neuronal morphology with visible long neurites and projections, in primary cells treated with microvesicles from FALS samples, as well as the healthy control (**Figure 5.6A**). We did not observe levels of 3H1 staining above background in the same cells treated with microvesicles from a SALS patient (**Figure 5.6A**). We also did not observe 3H1 staining in NonTg primary cultures not expressing HuWTSOD1 treated with the same microvesicle groups (data not shown).

When immunocytochemistry results were quantified, the % area labeled with 3H1 in primary cultures treated with microvesicles from FALS patient 93 was 28.7%, significantly higher relative to the same cells treated with microvesicles from all other patient groups **(Figure 5.6B**). FALS patient 83 and healthy control EV-treated cultures also displayed significantly higher 3H1-positive % area, at 14.0% and 13.5% respectively, when compared to SALS-treated cells (2.99% 3H1-positive area) (**Figure 5.6B)**. NonTg cells treated with human CNS-derived microvesicles from all patient groups had less than 4.05% 3H1-positive area, and were not significantly different between groups (**Figure 5.6B)**. These data suggest that microvesicles from FALS patient 93 induced propagated SOD1 misfolding in HuWTSOD1-expressing primary cultures with the highest efficiency, while FALS 83 and healthy control patient-derived EVs propagated to a lesser efficiency. Microvesicles from the SALS patient investigated did not appear to have induced misfolding of HuWTSOD1 in primary cultures.

To ensure that differences in results between patient groups were not due to variations in the numbers of cells counted, we quantified the DAPI-positive nuclei per field in each group. There were no significant differences in numbers of HuWTSOD1-expressing cells analyzed between treatment groups, as indicated by the number of DAPI-positive nuclei present in analyzed images **(Figure 5.6C).** Lower than average NonTg cell number were observed relative to HuWTSOD1 cells,

likely due to poor yield in those cultures, but no significant differences in number of NonTg cells counted were seen between patient groups **(Figure 5.6C)**. Taken together, these findings suggest that propagation of SOD1 misfolding occurs via CNS-derived EVs from individual patients but not others. Additional patient samples should be analyzed for determination of this result.

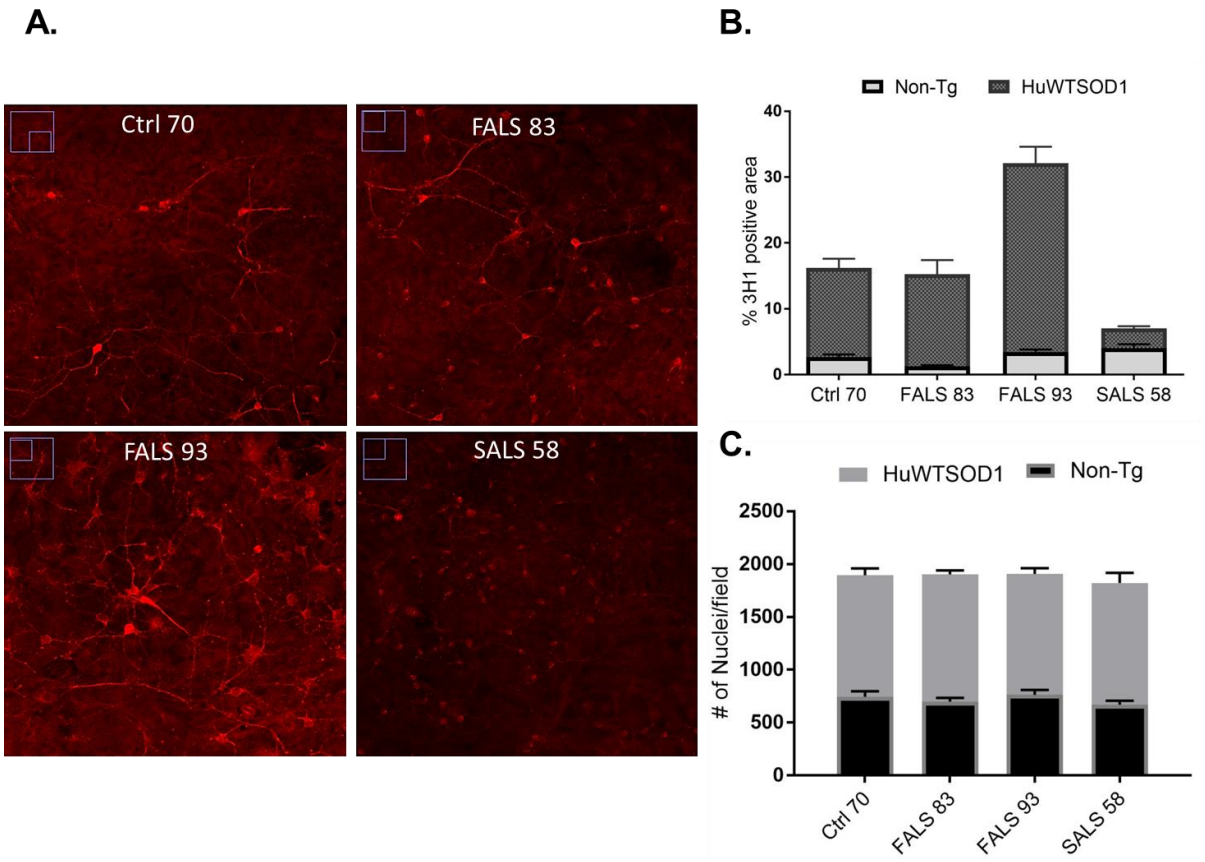

Figure 5.6 Propagation of SOD1 misfolding by human ALS tissue-derived EVs.

A. Confocal microscopy of primary mixed neuronal and glial cultures derived from spinal cord expressing HuWTSOD1 treated with spinal cord tissue-derived microvesicles from ALS patients and a healthy control. 3H1 immunopositivity above untreated background (not shown) is observed in primary cells treated with control patient EVs, and EVs from two different FALS patients, but not SALS. Staining was most intense in structures with neuronal morphology with visible neurites (arrows). Diffuse staining is also present in the background. **B.** Quantification of multiple immunocytochemistry experiments show highest levels of 3H1 immunopositivity in FALS 93 sample, lower levels in FALS 83 and healthy control patient 70, and lowest levels in the SALS patient. The % 3H1 positive area in FALS 93 EV-treated HuWTSOD1 cells is significantly higher than the same cells treated with Ctrl and FALS 83 EVs (N=10 technical replicates, $p<0.001$). Ctrl 70 and FALS 83 HuWTSOD1 cells are significantly higher than SALS 58, as is FALS 93 (N=10 technical replicates, $p<0.001$). There are no significant differences among patient groups for NonTg treated cells. **C.** There is no significant difference in the average number of EV-treated HuWTSOD1 or NonTg

primary cultured cells counted per image between treatment groups as indicated by DAPI-positive nuclei per field. Overall counted NonTg cell numbers are significantly lower than HuWTSOD1 cell numbers.

5.4 DISCUSSION

The data on human ALS patient tissue-derived EVs shown here are consistent with our findings in murine models of ALS. Namely, we show that spinal cord EVs from ALS patients are enriched with luminal misfolded SOD1 (**Figure 5.4**), similar to our findings in EVs from the transgenic mouse model $SOD1^{G93A}$ (**Figure 3.5 CNS tissue-derived exosomes and microvesicles SOD1G93A** mice contain luminal misfolded SOD1 cargo.). Moreover, we showed that CNS tissue-derived microvesicles can propagate SOD1 misfolding to recipient primary mixed neuronal and glial cells (**Figure 5.6)**, consistent with our findings using SOD^{G127X} mouse model EVs (**Figure 4.8)**. These data suggest that our findings in ALS mouse models are applicable to human ALS, and promote the ability to use *in vivo* mouse model tissue-derived EVs when investigating the pathobiology of human ALS disease.

Our observation that EVs isolated from the ALS patient spinal cords, but not frontal cortex, carry luminal misfolded SOD1, is consistent with an active EV-related mechanism of SOD1 secretion in areas of disease pathology in ALS. There is some evidence linking EVs to maintenance of protein homeostasis, or proteostasis, within the cell as some have shown trafficking to the multivesicular body, an early point in exosome biogenesis, prevents the accumulation of toxic protein burden within the cell [219]. Others have shown that exosome release is increased when there is impaired lysosomal or function, suggesting that EVs can compensate to maintain proteostasis in the event of failure of other protein clearance pathways [220]. Dysfunction in protein homeostasis is known to be an early event in neurodegenerative disease pathogenesis [205, 221]. Thus, EVs may be a mechanism of misfolded SOD1 secretion in ALS when protein burden within the cell surpasses the ability of other protein quality control systems such as autophagy and the ubiquitin proteasome system to manage.

In this study, we found that EVs from certain patients but not another, propagated SOD1 misfolding to recipient neuronal and glial cells. It was not wholly unexpected that EVs from an aged healthy patient induced SOD1 misfolding in cells. Others have shown misfolded SOD1 is not exclusive to ALS, but that levels of misfolded SOD1 exist in the normal population, and that it increases with age. The healthy control tissue used in this study was from a male patient of 76 years of age who died from an unrelated coronary condition. Thus, the age of the patient is within the realm as to suggest the possibility of misfolded protein cargo being present in his EVs. It was also not entirely surprising to find that although SALS-associated EVs contained luminal misfolded SOD1 protein, that they did not propagate SOD1 misfolding to cells in the patient investigated. A recent study found that misfolded SOD1 was not relevant to sporadic cases of ALS [30].

The findings presented here on EVs from the human CNS are consistent with our previous findings in mice models, and suggest that murine EVs are valuable tools for understanding EV biology in the CNS, and in the search for disease-relevant biomarkers and therapeutics. Human CNS tissue-derived EVs were investigated in our study with respect to circumscribed parameters such as misfolded SOD1 cargo and propagation competency. Further work using additional ALS patient material is essential for a comprehensive understanding of the role EVs play in the context of human ALS.

CHAPTER 6. DISCUSSION & CONCLUDING REMARKS

6.1 SUMMARY OF FINDINGS

The overall goal of this research was to investigate the *in vivo* relevance of extracellular vesicles to the pathobiology of ALS. To achieve this goal, we first required EVs isolated from an *in vivo* environment. Work published in 2012 by Perez-Gonzalez *et al.* put forth a novel protocol for the isolation of EVs from frozen, whole neural tissues from Alzheimer's disease patient material and murine models [222]. In Chapter 2 of this thesis, we modified and optimized this protocol for isolation of two EV subtypes from whole neural tissues of ALS mouse models which express FALS-associated SOD1 mutations, the SOD1^{G93A} and SOD1^{G127X} transgenic mice. The two EV subtypes, exosomes and microvesicles, were characterized by various parameters to demonstrate that they conform to EV-associated criteria established in literature. The results obtained strongly suggested that we were isolating pure populations of EVs free from major sources of contamination.

In Chapter 3, we used exosomes and microvesicles from SOD1^{G93A} mice to demonstrate that the isolated EVs possessed misfolded SOD1 cargo on the surface and within the luminal compartment. We found that misfolded SOD1 levels in SOD1^{G93A} CNS tissue-derived EVs were enriched in the lumen relative to surface, implicating active sorting and secretion of misfolded SOD1 via EVs. Concurrently, we observed that although surface misfolded SOD1 levels were low they were detectable using monoclonal antibodies 3H1 and 10C12 by both immunoprecipitation and immuno-EM techniques. When two different cultured cell types, HEK and NSC-34, were treated with routinely used concentrations of EVs, we also found that misfolded SOD1-bearing EVs did not cause significant cytotoxicity. Instead, we detected increased cell viability. Taken together, the results of Chapter 2

implicated active secretion of misfolded SOD1 protein via CNS tissue-derived EVs through an unconventional secretory pathway.

Next, in Chapter 4, we demonstrated that both exosomes and microvesicles from $SOD1^{G127X}$ mice propagate SOD1 misfolding to HuWTSOD1 cells, but not to HEK or NSC-34 cells at comparable levels. These results were not due to inefficient uptake of EVs since we also showed that all investigated cell types had similar EV uptake when treated with PKH67 dye-labeled EVs.

Finally, in Chapter 5 of this thesis, we showed preliminary findings from experiments conducted on human ALS patient tissue-derived EVs. We found that, similar to results observed in murine models, spinal cord tissue-derived microvesicles from ALS patients contained enriched levels of misfolded SOD1 protein that were significantly higher than levels observed in spinal cord microvesicles from either healthy controls or Alzheimer's disease patients. We also found that levels of EV-associated misfolded SOD1 were 7-fold lower in a region unaffected by pathology, the frontal cortex, when compared to the spinal cord. Overall, the implications and significance of these findings are many-fold, and are explored in greater depth in the following paragraphs.

6.2 A STARRING ROLE FOR TISSUE-DERIVED EVS IN THE SEARCH FOR BIOMARKERS IN ALS

Identification of biomarkers in biofluids such as CSF or plasma is difficult in neurodegenerative diseases because pathology is largely confined to specific cell types or discrete regions within the CNS [123]. Identifying reliable biomarkers in diseases such as ALS is crucial for patient disease diagnosis, improving therapy, conducting basic research, and for proper patient stratification in clinical trials [223]. Currently availably biomarkers in ALS are of limited diagnostic and prognostic value, and are hampered by a number of limitations including inability to distinguish

between ALS and other diseases like primary lateral sclerosis which mimic the symptoms of ALS [223]. In Parkinson's disease, attempts at using total α-synuclein levels in CSF or plasma as a diagnostic measure have yielded inconsistent and discouraging results, reviewed in a paper by Kasuga *et al.* [224]. More hopeful results were produced in a study that first enriched for EVs expressing the neural cell adhesion molecule (L1CAM), a CNS-specific marker, and subsequently probed for α-synuclein [217].

Herein we have presented data from both mouse models and human ALS patients that intimate the potential for misfolded SOD1 within EVs to be used as biomarkers in this disease. For example, since we have demonstrated misfolded SOD1 on the surface of EVs from ALS patients and murine models, misfolded SOD1-specific antibodies such as 3H1 and 10C12 could be used to enrich for blood or CSF-derived EVs also possessing surface misfolded SOD1 protein. We have also shown evidence in this work that luminal misfolded SOD1 protein is a more reliable marker for distinguishing between disease and healthy EVs than is surface misfolded protein. Therefore, a method which first enriches for neuron-specific EVs in a CSF preparation, such as pull-down of L1CAM-expressing EVs as demonstrated by Shi *et al*. [217], would enable subsequent detergent lysis and detection of luminal misfolded SOD1. The possibility of using misfolded SOD1 within EVs is an attractive biomarker option which warrants further exploration. In the future, fully characterizing the proteome of ALS patient tissue-derived EVs could identify other higher abundant proteins that are specific to disease. Such high abundant markers could then be used to enrich for EV biomarkers in minute amounts of CSF or plasma.

6.3 Mechanistic implications of EVs in ALS

Association with EVs may promote protein aggregation

Since misfolded SOD1 has been demonstrated to be secreted by EV-dependent and independent avenues, it is interesting to consider the specific effects and

contribution of EVs to overall disease pathogenesis. A recent study published by Grey *et al.* in the *Journal for Biological Chemistry* showed that aggregation of α-synuclein was accelerated in the presence of exosomes or exosome-derived lipids [225]. Using exosomes isolated from neuroblastoma cells and a thioflavin T assay to monitor aggregation, they found that the lag time to formation of α-synuclein fibrils was reduced in the presence of exosomes from either control cells or cells overexpressing α-synuclein, and that exosomes catalyzed the formation of α-synuclein aggregates to the same extent as incubation with pre-formed fibrils [225]. There is also an established tendency for gangliosides, a lipid enriched in exosomes, to interact with Alzheimer's-associated Aβ, and higher concentrations of ganglioside-bound Aβ have been found in the CSF of AD patients [226-228]. Remarkably, another study demonstrated that Aβ fibril formation was accelerated in the presence of ganglioside-containing membrane vesicles [229]. These findings suggest that EVs, and more specifically their unique lipid composition, can catalyze the aggregation of proteins that are involved in neurodegenerative diseases. We did not explore the aggregation dynamics of isolated EV-associated misfolded SOD1 in this work, but evidence from the above studies indicates that it is an important avenue to investigate further. Thus, although misfolded SOD1 is released from cells both as naked protein and in associate with exosomes, EVs may specifically promote SOD1 aggregate-formation, and may contribute to disease pathogenesis above and beyond the capability of non-vesicle-associated extracellular SOD1.

EV-associated nucleic acids and intercellular communication

Exosomes are enriched in nucleic acid cargo, especially small RNA transcripts such as piRNA, tRNA, and miRNAs, which they protect from extracellular ribonucleases by enclosing them within a double membrane [230, 231]. In the CNS, such nucleic-acid containing EVs can traverse through the endothelial cells of the blood-brain barrier and mediate long-distance communication between the CNS and periphery [128, 231, 232]. Converging lines of evidence show that RNA and DNA material within EVs are stable in the extracellular environment, and can exert a biological

effects in recipient cells by repressing or inhibiting gene translation [174, 230, 233-235]. These exosomes can also have a detrimental effect on the function of recipient cells in the context of neurodegenerative diseases. *In vivo* studies in prion disease models have identified specific enrichment of miRNAs such as miR-342 and miR-146 in EVs which were found to activate microglia and promote formation of plaques [231, 236-238]. A significantly altered miRNA profile was also detected in EVs from prion-infected neuronal cells [236]. Furthermore, small RNAs are increasingly found to modulate vital processes in the CNS including synaptic plasticity, and neuronal viability and development which frequently go awry in neurodegenerative disease [231, 239]. However, to our knowledge, no work has been conducted on exosome-derived miRNAs in the context of ALS. The above lines of evidence suggest that RNA deep-sequencing of tissue-derived EVs from affected CNS regions in ALS can be used to identify disease-specific miRNA signatures in ALS and potential functional effects of those transcripts in recipient cells, and should be investigated.

EVs work in concert with other protein clearance pathways

EV secretion is also increasingly found to work in concert with other protein clearance pathways in the cell. Alvarez-Erviti *et al.* showed that lysosomal dysfunction, an early event in Parkinson's disease, ALS, and several other neurodegenerative diseases, increases the release of exosomes containing α-synuclein from cultured neuroblastoma cells, and the intercellular transmission of α-synuclein [220]. A close relationship also seems to exist between the biogenesis and secretion of exosomes and autophagy. Biochemical and morphological studies demonstrate that the autophagosome, the initiating organelle in the autophagy pathway, can fuse with the multivesicular body (MVB), a starting structure in the exosome release pathway, to form a hybrid structure called the amphisome **(Figure 6.1)** [240]. The MVB is the autophagosome's main endocytic fusion partner [241]. Induction of autophagy is also shown to inhibit exosome release and increase fusion of autophagosomes to MVBs, generating enlarged amphisomes in an erythroleukemic cell line [242].

A concerted autophagy and exosome release pathway appears to play an important yet poorly understood role in neurodegenerative disease. Mutations in the endosomal sorting complex required for transport (ESCRT)-III subunit charged multivesicular body protein 2B (CHMP2B) are associated with a subset ALS [243]. ESCRT subunits select and sequester cargo into intraluminal vesicles of the late endosome, initiating exosome biogenesis [244]. Functional studies show that ESCRT subunits are also required for efficient fusion of autophagosomes to MVBs and successful autophagic degradation of cargo [243]. Defects in ESCRT function also lead to accumulation of cytoplasmic TDP-43 within inclusions, a hallmark of ALS and FTD [243]. Even more remarkably, C9ORF72, gene mutations of which is the major cause of ALS, has recently been shown to regulate both endosomal trafficking and autophagy [245]. Thus there seems to be a dynamic interplay between autophagy and EV release pathways which may be detrimentally altered in ALS. Further investigation of this coordinated pathway should be conducted using tissue-derived EVs from the CNS in order to understand the contribution of autophagy and EVs to ALS pathobiology.

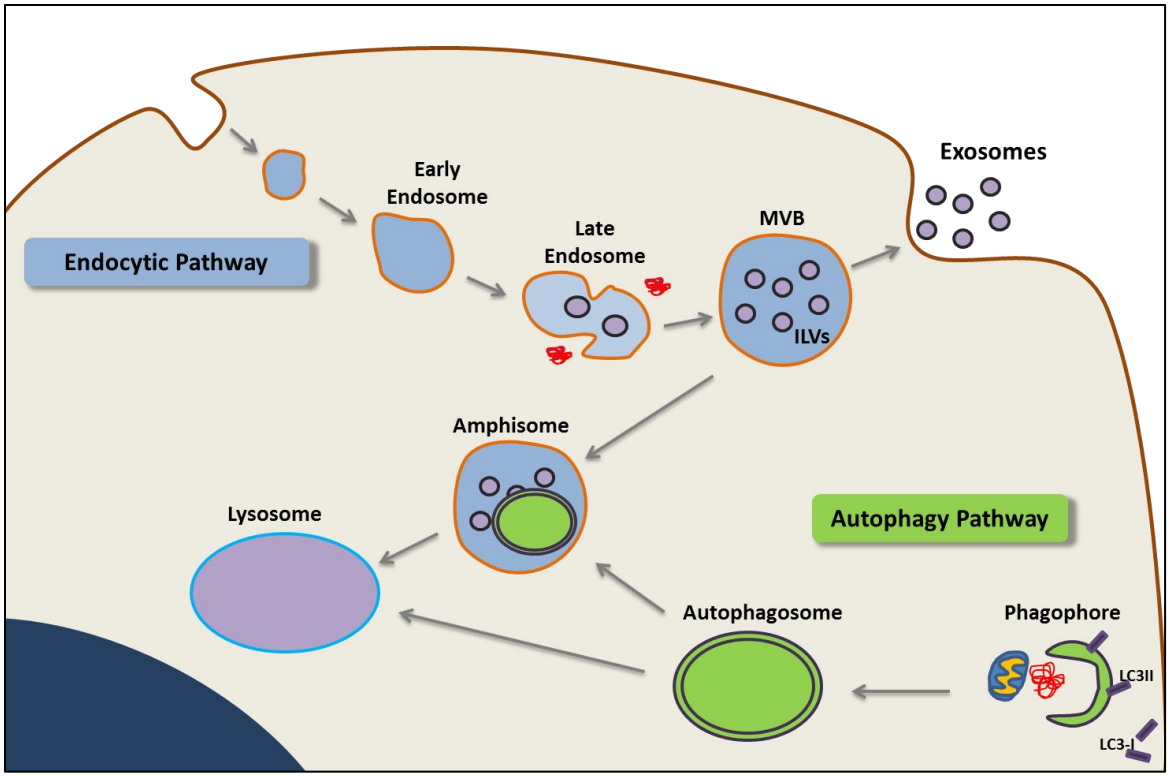

Figure 6.1 The exosome release pathway works in concert with other protein clearance pathways.

The exosome biogenesis pathway begins at the late endosome with the formation of invaginations in the endosomal membrane to form intraluminal vesicles (ILVs), and matures into an organelle termed the multivesicular body (MVB). The initiating structure of the autophagy pathway is the autophagosome, which forms by elongation of a phagophore. The autophagosome can either directly fuse with the lysosome for degradation of intraluminal contents, or fuse with the MVB to form a structure called the amphisome. Induction of autophagy has been shown to inhibit exosome release and increase fusion of autophagosomes to MVBs. The EV biogenesis pathway appears to works in concert with autophagy to maintain cellular proteostasis.
Figure adapted and redrawn with permission from Baixauli, F. *et al.* Exosomes and Autophagy: Coordinated Mechanisms for the Maintenance of Cellular Fitness. *Front. Immunol.* **5,** (2014) [240]

6.4 PRION-LIKE PROPAGATION OF PROTEIN MISFOLDING VIA EVS

In prion disease, pathology is conferred from cell to cell by infectious proteins which induce conformational changes in their normal counterparts and recruit them into pathological aggregates [246]. Increasing evidence suggests that such a mechanism also exists for a wider array of proteins involved in neurodegenerative diseases such

as tau, Aβ, α-synuclein, mutant huntingtin, and SOD1, reviewed in excellent articles by Jucker and Walker, and Brettschneider *et al.* [190, 247].

The exact mechanism whereby pathology is transmitted in ALS patients or disease models is unknown. Recently, a series of compelling studies gave *in-vivo* evidence for propagative SOD1 misfolding being a primary driver of disease symptoms in ALS [86, 87, 248]. Ayers et al. introduced whole-brain homogenates from paralyzed $SOD1^{G93A}$ mice into newborn mice transgenic for a YFP-tagged SOD1 mutant G85R ($SOD1^{G85R\text{-}YFP}$) [86].They found that all $SOD1^{G93A}$-injected $SOD1^{G85R\text{-}YFP}$ mice became paralyzed by 3 months of age and had YFP accumulations in the brain and spinal cord, mimicking the pathology and phenotype seen in ALS patients [86]. Heterozygous $SOD1^{G85R}$ mice usually never develop symptoms during their lifetime, so the observed changes were highly significant. Remarkably, they showed that a second passage injection of brain homogenates from paralyzed $SOD1^{G85R\text{-}YFP}$ mice which were previously injected with $SOD1^{G93A}$, into naïve newborn $SOD1^{G85R\text{-}YFP}$ mice caused a significant decrease in age to paralysis in all mice [86]. This finding is reminiscent of host adaptation seen in prion diseases whereby the second passage of prion protein into a host that is of the same species results in faster incubation times [249].

However, in order for propagation to occur in a prion-like manner, pathogenic proteins must be released and taken up by neighbouring cells. Studies have shown that tau fibrils are released directly into the extracellular space [250], while oligomers of both tau and α-synuclein are released encapsulated within exosomes [171, 214, 251]. Interestingly, some have shown that EV-associated α-synuclein is more oligomeric and aggregation-prone than free α-synuclein in the extracellular milieu, and therefore, potentially more pathological [170, 195]. The cellular uptake of mutant tau, SOD1, and oligomeric α -synuclein have been shown to be mediated by mechanisms such as fluid-phase uptake, receptor-mediated endocytosis and micropinocytosis [167, 247, 252-254]. A group has also shown that aggregates of

mutant huntingtin can directly penetrate cell membranes, bypassing the endosome and other intracellular compartments [255]. Based on these data and our own, we propose that misfolded SOD1 can be propagated in a prion-like manner via both EVs released from living cells and aggregated SOD1 species that are released from dead or dying cells **(Figure 6.2)**. However, the manner by which misfolded SOD1 protein is sorted to EVs or the mechanisms responsible for uptake of these EVs remain unknown, and future mechanistic studies should focus on elucidating these pathways.

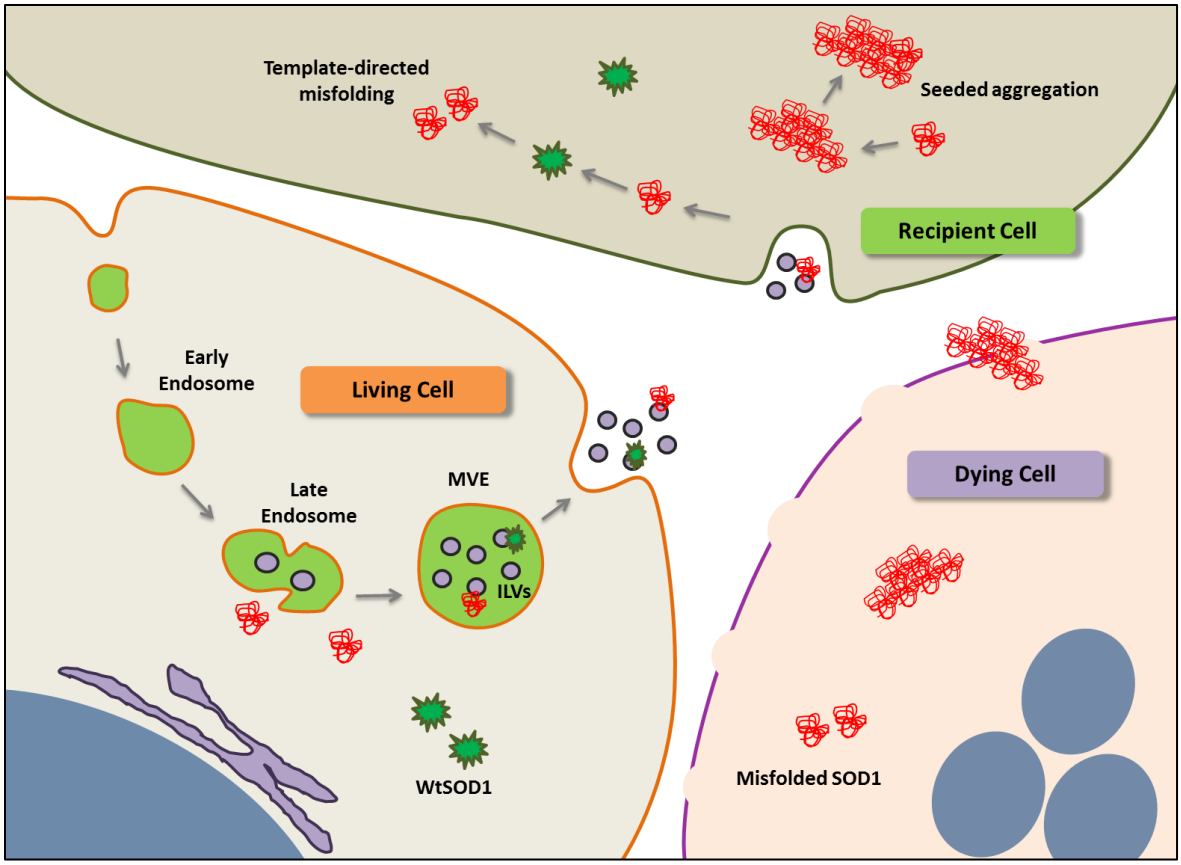

Figure 6.2 Intercellular transmission and seeding of SOD1 misfolding via EVs

Misfolded SOD1 is packaged into intraluminal vesicles (ILVs) within the late endosome and secreted into the extracellular space as exosomes. Microvesicles are released by direct budding off of the plasma membrane, and results in vesicles similar to exosomes in the extracellular space. Exosomes and microvesicles can be taken up by neighboring cells via endocytosis, micropinocytosis or receptor-mediated endocytosis. Within the recipient cell, the misfolded SOD1 species can escape into the cytosol and template the misfolding of normally folded wild-type SOD1. Simultaneously, dead or dying cells can release SOD1 aggregates which can be taken up by recipient cells via macropinocytosis. Seeded aggregation ensues when a SOD1 aggregate composed of misfolded protein recruits additional proteins to enlarge the aggregate.

Figure and portions of the caption are reproduced with permission from Silverman J, **Fernando S**, et al. 2016. Disease Mechanisms in ALS: Misfolded SOD1 Transferred Through Exosome-Dependent and Exosome-Independent Pathways. *Cellular and molecular neurobiology* 36: 377-81

An interesting finding from the work in this thesis is that CNS-sourced EVs bearing misfolded protein are not directly cytotoxic to certain cell lines at concentrations routinely using in literature for treatment of cells **(Chapter 3, Figure 3.8**). However, we observed propagation of SOD1 misfolding to recipient neuronal and glial cells at the same concentration of EVs **(Chapter 4, Figure 4.6)**. In literature, prion infectivity

(or propagation) and prion toxicity are shown to be at least partially distinct from each other [190, 256]. Interesting work by Sandberg *et al.* showed that the propagation of prions and their toxicity occur in two distinct mechanistic phases: a phenotypically silent phase in which prions propagate exponentially until a threshold is reached, and a second plateau phase which is accompanied by onset of clinical disease [256]. Thus, the phenomenon of propagated SOD1 misfolding may not result in direct toxicity to neurons below a certain threshold of either EV concentration or failure of other cellular homeostasis pathways.

6.5 MISFOLDED SOD1-BEARING EVS AS A THERAPEUTIC TARGET

Concurrently, EVs can potentially be used as a therapeutic target. Due to the temporal separation of toxicity and propagation, prion-like template-directed misfolding of SOD1 (and potentially others proteins such as TDP-43), is likely to be an early event in the pathogenesis of ALS. Specifically targeting misfolded SOD1 bearing EVs for degradation by the immune system or protein clearance pathways can therefore act as a viable therapeutic option. We showed here that the monoclonal antibodies 3H1 and 10C12 can be used to detect misfolded SOD1 on CNS tissue-derived EVs. Indeed, such a mechanism has been shown to clear extracellular α-synuclein by targeting to microglia when a transgenic mouse model of Parkinson's disease was passively immunized with an anti-α-synuclein antibody [257]. Thus, 3H1 and 10C12 antibodies, or other high affinity antibodies of a similar nature, can be used to target potentially pathogenic EVs bearing misfolded SOD1 protein before ALS disease progression worsens. Alternatively, receptors which mediate the uptake of such EVs can be targeted. However, targeting EV-receptors is likely to yield unfavourable side effects since they are known to multitask for endocytosis of multiple cell-essential components.

Neuronal and glial EVs also have known neuroprotective roles in the CNS. Takeuchi *et al.* showed that the secretion and uptake of exosomes packaged with

molecular chaperones improved protein homeostasis at the organism level in a *Drosophila* model, and reduced protein aggregation in neuroblastoma cells [258]. More recently, Deng *et al.* demonstrated that extracellular vesicles enriched in both misfolded proteins and cysteine string protein, a protein essential for maintaining proteostasis at neuronal synapses, are co-exported from neurons [259]. Their work indicated that EV-mediated removal of misfolded proteins compensate for dysfunction in lysosomal and proteosomal pathways, and is beneficial to cells [259]. Thus, EVs from certain environments are neuroprotective, and are a potential means of therapy in neurodegenerative diseases. Further works exploring exactly which EVs are neuroprotective, for example whether EVs secreted from a certain cell type such as astrocytes or microglia, would aid the potential development of such therapeutics.

6.6 EXTRACELLULAR VESICLES: PLEIOTROPIC ACTORS IN THE CNS

Cytoplasmic inclusions containing SOD1 protein are found in astrocytes and motor neurons from ALS patients with SOD1 gene mutations [45, 260]. This observed inclusion pathology can be exacerbated either by the increased release and uptake of misfolded SOD1 from the extracellular space, or from decreased release and retention of SOD1 species within the cell, promoting formation of protein aggregates. There is evidence to suggest that both are involved in ALS, and that a balance of protein clearance is essential [261].

Taken together, the work depicted in this thesis, and the findings of others, suggest that extracellular vesicles play a pleiotropic role in the CNS and in ALS, as first hypothesized by Dr. Efrat Levy's research group [135, 262]: In one aspect, EVs bearing misfolded protein cargo can seed a prion-like protein misfolding cascade in recipient cells, causing widespread transmission of disease pathology. On the other hand, EV-mediated clearance of pathological proteins is likely beneficial to the cell,

and can compensate for the failure of other protein clearance pathways. Thus, it appears that EV-mediated export of misfolded protein can be beneficial to the individual cell, but may be detrimental at the organ or organism level.

6.7 LOOKING TO THE FUTURE: RESEARCH ON EVS IN NEURODEGENERATIVE DISEASE

Propagation of protein misfolding and impairment of protein homeostasis appear to be general, unifying phenomenon in neurodegenerative disease, with contributing evidence from several different diseases. However, some important questions remain unanswered. For one, the initiating events in the protein misfolding cascade are unknown, meaning that we do not completely understand why neurodegenerative diseases are associated with aging. We also do not know what causes cell-type specificity of neurodegeneration in different neurodegenerative diseases; for example, motor neurons in ALS, striatal neurons in PD, and cortical neurons in AD. Future research on EVs may provide insight into some aspects of these questions. For instance, using murine and rat models of aging, two different groups have shown an abnormal accumulation of exosomes at the neuromuscular junction and axon terminals, among other regions, in the CNS [263, 264]. An age-related increase in exosome release has also been observed in rhesus monkeys and humans [265, 266]. Further analysis of age-related changes in CNS EVs can potentially help identify disease-relevant factors that occur with aging. For example, using plasma or serum-sourced EVs obtained at serial time points from diagnosed patients, longitudinal analyses can be conducted, and has the potential to yield interesting results.

Finally, the pathogenesis of neurodegenerative diseases like ALS is most likely non-cell autonomous, with evidence for microglia, astrocytes and other supporter cells in the CNS playing crucial roles. The extent to which EVs released from these cell types contribute to disease pathology and neuronal death is a research area that is

also likely to yield very interesting results. The protocol described in this work can be used to isolate CNS-sourced EV populations that can subsequently be separated by cell-type specific surface markers to distinguish between EVs of neuronal and glial origin. The physiological relevance and disease-specificity of CNS tissue-derived EVs can greatly aid such investigations.

Holistically, the field of extracellular vesicle biology is relatively new and the importance of these small vesicles in multiple diseases is only now being fully appreciated. Continued research into the role of EVs in neurodegenerative diseases using physiologically relevant models will allow for a basic understanding EVs in the CNS, and inform their use as much-needed biomarkers and therapeutic targets in disease.

BIBLIOGRAPHY

1. Robberecht, W. and T. Philips, *The changing scene of amyotrophic lateral sclerosis.* Nat Rev Neurosci, 2013. **14**(4): p. 248-64.
2. Swinnen, B. and W. Robberecht, *The phenotypic variability of amyotrophic lateral sclerosis.* Nat Rev Neurol, 2014. **10**(11): p. 661-70.
3. Rowland, L.P., *How amyotrophic lateral sclerosis got its name: The clinical-pathologic genius of jean-martin charcot.* Archives of Neurology, 2001. **58**(3): p. 512-515.
4. Ravits, J.M. and A.R. La Spada, *ALS motor phenotype heterogeneity, focality, and spread: deconstructing motor neuron degeneration.* Neurology, 2009. **73**(10): p. 805-11.
5. *Full text of Lou Gehrig's farewell speech*. 2016; Available from: http://www.si.com/mlb/2009/07/04/gehrig-text.
6. Le, S.C., et al., *Genetics of amyotrophic lateral sclerosis: an update.* 2013.
7. Pratt, A.J., E.D. Getzoff, and J.J. Perry, *Amyotrophic lateral sclerosis: update and new developments.* Degener Neurol Neuromuscul Dis, 2012. **2012**(2): p. 1-14.
8. Cronin, S. and et al., *Ethnic variation in the incidence of ALS: a systematic review. - PubMed - NCBI.* 2016.
9. Kiernan, M.C., et al., *Amyotrophic lateral sclerosis.* Lancet, 2011. **377**(9769): p. 942-55.
10. Cox, P.A.P.A., *Cycad neurotoxins, consumption of flying foxes, and ALS-PDC disease in Guam.* Neurology. **58**(6): p. 956-959.
11. Ow, C.P.A. and Sacks, *Cycad neurotoxins, consumption of flying foxes, and ALS-PDC disease in Guam. - PubMed - NCBI.* 2016.
12. Ingre, C., et al., *Risk factors for amyotrophic lateral sclerosis.* Clin Epidemiol, 2015. **7**: p. 181-93.
13. Al-Chalabi, A., et al., *The genetics and neuropathology of amyotrophic lateral sclerosis.* Acta Neuropathol, 2012. **124**(3): p. 339-52.
14. Taylor, J.P., R.H. Brown, Jr., and D.W. Cleveland, *Decoding ALS: from genes to mechanism.* Nature, 2016. **539**(7628): p. 197-206.
15. Al-Chalabi, A. and O. Hardiman, *The epidemiology of ALS: a conspiracy of genes, environment and time.* Nat Rev Neurol, 2013. **9**(11): p. 617-28.
16. 2016; Available from: http://alsod.iop.kcl.ac.uk/Overview/gene.aspx?gene_id=SOD1.
17. Andersen, P.M., et al., *Phenotypic heterogeneity in motor neuron disease patients with CuZn-superoxide dismutase mutations in Scandinavia.* Brain, 1997. **120 (Pt 10)**: p. 1723-37.
18. Chen, S., et al., *Genetics of amyotrophic lateral sclerosis: an update.* Mol Neurodegener, 2013. **8**: p. 28.
19. Therrien, M., P.A. Dion, and G.A. Rouleau, *ALS: Recent Developments from Genetics Studies.* Curr Neurol Neurosci Rep, 2016. **16**(6): p. 59.
20. Renton, A.E., et al., *A hexanucleotide repeat expansion in C9ORF72 is the cause of chromosome 9p21-linked ALS-FTD.* Neuron, 2011. **72**(2): p. 257-68.
21. DeJesus-Hernandez, M., et al., *Expanded GGGGCC hexanucleotide repeat in noncoding region of C9ORF72 causes chromosome 9p-linked FTD and ALS.* Neuron, 2011. **72**(2): p. 245-56.
22. Al-Chalabi, A., L.H. van den Berg, and J. Veldink, *Gene discovery in amyotrophic lateral sclerosis: implications for clinical management.* Nat Rev Neurol, 2016.

23. Paez-Colasante, X., et al., *Amyotrophic lateral sclerosis: mechanisms and therapeutics in the epigenomic era.* Nat Rev Neurol, 2015. **11**(5): p. 266-279.
24. Nishimura, A.L., et al., *A mutation in the vesicle-trafficking protein VAPB causes late-onset spinal muscular atrophy and amyotrophic lateral sclerosis.* Am J Hum Genet, 2004. **75**(5): p. 822-31.
25. Skibinski, G., et al., *Mutations in the endosomal ESCRTIII-complex subunit CHMP2B in frontotemporal dementia.* Nat Genet, 2005. **37**(8): p. 806-8.
26. Aoki, Y., et al., *C9orf72 and RAB7L1 regulate vesicle trafficking in amyotrophic lateral sclerosis and frontotemporal dementia.* Brain, 2017. **140**(4): p. 887-897.
27. Blokhuis, A.M., et al., *Protein aggregation in amyotrophic lateral sclerosis.* Acta Neuropathol, 2013. **125**(6): p. 777-94.
28. Mackenzie, I.R.A., R. Rademakers, and M. Neumann, *TDP-43 and FUS in amyotrophic lateral sclerosis and frontotemporal dementia.* The Lancet Neurology, 2010. **9**(10): p. 995-1007.
29. Pokrishevsky, E., et al., *Aberrant Localization of FUS and TDP43 Is Associated with Misfolding of SOD1 in Amyotrophic Lateral Sclerosis.* PLoS One, 2012. **7**(4).
30. Da Cruz, S., et al., *Misfolded SOD1 is not a primary component of sporadic ALS.* Acta Neuropathol, 2017.
31. Van Den Bosch, L., et al., *Ca(2+)-permeable AMPA receptors and selective vulnerability of motor neurons.* J Neurol Sci, 2000. **180**(1-2): p. 29-34.
32. Van Den Bosch, L., et al., *The role of excitotoxicity in the pathogenesis of amyotrophic lateral sclerosis.* Biochim Biophys Acta, 2006. **1762**(11-12): p. 1068-82.
33. Urca, G. and R. Urca, *Neurotoxic effects of excitatory amino acids in the mouse spinal cord: quisqualate and kainate but not N-methyl-D-aspartate induce permanent neural damage.* Brain Res, 1990. **529**(1-2): p. 7-15.
34. Hugon, J., et al., *Kainic acid induces early and delayed degenerative neuronal changes in rat spinal cord.* Neurosci Lett, 1989. **104**(3): p. 258-62.
35. Curtis, D.R. and R. Malik, *A neurophysiological analysis of the effect of kainic acid on nerve fibres and terminals in the cat spinal cord.* J Physiol, 1985. **368**: p. 99-108.
36. Van Den Bosch, L., et al., *The role of excitotoxicity in the pathogenesis of amyotrophic lateral sclerosis.* Biochimica et Biophysica Acta (BBA) - Molecular Basis of Disease, 2006. **1762**(11–12): p. 1068-1082.
37. Damme, M., et al., *Autophagy in neuronal cells: general principles and physiological and pathological functions.* Acta Neuropathol, 2015. **129**(3): p. 337-62.
38. Nedelsky, N.B., P.K. Todd, and J.P. Taylor, *Autophagy and the ubiquitin-proteasome system: collaborators in neuroprotection.* Biochim Biophys Acta, 2008. **1782**(12): p. 691-9.
39. Nah, J., J. Yuan, and Y.-K. Jung, *Autophagy in Neurodegenerative Diseases: From Mechanism to Therapeutic Approach.* Molecules and Cells, 2015. **38**(5): p. 381-389.
40. Wong, E. and A.M. Cuervo, *Autophagy gone awry in neurodegenerative diseases.* Nat Neurosci, 2010. **13**(7): p. 805-11.
41. Caberlotto, L. and T.-P. Nguyen, *A systems biology investigation of neurodegenerative dementia reveals a pivotal role of autophagy.* BMC Systems Biology, 2014. **8**(1): p. 1-15.
42. Sasaki, S., *Autophagy in spinal cord motor neurons in sporadic amyotrophic lateral sclerosis.* J Neuropathol Exp Neurol, 2011. **70**(5): p. 349-59.
43. Morimoto, N., et al., *Increased autophagy in transgenic mice with a G93A mutant SOD1 gene.* Brain Res, 2007. **1167**: p. 112-7.
44. Li, L., X. Zhang, and W. Le, *Altered macroautophagy in the spinal cord of SOD1 mutant mice.* Autophagy, 2008. **4**(3): p. 290-3.

45. Lee, S. and H.J. Kim, *Prion-like Mechanism in Amyotrophic Lateral Sclerosis: are Protein Aggregates the Key?* Exp Neurobiol, 2015. **24**(1): p. 1-7.
46. Nassif, M., et al., *Pathogenic role of BECN1/Beclin 1 in the development of amyotrophic lateral sclerosis.* Autophagy, 2014. **10**(7): p. 1256-71.
47. Zhang, X., et al., *Rapamycin treatment augments motor neuron degeneration in SOD1(G93A) mouse model of amyotrophic lateral sclerosis.* Autophagy, 2011. **7**(4): p. 412-25.
48. Lim, J. and Z. Yue, *Neuronal aggregates: formation, clearance, and spreading.* Dev Cell, 2015. **32**(4): p. 491-501.
49. Schubert, U., et al., *Rapid degradation of a large fraction of newly synthesized proteins by proteasomes.* Nature, 2000. **404**(6779): p. 770-4.
50. Mallucci, H.L.S. and R. Giovanna, *The unfolded protein response: mechanisms and therapy of neurodegeneration.* 2016.
51. Soto, C., *Unfolding the role of protein misfolding in neurodegenerative diseases.* Nat Rev Neurosci, 2003. **4**(1): p. 49-60.
52. Pradat, P.F., E. Kabashi, and C. Desnuelle, *Deciphering spreading mechanisms in amyotrophic lateral sclerosis: clinical evidence and potential molecular processes.* Curr Opin Neurol, 2015. **28**(5): p. 455-61.
53. Polymenidou, M. and Don W. Cleveland, *The Seeds of Neurodegeneration: Prion-like Spreading in ALS.* Cell. **147**(3): p. 498-508.
54. Shimonaka, S., et al., *Templated Aggregation of TAR DNA-binding Protein of 43 kDa (TDP-43) by Seeding with TDP-43 Peptide Fibrils.* J Biol Chem, 2016. **291**(17): p. 8896-907.
55. Smethurst, P., et al., *In vitro prion-like behaviour of TDP-43 in ALS.* Neurobiol Dis, 2016. **96**: p. 236-47.
56. Jonsson, P.A., et al., *Minute quantities of misfolded mutant superoxide dismutase-1 cause amyotrophic lateral sclerosis.* Brain, 2004. **127**(1): p. 73-88.
57. Nonaka, T., et al., *Prion-like properties of pathological TDP-43 aggregates from diseased brains.* Cell Rep, 2013. **4**(1): p. 124-34.
58. Chia, R., et al., *Superoxide dismutase 1 and tgSOD1 mouse spinal cord seed fibrils, suggesting a propagative cell death mechanism in amyotrophic lateral sclerosis.* PLoS One, 2010. **5**(5): p. e10627.
59. Rosen, D.R., et al., *Mutations in Cu/Zn superoxide dismutase gene are associated with familial amyotrophic lateral sclerosis.* Nature, 1993. **362**(6415): p. 59-62.
60. Gurney, M.E., et al., *Motor neuron degeneration in mice that express a human Cu,Zn superoxide dismutase mutation.* Science, 1994. **264**(5166): p. 1772-5.
61. Philips, T. and J.D. Rothstein, *Rodent Models of Amyotrophic Lateral Sclerosis.* Curr Protoc Pharmacol, 2015. **69**: p. 5.67.1-21.
62. Mondola, P., et al., *The Cu, Zn Superoxide Dismutase: Not Only a Dismutase Enzyme.* Front Physiol, 2016. **7**.
63. Corson, L.B., et al., *Chaperone-facilitated copper binding is a property common to several classes of familial amyotrophic lateral sclerosis-linked superoxide dismutase mutants.* Proc Natl Acad Sci U S A, 1998. **95**(11): p. 6361-6.
64. Bunton-Stasyshyn, R.K., et al., *SOD1 Function and Its Implications for Amyotrophic Lateral Sclerosis Pathology: New and Renascent Themes.* Neuroscientist, 2014. **21**(5): p. 519-29.
65. Kaur, S.J., S.R. McKeown, and S. Rashid, *Mutant SOD1 mediated pathogenesis of Amyotrophic Lateral Sclerosis.* Gene, 2016. **577**(2): p. 109-18.
66. Szpryngiel, S., M. Oliveberg, and L. Mäler, *Diffuse binding of Zn2+ to the denatured ensemble of Cu/Zn superoxide dismutase 1.* FEBS Open Bio, 2015. **5**: p. 56-63.

67. Kayatekin, C., J.A. Zitzewitz, and C.R. Matthews, *Zinc binding modulates the entire folding free energy surface of human Cu,Zn superoxide dismutase.* J Mol Biol, 2008. **384**(2): p. 540-55.
68. McCord, J.M. and I. Fridovich, *Superoxide dismutase. An enzymic function for erythrocuprein (hemocuprein).* J Biol Chem, 1969. **244**(22): p. 6049-55.
69. Cleveland, D.W., et al., *Toxic mutants in Charcot's sclerosis.* Nature, 1995. **378**(6555): p. 342-3.
70. Kabashi, E., et al., *Oxidized/misfolded superoxide dismutase-1: the cause of all amyotrophic lateral sclerosis?* Ann Neurol, 2007. **62**(6): p. 553-9.
71. Bruijn, L.I., et al., *Aggregation and motor neuron toxicity of an ALS-linked SOD1 mutant independent from wild-type SOD1.* Science, 1998. **281**(5384): p. 1851-4.
72. Nagai, M., et al., *Astrocytes expressing ALS-linked mutated SOD1 release factors selectively toxic to motor neurons.* Nat Neurosci, 2007. **10**(5): p. 615-22.
73. Ezzi, S.A., M. Urushitani, and J.P. Julien, *Wild-type superoxide dismutase acquires binding and toxic properties of ALS-linked mutant forms through oxidation.* J Neurochem, 2007. **102**(1): p. 170-8.
74. Durazo, A., et al., *Metal-free superoxide dismutase-1 and three different amyotrophic lateral sclerosis variants share a similar partially unfolded beta-barrel at physiological temperature.* J Biol Chem, 2009. **284**(49): p. 34382-9.
75. Estevez, A.G., et al., *Induction of nitric oxide-dependent apoptosis in motor neurons by zinc-deficient superoxide dismutase.* Science, 1999. **286**(5449): p. 2498-500.
76. Rakhit, R., et al., *Oxidation-induced misfolding and aggregation of superoxide dismutase and its implications for amyotrophic lateral sclerosis.* J Biol Chem, 2002. **277**(49): p. 47551-6.
77. Bosco, D.A., et al., *Wild-type and mutant SOD1 share an aberrant conformation and a common pathogenic pathway in ALS.* Nat Neurosci, 2010. **13**(11): p. 1396-403.
78. Forsberg, K., et al., *Novel antibodies reveal inclusions containing non-native SOD1 in sporadic ALS patients.* PLoS One, 2010. **5**(7): p. e11552.
79. Liu, H.N., et al., *Lack of evidence of monomer/misfolded superoxide dismutase-1 in sporadic amyotrophic lateral sclerosis.* Ann Neurol, 2009. **66**(1): p. 75-80.
80. Joyce, P.I., et al., *SOD1 and TDP-43 animal models of amyotrophic lateral sclerosis: recent advances in understanding disease toward the development of clinical treatments.* Mammalian Genome, 2011. **22**(7): p. 420-448.
81. Turner, B.J. and K. Talbot, *Transgenics, toxicity and therapeutics in rodent models of mutant SOD1-mediated familial ALS.* Prog Neurobiol, 2008. **85**(1): p. 94-134.
82. Chiu, A.Y., et al., *Age-dependent penetrance of disease in a transgenic mouse model of familial amyotrophic lateral sclerosis.* Mol Cell Neurosci, 1995. **6**(4): p. 349-62.
83. Grad, L.I., et al., *Intermolecular transmission of superoxide dismutase 1 misfolding in living cells.* Proc Natl Acad Sci U S A, 2011. **108**(39): p. 16398-403.
84. Grad, L.I., et al., *Intercellular propagated misfolding of wild-type Cu/Zn superoxide dismutase occurs via exosome-dependent and -independent mechanisms.* Proc Natl Acad Sci U S A, 2014. **111**(9): p. 3620-5.
85. Pokrishevsky, E., L.I. Grad, and N.R. Cashman, *TDP-43 or FUS-induced misfolded human wild-type SOD1 can propagate intercellularly in a prion-like fashion.* Sci Rep, 2016. **6**: p. 22155.
86. Ayers, J.I., et al., *Experimental transmissibility of mutant SOD1 motor neuron disease.* Acta Neuropathol, 2014. **128**(6): p. 791-803.
87. Ayers, J.I., et al., *Prion-like propagation of mutant SOD1 misfolding and motor neuron disease spread along neuroanatomical pathways.* Acta Neuropathol, 2016. **131**(1): p. 103-14.

88. Proctor, E.A., et al., *Nonnative SOD1 trimer is toxic to motor neurons in a model of amyotrophic lateral sclerosis.* Proc Natl Acad Sci U S A, 2016. **113**(3): p. 614-9.
89. Bosco, D.A., et al., *Wild-type and mutant SOD1 share an aberrant conformation and a common pathogenic pathway in ALS.* Nat Neurosci, 2010. **13**(11): p. 1396-1403.
90. Candelario, K.M. and D.A. Steindler, *The role of extracellular vesicles in the progression of neurodegenerative disease and cancer.* Trends Mol Med, 2014. **20**(7): p. 368-74.
91. Théry, M.C., R. Graça, and Clotilde, *Biogenesis, Secretion, and Intercellular Interactions of Exosomes and Other Extracellular Vesicles.* http://dx.doi.org/10.1146/annurev-cellbio-101512-122326, 2014.
92. Johnstone, R.M., et al., *Vesicle formation during reticulocyte maturation. Association of plasma membrane activities with released vesicles (exosomes).* J Biol Chem, 1987. **262**(19): p. 9412-20.
93. Raposo, G., et al., *B lymphocytes secrete antigen-presenting vesicles.* J Exp Med, 1996. **183**(3): p. 1161-72.
94. Amigorena, L.Z., et al., *Eradication of established murine tumors using a novel cell-free vaccine: dendritic cell derived exosomes.* Nature Medicine, 1998. **4**(5): p. 594-600.
95. Lötvall, H.V., et al., *Exosome-mediated transfer of mRNAs and microRNAs is a novel mechanism of genetic exchange between cells.* Nature Cell Biology, 2007. **9**(6): p. 654-659.
96. Thompson, A.G., et al., *Extracellular vesicles in neurodegenerative disease [mdash] pathogenesis to biomarkers.* Nat Rev Neurol, 2016. **12**(6): p. 346-357.
97. Gould, S.J. and G. Raposo, *As we wait: coping with an imperfect nomenclature for extracellular vesicles.* J Extracell Vesicles, 2013. **2**.
98. Raposo, G. and W. Stoorvogel, *Extracellular vesicles: exosomes, microvesicles, and friends.* J Cell Biol, 2013. **200**(4): p. 373-83.
99. Colombo, M., G. Raposo, and C. Thery, *Biogenesis, secretion, and intercellular interactions of exosomes and other extracellular vesicles.* Annu Rev Cell Dev Biol, 2014. **30**: p. 255-89.
100. J.A, E.W., et al., *Cells release subpopulations of exosomes with distinct molecular and biological properties.* Scientific Reports, Published online: 2 March 2016; | doi:10.1038/srep22519, 2016.
101. Théry, A.B., et al., *Diverse subpopulations of vesicles secreted by different intracellular mechanisms are present in exosome preparations obtained by differential ultracentrifugation.* 1, 2012.
102. Duelli, J.P., et al., *MicroRNAs are exported from malignant cells in customized particles.* 2012.
103. Yáñez-Mó, M., et al., *Biological properties of extracellular vesicles and their physiological functions.* J Extracell Vesicles, 2015. **4**.
104. Zitvogel, L., et al., *Eradication of established murine tumors using a novel cell-free vaccine: dendritic cell-derived exosomes.* Nat Med, 1998. **4**(5): p. 594-600.
105. Bobrie, A., et al., *Exosome secretion: molecular mechanisms and roles in immune responses.* Traffic, 2011. **12**(12): p. 1659-68.
106. Fauré, J. and et al., *Exosomes are released by cultured cortical neurones. - PubMed - NCBI.* 2016.
107. Guescini, M., et al., *Astrocytes and Glioblastoma cells release exosomes carrying mtDNA.* J Neural Transm (Vienna), 2009. **117**(1): p. 1-4.
108. Asai, H. and et al., *Depletion of microglia and inhibition of exosome synthesis halt tau propagation. - PubMed - NCBI.* 2016.

109. Fitzner, D. and et al., *Selective transfer of exosomes from oligodendrocytes to microglia by macropinocytosis. - PubMed - NCBI.* 2016.
110. Kramer-Albers, E.M. and A.F. Hill, *Extracellular vesicles: interneural shuttles of complex messages.* Curr Opin Neurobiol, 2016. **39**: p. 101-107.
111. Budnik, V., C. Ruiz-Canada, and F. Wendler, *Extracellular vesicles round off communication in the nervous system.* Nat Rev Neurosci, 2016. **17**(3): p. 160-172.
112. Janas, A.M., et al., *Exosomes and other extracellular vesicles in neural cells and neurodegenerative diseases.* Biochim Biophys Acta, 2016. **1858**(6): p. 1139-1151.
113. Toulouse, M.R. michel.record@inserm.fr, and U.I.-. Université, *Exosomal Lipids in Cell–Cell Communication.* 2016: p. 47-68.
114. Yanez-Mo, M., et al., *Biological properties of extracellular vesicles and their physiological functions.* J Extracell Vesicles, 2015. **4**: p. 27066.
115. Trajkovic, K., et al., *Ceramide triggers budding of exosome vesicles into multivesicular endosomes.* Science, 2008. **319**(5867): p. 1244-7.
116. Llorente, A., B. van Deurs, and K. Sandvig, *Cholesterol regulates prostasome release from secretory lysosomes in PC-3 human prostate cancer cells.* Eur J Cell Biol, 2007. **86**(7): p. 405-15.
117. Kim, C.W., et al., *Extracellular membrane vesicles from tumor cells promote angiogenesis via sphingomyelin.* Cancer Res, 2002. **62**(21): p. 6312-7.
118. Palmerini, C.A., et al., *Role of cholesterol, DOTAP, and DPPC in prostasome/spermatozoa interaction and fusion.* J Membr Biol, 2006. **211**(3): p. 185-90.
119. Simpson, R.J., H. Kalra, and S. Mathivanan, *ExoCarta as a resource for exosomal research*, in *J Extracell Vesicles*. 2012.
120. *PLOS Biology: Vesiclepedia: A Compendium for Extracellular Vesicles with Continuous Community Annotation*. 2016; Available from: http://journals.plos.org/plosbiology/article?id=10.1371/journal.pbio.1001450.
121. Kim, D.K., et al., *EVpedia: an integrated database of high-throughput data for systemic analyses of extracellular vesicles.* J Extracell Vesicles, 2013. **2**.
122. Alais, S., et al., *Mouse neuroblastoma cells release prion infectivity associated with exosomal vesicles.* Biol Cell, 2008. **100**(10): p. 603-15.
123. Turner, A.G.T., et al., *Extracellular vesicles in neurodegenerative disease [mdash] pathogenesis to biomarkers.* Nature Reviews Neurology, 2016.
124. Fevrier, B., et al., *Cells release prions in association with exosomes.* Proceedings of the National Academy of Sciences of the United States of America, 2004. **101**(26): p. 9683-9688.
125. Vella, L.J., et al., *Packaging of prions into exosomes is associated with a novel pathway of PrP processing.* J Pathol, 2007. **211**(5): p. 582-90.
126. Guo, B.B., S.A. Bellingham, and A.F. Hill, *Stimulating the Release of Exosomes Increases the Intercellular Transfer of Prions.* J Biol Chem, 2016. **291**(10): p. 5128-37.
127. Lee, H.-J.L., P. Smita, and J. Seung, *Intravesicular Localization and Exocytosis of α-Synuclein and its Aggregates.* 2005.
128. Bellingham, S.A., et al., *Exosomes: vehicles for the transfer of toxic proteins associated with neurodegenerative diseases?* Front Physiol, 2012. **3**: p. 124.
129. Stuendl, A., et al., *Induction of alpha-synuclein aggregate formation by CSF exosomes from patients with Parkinson's disease and dementia with Lewy bodies.* Brain, 2016. **139**(Pt 2): p. 481-94.
130. Gomes, C., et al., *Evidence for secretion of Cu,Zn superoxide dismutase via exosomes from a cell model of amyotrophic lateral sclerosis.* Neurosci Lett, 2007. **428**(1): p. 43-6.

131. Crescitelli, R., et al., *Distinct RNA profiles in subpopulations of extracellular vesicles: apoptotic bodies, microvesicles and exosomes.* J Extracell Vesicles, 2013. **2**.
132. Ilieva, H., M. Polymenidou, and D.W. Cleveland, *Non–cell autonomous toxicity in neurodegenerative disorders: ALS and beyond.* J Cell Biol, 2009. **187**(6): p. 761-72.
133. Yamanaka, K., et al., *Astrocytes as determinants of disease progression in inherited ALS.* Nat Neurosci, 2008. **11**(3): p. 251-3.
134. Gallart-Palau, X., A. Serra, and S.K. Sze, *Enrichment of extracellular vesicles from tissues of the central nervous system by PROSPR.* Molecular Neurodegeneration, 2016. **11**(1): p. 41.
135. Levy, R.P.-G., et al., *The Exosome Secretory Pathway Transports Amyloid Precursor Protein Carboxyl-terminal Fragments from the Cell into the Brain Extracellular Space.* 2012.
136. Polanco, J.C., et al., *Extracellular Vesicles Isolated from the Brains of rTg4510 Mice Seed Tau Protein Aggregation in a Threshold-dependent Manner.* J Biol Chem, 2016. **291**(24): p. 12445-66.
137. Banigan, M.G., et al., *Differential expression of exosomal microRNAs in prefrontal cortices of schizophrenia and bipolar disorder patients.* PLoS One, 2013. **8**(1): p. e48814.
138. Lotvall, J., et al., *Minimal experimental requirements for definition of extracellular vesicles and their functions: a position statement from the International Society for Extracellular Vesicles.* J Extracell Vesicles, 2014. **3**: p. 26913.
139. Willms, E., et al., *Cells release subpopulations of exosomes with distinct molecular and biological properties.* Sci Rep, 2016. **6**: p. 22519.
140. Bobrie, A., et al., *Diverse subpopulations of vesicles secreted by different intracellular mechanisms are present in exosome preparations obtained by differential ultracentrifugation.* J Extracell Vesicles, 2012. **1**.
141. Dragovic, R.A., et al., *Sizing and phenotyping of cellular vesicles using Nanoparticle Tracking Analysis.* Nanomedicine, 2011. **7**(6): p. 780-8.
142. Yuana, Y., et al., *Co-isolation of extracellular vesicles and high-density lipoproteins using density gradient ultracentrifugation.* J Extracell Vesicles, 2014. **3**.
143. Schindelin, J., et al., *Fiji: an open-source platform for biological-image analysis.* Nat Methods, 2012. **9**(7): p. 676-82.
144. Lee, A.S., *The ER chaperone and signaling regulator GRP78/BiP as a monitor of endoplasmic reticulum stress.* Methods, 2005. **35**(4): p. 373-81.
145. Horváth, I., et al., *Membrane-associated stress proteins: More than simply chaperones.* Biochimica et Biophysica Acta (BBA) - Biomembranes, 2008. **1778**(7–8): p. 1653-1664.
146. Fevrier, B., et al., *Exosomes: a bubble ride for prions?* Traffic, 2005. **6**(1): p. 10-7.
147. Delpino, A. and M. Castelli, *The 78 kDa glucose-regulated protein (GRP78/BIP) is expressed on the cell membrane, is released into cell culture medium and is also present in human peripheral circulation.* Biosci Rep, 2002. **22**(3-4): p. 407-20.
148. Chiou, N.-T. and K.M. Ansel, *Improved exosome isolation by sucrose gradient fractionation of ultracentrifuged crude exosome pellets.* 2016.
149. Quillin, M.L. and B.W. Matthews, *Accurate calculation of the density of proteins.* Acta Crystallogr D Biol Crystallogr, 2000. **56**(Pt 7): p. 791-4.
150. Théry, C., et al., *Isolation and Characterization of Exosomes from Cell Culture Supernatants and Biological Fluids*, in *Current Protocols in Cell Biology*. 2001, John Wiley & Sons, Inc.
151. Lazaro-Ibanez, E., et al., *Different gDNA content in the subpopulations of prostate cancer extracellular vesicles: apoptotic bodies, microvesicles, and exosomes.* Prostate, 2014. **74**(14): p. 1379-90.

152. Laulagnier, K., et al., *Characterization of exosome subpopulations from RBL-2H3 cells using fluorescent lipids.* Blood Cells Mol Dis, 2005. **35**(2): p. 116-21.
153. Sinha, S., et al., *Cortactin promotes exosome secretion by controlling branched actin dynamics.* The Journal of Cell Biology, 2016.
154. Kim, D.K., et al., *EVpedia: A community web resource for prokaryotic and eukaryotic extracellular vesicles research.* Semin Cell Dev Biol, 2015. **40**: p. 4-7.
155. Choi, D.S., et al., *Proteomics, transcriptomics and lipidomics of exosomes and ectosomes.* Proteomics, 2013. **13**(10-11): p. 1554-71.
156. Basso, M., et al., *Mutant copper-zinc superoxide dismutase (SOD1) induces protein secretion pathway alterations and exosome release in astrocytes: implications for disease spreading and motor neuron pathology in amyotrophic lateral sclerosis.* J Biol Chem, 2013. **288**(22): p. 15699-711.
157. Properzi, F., M. Logozzi, and S. Fais, *Exosomes: the future of biomarkers in medicine.* Biomark Med, 2013. **7**(5): p. 769-78.
158. Cortez, M.A., et al., *MicroRNAs in body fluids--the mix of hormones and biomarkers.* Nat Rev Clin Oncol, 2011. **8**(8): p. 467-77.
159. Blennow, K. and H. Zetterberg, *Understanding biomarkers of neurodegeneration: Ultrasensitive detection techniques pave the way for mechanistic understanding.* Nat Med, 2015. **21**(3): p. 217-9.
160. Rotunno, M. and D. Bosco, *An emerging role for misfolded wild-type SOD1 in sporadic ALS pathogenesis.* Frontiers in Cellular Neuroscience, 2013. **7**(253).
161. Turner, B.J., et al., *Impaired extracellular secretion of mutant superoxide dismutase 1 associates with neurotoxicity in familial amyotrophic lateral sclerosis.* J Neurosci, 2005. **25**(1): p. 108-17.
162. Urushitani, M., et al., *Chromogranin-mediated secretion of mutant superoxide dismutase proteins linked to amyotrophic lateral sclerosis.* Nat Neurosci, 2006. **9**(1): p. 108-18.
163. Lafon-Cazal, M., et al., *Proteomic analysis of astrocytic secretion in the mouse. Comparison with the cerebrospinal fluid proteome.* J Biol Chem, 2003. **278**(27): p. 24438-48.
164. Jacobsson, J., et al., *Superoxide dismutase in CSF from amyotrophic lateral sclerosis patients with and without CuZn-superoxide dismutase mutations.* Brain, 2001. **124**(Pt 7): p. 1461-6.
165. Zetterstrom, P., et al., *Misfolded superoxide dismutase-1 in CSF from amyotrophic lateral sclerosis patients.* J Neurochem, 2011. **117**(1): p. 91-9.
166. Mondola, P., et al., *Secretion and Increase of Intracellular CuZn Superoxide Dismutase Content in Human Neuroblastoma SK-N-BE Cells Subjected to Oxidative Stress.* Brain Research Bulletin, 1998. **45**(5): p. 517-520.
167. Münch, C., J. O'Brien, and A. Bertolotti, *Prion-like propagation of mutant superoxide dismutase-1 misfolding in neuronal cells.* Proceedings of the National Academy of Sciences, 2011. **108**(9): p. 3548-3553.
168. Zhao, W., et al., *Extracellular Mutant SOD1 Induces Microglial-Mediated Motoneuron Injury.* Glia, 2010. **58**(2): p. 231-43.
169. Mondola, P., et al., *The Cu,Zn superoxide dismutase in neuroblastoma SK-N-BE cells is exported by a microvesicles dependent pathway.* Molecular Brain Research, 2003. **110**(1): p. 45-51.
170. Lee, H.-J., E.-J. Bae, and S.-J. Lee, *Extracellular [alpha]-synuclein[mdash]a novel and crucial factor in Lewy body diseases.* Nat Rev Neurol, 2014. **10**(2): p. 92-98.
171. Danzer, K.M., et al., *Exosomal cell-to-cell transmission of alpha synuclein oligomers.* Mol Neurodegener, 2012. **7**: p. 42.

172. Grad, L.I., S.M. Fernando, and N.R. Cashman, *From molecule to molecule and cell to cell: prion-like mechanisms in amyotrophic lateral sclerosis.* Neurobiol Dis, 2015. **77**: p. 257-65.
173. Tiwari, A. and L.J. Hayward, *Mutant SOD1 instability: implications for toxicity in amyotrophic lateral sclerosis.* Neurodegener Dis, 2005. **2**(3-4): p. 115-27.
174. El-Andaloussi, S., et al., *Exosome-mediated delivery of siRNA in vitro and in vivo.* Nat. Protocols, 2012. **7**(12): p. 2112-2126.
175. Lee, J.K., et al., *Exosomes derived from mesenchymal stem cells suppress angiogenesis by down-regulating VEGF expression in breast cancer cells.* PLoS One, 2013. **8**(12): p. e84256.
176. Christianson, H.C., et al., *Cancer cell exosomes depend on cell-surface heparan sulfate proteoglycans for their internalization and functional activity.* Proceedings of the National Academy of Sciences, 2013. **110**(43): p. 17380-17385.
177. Costa-Silva, B., et al., *Pancreatic cancer exosomes initiate pre-metastatic niche formation in the liver.* Nat Cell Biol, 2015. **17**(6): p. 816-826.
178. Braicu, C., et al., *Exosomes as divine messengers: are they the Hermes of modern molecular oncology?* Cell Death Differ, 2015. **22**(1): p. 34-45.
179. Coleman, B.M. and A.F. Hill, *Extracellular vesicles--Their role in the packaging and spread of misfolded proteins associated with neurodegenerative diseases.* Semin Cell Dev Biol, 2015. **40**: p. 89-96.
180. Silverman, J.M., et al., *Disease Mechanisms in ALS: Misfolded SOD1 Transferred Through Exosome-Dependent and Exosome-Independent Pathways.* Cell Mol Neurobiol, 2016. **36**(3): p. 377-81.
181. Jang, A., et al., *Non-classical exocytosis of alpha-synuclein is sensitive to folding states and promoted under stress conditions.* J Neurochem, 2010. **113**(5): p. 1263-74.
182. Beninson, L.A., et al., *12. Exposure to acute stress modifies plasma exosomes capable of improving host defense to bacterial challenge.* Brain, Behavior, and Immunity, 2014. **40, Supplement**: p. e4.
183. Akers, J.C., et al., *miRNA contents of cerebrospinal fluid extracellular vesicles in glioblastoma patients.* J Neurooncol, 2015. **123**(2): p. 205-16.
184. Tietje, A., et al., *Cerebrospinal fluid extracellular vesicles undergo age dependent declines and contain known and novel non-coding RNAs.* PLoS One, 2014. **9**(11): p. e113116.
185. Choi, H. and D.S. Lee, *Illuminating the physiology of extracellular vesicles.* Stem Cell Research & Therapy, 2016. **7**(1): p. 55.
186. Wiklander, O.P., et al., *Extracellular vesicle in vivo biodistribution is determined by cell source, route of administration and targeting.* J Extracell Vesicles, 2015. **4**.
187. Di Giorgio, F.P., et al., *Non-cell autonomous effect of glia on motor neurons in an embryonic stem cell-based ALS model.* Nat Neurosci, 2007. **10**(5): p. 608-14.
188. Yang, L., et al., *Bladder cancer cell-derived exosomes inhibit tumor cell apoptosis and induce cell proliferation in vitro.* Mol Med Rep, 2013. **8**(4): p. 1272-8.
189. Demory Beckler, M., et al., *Proteomic Analysis of Exosomes from Mutant KRAS Colon Cancer Cells Identifies Intercellular Transfer of Mutant KRAS.* Mol Cell Proteomics, 2013. **12**(2): p. 343-55.
190. Jucker, M. and L.C. Walker, *Self-propagation of pathogenic protein aggregates in neurodegenerative diseases.* Nature, 2013. **501**(7465): p. 45-51.
191. Soto, C., *Transmissible Proteins: Expanding the Prion Heresy.* Cell. **149**(5): p. 968-977.
192. Zeineddine, R., et al., *SOD1 protein aggregates stimulate macropinocytosis in neurons to facilitate their propagation.* Mol Neurodegener, 2015. **10**: p. 57.

193. Sundaramoorthy, V., et al., *Extracellular wildtype and mutant SOD1 induces ER–Golgi pathology characteristic of amyotrophic lateral sclerosis in neuronal cells.* Cellular and Molecular Life Sciences, 2013. **70**(21): p. 4181-4195.
194. Chivet, M., et al., *Emerging Role of Neuronal Exosomes in the Central Nervous System.* Frontiers in Physiology, 2012. **3**.
195. Lee, H.J., S. Patel, and S.J. Lee, *Intravesicular localization and exocytosis of alpha-synuclein and its aggregates.* J Neurosci, 2005. **25**(25): p. 6016-24.
196. Rajendran, L., et al., *Alzheimer's disease beta-amyloid peptides are released in association with exosomes.* Proc Natl Acad Sci U S A, 2006. **103**(30): p. 11172-7.
197. Talbot, K., *Amyotrophic lateral sclerosis: cell vulnerability or system vulnerability?* J Anat, 2014. **224**(1): p. 45-51.
198. Oztug Durer, Z.A., et al., *Loss of Metal Ions, Disulfide Reduction and Mutations Related to Familial ALS Promote Formation of Amyloid-Like Aggregates from Superoxide Dismutase.* PLoS ONE, 2009. **4**(3).
199. Banci, L., et al., *Metal-free superoxide dismutase forms soluble oligomers under physiological conditions: a possible general mechanism for familial ALS.* Proc Natl Acad Sci U S A, 2007. **104**(27): p. 11263-7.
200. Wang, L., D.H. Gutmann, and R.P. Roos, *Astrocyte loss of mutant SOD1 delays ALS disease onset and progression in G85R transgenic mice.* Hum Mol Genet, 2011. **20**(2): p. 286-93.
201. Charoenviriyakul, C., et al., *Cell type-specific and common characteristics of exosomes derived from mouse cell lines: Yield, physicochemical properties, and pharmacokinetics.* European Journal of Pharmaceutical Sciences, 2017. **96**: p. 316-322.
202. Haidet-Phillips, A.M., et al., *Astrocytes from familial and sporadic ALS patients are toxic to motor neurons.* Nat Biotech, 2011. **29**(9): p. 824-828.
203. Zhang, L., et al., *Microenvironment-induced PTEN loss by exosomal microRNA primes brain metastasis outgrowth.* Nature, 2015. **527**(7576): p. 100-104.
204. Fukai, T. and M. Ushio-Fukai, *Superoxide Dismutases: Role in Redox Signaling, Vascular Function, and Diseases.* Antioxid Redox Signal, 2011. **15**(6): p. 1583-606.
205. Hetz, C., *Protein Misfolding Disorders: A Trip Into the ER*. 2009: Bentham eBooks.
206. Ikemoto, A., et al., *Differential expression between synaptic vesicle proteins and presynaptic plasma membrane proteins in the anterior horn of amyotrophic lateral sclerosis.* Acta Neuropathol, 2002. **103**(2): p. 179-87.
207. Schiffer, D., et al., *Synaptic vesicle proteins, synaptophysin and chromogranin A in amyotrophic lateral sclerosis.* J Neurol Sci, 1995. **129 Suppl**: p. 68-74.
208. Lee, H.J., et al., *Dopamine promotes formation and secretion of non-fibrillar alpha-synuclein oligomers.* Exp Mol Med, 2011. **43**(4): p. 216-22.
209. Lee, H.J., et al., *Autophagic failure promotes the exocytosis and intercellular transfer of alpha-synuclein.* Exp Mol Med, 2013. **45**: p. e22.
210. Kim, C., et al., *Neuron-released oligomeric alpha-synuclein is an endogenous agonist of TLR2 for paracrine activation of microglia.* Nat Commun, 2013. **4**: p. 1562.
211. Howitt, J. and A.F. Hill, *Exosomes in the Pathology of Neurodegenerative Diseases.* J Biol Chem, 2016. **291**(52): p. 26589-26597.
212. Eitan, E., et al., *Extracellular Vesicle-Associated Abeta Mediates Trans-Neuronal Bioenergetic and Ca2+-Handling Deficits in Alzheimer's Disease Models.* NPJ Aging Mech Dis, 2016. **2**.
213. Jeon, I., et al., *Human-to-mouse prion-like propagation of mutant huntingtin protein.* Acta Neuropathol, 2016. **132**(4): p. 577-92.

214. Saman, S., et al., *Exosome-associated tau is secreted in tauopathy models and is selectively phosphorylated in cerebrospinal fluid in early Alzheimer disease.* J Biol Chem, 2012. **287**(6): p. 3842-9.
215. Asai, H., et al., *Depletion of microglia and inhibition of exosome synthesis halt tau propagation.* Nat Neurosci, 2015. **18**(11): p. 1584-1593.
216. Huang, X., et al., *Characterization of human plasma-derived exosomal RNAs by deep sequencing.* BMC Genomics, 2013. **14**(1): p. 319.
217. Shi, M., et al., *Plasma exosomal alpha-synuclein is likely CNS-derived and increased in Parkinson's disease.* Acta Neuropathol, 2014. **128**(5): p. 639-50.
218. Gardiner, C., et al., *Extracellular vesicle sizing and enumeration by nanoparticle tracking analysis.* J Extracell Vesicles, 2013. **2**.
219. Wang, S., G. Thibault, and D.T.W. Ng, *Routing Misfolded Proteins through the Multivesicular Body (MVB) Pathway Protects against Proteotoxicity.* J Biol Chem, 2011. **286**(33): p. 29376-87.
220. Alvarez-Erviti, L., et al., *Lysosomal dysfunction increases exosome-mediated alpha-synuclein release and transmission.* Neurobiol Dis, 2011. **42**(3): p. 360-7.
221. Hetz, C. and B. Mollereau, *Disturbance of endoplasmic reticulum proteostasis in neurodegenerative diseases.* Nat Rev Neurosci, 2014. **15**(4): p. 233-249.
222. Perez-Gonzalez, R., et al., *The exosome secretory pathway transports amyloid precursor protein carboxyl-terminal fragments from the cell into the brain extracellular space.* J Biol Chem, 2012. **287**.
223. Chio, A. and B.J. Traynor, *Motor neuron disease in 2014: Biomarkers for ALS[mdash]in search of the Promised Land.* Nat Rev Neurol, 2015. **11**(2): p. 72-74.
224. Kasuga, K., M. Nishizawa, and T. Ikeuchi, *α-Synuclein as CSF and Blood Biomarker of Dementia with Lewy Bodies.* Int J Alzheimers Dis, 2012. **2012**.
225. Grey, M., et al., *Acceleration of alpha-synuclein aggregation by exosomes.* J Biol Chem, 2015. **290**(5): p. 2969-82.
226. Hong, S., et al., *Soluble Abeta oligomers are rapidly sequestered from brain ISF in vivo and bind GM1 ganglioside on cellular membranes.* Neuron, 2014. **82**(2): p. 308-19.
227. Ariga, T., et al., *Characterization of high-affinity binding between gangliosides and amyloid beta-protein.* Arch Biochem Biophys, 2001. **388**(2): p. 225-30.
228. Blennow, K., et al., *Gangliosides in cerebrospinal fluid in 'probable Alzheimer's disease'.* Arch Neurol, 1991. **48**(10): p. 1032-5.
229. Choo-Smith, L.P., et al., *Acceleration of amyloid fibril formation by specific binding of Abeta-(1-40) peptide to ganglioside-containing membrane vesicles.* J Biol Chem, 1997. **272**(37): p. 22987-90.
230. Valadi, H., et al., *Exosome-mediated transfer of mRNAs and microRNAs is a novel mechanism of genetic exchange between cells.* Nat Cell Biol, 2007. **9**(6): p. 654-659.
231. Quek, C. and A.F. Hill, *The role of extracellular vesicles in neurodegenerative diseases.* Biochem Biophys Res Commun, 2017. **483**(4): p. 1178-1186.
232. Théry, C., *Exosomes: secreted vesicles and intercellular communications.* F1000 Biol Rep, 2011. **3**.
233. Alvarez-Erviti, L., et al., *Delivery of siRNA to the mouse brain by systemic injection of targeted exosomes.* Nat Biotechnol, 2011. **29**.
234. Montecalvo, A., et al., *Mechanism of transfer of functional microRNAs between mouse dendritic cells via exosomes.* Blood, 2012. **119**(3): p. 756-66.
235. Mittelbrunn, M., et al., *Unidirectional transfer of microRNA-loaded exosomes from T cells to antigen-presenting cells.* Nat Commun, 2011. **2**.

236. Bellingham, S.A., B.M. Coleman, and A.F. Hill, *Small RNA deep sequencing reveals a distinct miRNA signature released in exosomes from prion-infected neuronal cells.* Nucleic Acids Res, 2012. **40**(21): p. 10937-49.
237. Montag, J., et al., *Upregulation of miRNA hsa-miR-342-3p in experimental and idiopathic prion disease.* Mol Neurodegener, 2009. **4**: p. 36.
238. Saba, R., et al., *MicroRNA 146a (miR-146a) is over-expressed during prion disease and modulates the innate immune response and the microglial activation state.* PLoS One, 2012. **7**(2): p. e30832.
239. Sonntag, K.C., *MicroRNAs and deregulated gene expression networks in neurodegeneration.* Brain Res, 2010. **1338**: p. 48-57.
240. Baixauli, F., C. López-Otín, and M. Mittelbrunn, *Exosomes and Autophagy: Coordinated Mechanisms for the Maintenance of Cellular Fitness.* Front Immunol, 2014. **5**.
241. Fader, C.M. and M.I. Colombo, *Autophagy and multivesicular bodies: two closely related partners.* Cell Death Differ, 2009. **16**(1): p. 70-8.
242. Fader, C.M., et al., *Induction of autophagy promotes fusion of multivesicular bodies with autophagic vacuoles in k562 cells.* Traffic, 2008. **9**(2): p. 230-50.
243. Rusten, T.E. and A. Simonsen, *ESCRT functions in autophagy and associated disease.* Cell Cycle, 2008. **7**(9): p. 1166-72.
244. Thery, C., L. Zitvogel, and S. Amigorena, *Exosomes: composition, biogenesis and function.* Nat Rev Immunol, 2002. **2**.
245. Farg, M.A., et al., *C9ORF72, implicated in amytrophic lateral sclerosis and frontotemporal dementia, regulates endosomal trafficking.* Hum Mol Genet, 2014. **23**(13): p. 3579-95.
246. Prusiner, S.B., *Novel proteinaceous infectious particles cause scrapie.* Science, 1982. **216**(4542): p. 136-44.
247. Brettschneider, J., et al., *Spreading of pathology in neurodegenerative diseases: a focus on human studies.* Nat Rev Neurosci, 2015. **16**(2): p. 109-20.
248. Ayers, J.I., et al., *Distinct conformers of transmissible misfolded SOD1 distinguish human SOD1-FALS from other forms of familial and sporadic ALS.* Acta Neuropathol, 2016.
249. Bian, J., et al., *Prion replication without host adaptation during interspecies transmissions.* Proceedings of the National Academy of Sciences, 2017. **114**(5): p. 1141-1146.
250. Kfoury, N., et al., *Trans-cellular propagation of Tau aggregation by fibrillar species.* J Biol Chem, 2012. **287**(23): p. 19440-51.
251. Emmanouilidou, E., et al., *Cell-Produced α-Synuclein Is Secreted in a Calcium-Dependent Manner by Exosomes and Impacts Neuronal Survival.* J Neurosci, 2010. **30**(20): p. 6838-51.
252. Frost, B., R.L. Jacks, and M.I. Diamond, *Propagation of tau misfolding from the outside to the inside of a cell.* J Biol Chem, 2009. **284**(19): p. 12845-52.
253. Wu, J.W., et al., *Small misfolded Tau species are internalized via bulk endocytosis and anterogradely and retrogradely transported in neurons.* J Biol Chem, 2013. **288**(3): p. 1856-70.
254. Lee, H.J., et al., *Assembly-dependent endocytosis and clearance of extracellular alpha-synuclein.* Int J Biochem Cell Biol, 2008. **40**(9): p. 1835-49.
255. Ren, P.H., et al., *Cytoplasmic penetration and persistent infection of mammalian cells by polyglutamine aggregates.* Nat Cell Biol, 2009. **11**(2): p. 219-25.
256. Sandberg, M.K., et al., *Prion propagation and toxicity in vivo occur in two distinct mechanistic phases.* Nature, 2011. **470**(7335): p. 540-542.

257. Bae, E.J., et al., *Antibody-aided clearance of extracellular alpha-synuclein prevents cell-to-cell aggregate transmission.* J Neurosci, 2012. **32**(39): p. 13454-69.
258. Takeuchi, T., et al., *Intercellular chaperone transmission via exosomes contributes to maintenance of protein homeostasis at the organismal level.* Proceedings of the National Academy of Sciences, 2015. **112**(19): p. E2497-E2506.
259. Deng, J., et al., *Neurons Export Extracellular Vesicles Enriched in Cysteine String Protein and Misfolded Protein Cargo.* Scientific Reports, 2017. **7**(1): p. 956.
260. Kato, S., et al., *New consensus research on neuropathological aspects of familial amyotrophic lateral sclerosis with superoxide dismutase 1 (SOD1) gene mutations: inclusions containing SOD1 in neurons and astrocytes.* Amyotroph Lateral Scler Other Motor Neuron Disord, 2000. **1**(3): p. 163-84.
261. Ruegsegger, C. and S. Saxena, *Proteostasis impairment in ALS.* Brain Res, 2016. **1648**(Pt B): p. 571-579.
262. Levy, E., *Exosomes in the Diseased Brain: First Insights from In vivo Studies.* Frontiers in Neuroscience, 2017. **11**(142).
263. Johnson, J.E., W.R. Mehler, and J. Miquel, *A fine structural study of degenerative changes in the dorsal column nuclei of aging mice. Lack of protection by vitamin E.* J Gerontol, 1975. **30**(4): p. 395-411.
264. de la Roza, C., J. Cano, and F. Reinoso-Suarez, *An electron microscopic study of astroglia and oligodendroglia in the lateral geniculate nucleus of aged rats.* Mech Ageing Dev, 1985. **29**(3): p. 267-81.
265. Townes-Anderson, E. and G. Raviola, *Degeneration and regeneration of autonomic nerve endings in the anterior part of rhesus monkey ciliary muscle.* J Neurocytol, 1978. **7**(5): p. 583-600.
266. Schroer, J.A., S.B. Plurad, and R.E. Schmidt, *Fine structure of presynaptic axonal terminals in sympathetic autonomic ganglia of aging and diabetic human subjects.* Synapse, 1992. **12**(1): p. 1-13.

APPENDIX 1

Gene Mutations Associated with Amyotrophic Lateral Sclerosis

Genetic subtype	Chromosomal locus	Gene	Protein
ALS1	21q22.1	SOD1	Cu/Zn SOD-1
ALS2	2q33-2q35	Alsin	Alsin
ALS3	18q21	Unknown	Unknown
ALS4	9q34	SETX	Senataxin
ALS5	15q15-21	SPG 11	Spatacsin
ALS6	16p11.2	FUS	Fused in Sarcoma
ALS8	20q13.3	VAPB	VAPB
ALS9	14q11.2	ANG	Angiogenin
ALS10	1p36.2	TARDBP	DNA-binding protein
ALS11	6q21	FIG 4	Phosphoinositide-5phosphatease
ALS12	10p13	OPTN	Optineurin
ALS14	9p13.3	VCP	VCP
ALS15/ALSX	Xp11	UBQLN2	Ubiquilin 2

Genetic subtype	**Chromosomal locus**	**Gene**	**Protein**
ALS16	9p13.2-21.3	SIGMAR1	SIGMAR1
ALS-FTD1	9q21-22	unknown	unknown
ALS-FTD2	9p21	C9ORF72	C9ORF72
NA	2p13	DCTN1	Dynactin

*Table adapted from [18]